Università degli Studi di Trieste

Graduate School in MOLECULAR BIOMEDICINE

PhD Thesis

The Unfolded Protein Response is required early during TBEV infection to trigger the Interferon Response

Tea Carletti

XXVII ciclo – Anno Accademico 2014/2015

UNIVERSITÀ DEGLI STUDI DI TRIESTE

XXVII CICLO DEL DOTTORATO DI RICERCA IN

BIOMEDICINA MOLECOLARE

The Unfolded Protein Response is required early during TBEV infection to trigger the Interferon Response

Settore scientifico-disciplinare: BIO/11 BIOLOGIA MOLECOLARE

DOTTORANDA
TEA CARLETTI

COORDINATORE
PROF. GUIDALBERTO MANFIOLETTI

SUPERVISORE DI TESI
ALESSANDRO MARCELLO

ANNO ACCADEMICO 2014 / 2015

Flaviviruses are a major cause of disease in humans and animals worldwide. Tick-borne encephalitis virus (TBEV) is the most important arthropod-borne flavivirus endemic in Europe and is the etiological agent of tick-borne encephalitis, a potentially fatal infection of the central nervous system. In collaboration with the local hospital we identified the first cases of human transmission of TBEV in the area of Trieste (Caracciolo et al., 2015).

By studying the interplay of TBEV with the infected cell we recently demonstrated that TBEV is able to trigger the stress response of infected cells leading to the formation of stress granules (SG) (Albornoz et al. 2014). Indeed, by immunofluorescence analysis of infected cells we were able to identify SG containing the typical marker of stress: G3BP1, eIF3 and eIF4B. Moreover, by immunoblot analysis we demonstrated that in infected cells the initiation of translation factor eIF2α, a key regulator for the formation of SG, is phosphorylated. We also have evidences that stress and immune response to viral infection are strictly related. In particular we found that the formation of SG in TBEV infected cells is delayed, following the same delayed kinetic of the IFN response (16 h p.i.). Interestingly we found that all the possible agonists of the interferon response are present in the cells at early time after infection: viral RNA is increasing from 8 h.p.i. and infectious particles are produced from 10 h.p.i. These data suggest that the virus is able to escape the host defence machinery.

To better understand what is happening during infection we performed a transcriptome analysis of infected cells comparing two critical time of the infection: 10 h p.i. when TBEV is already replicating but not inducing the IFN and the stress response, and 24 h p.i. when both cellular responses are activated. From the analysis of these data results that several cellular responses are upregulated during infection. Among the most significantly upregulated we found the Unfolded Protein Response (UPR) and the ER stress response.

By performing time course experiments we found that the nuclear translocation of ATF6, the splicing of XBP1 and the phosphorylation of PERK are early events during infection (8-12 h p.i.) indicating that the UPR occurs before the induction of interferon.

We then investigated the role of the UPR as an early cellular response to the infection and as a possible trigger of the interferon response. Interestingly, when cells were infected and, at the same time, treated with Tunicamycin, a known inducer of the UPR, the IFN response was already active at 8 h.p.i. In this condition we found that viral replication was significantly affected by the activation of the UPR and the virus titres

were significantly decreased. Consistent with our previous results we found that also in this condition interferon and stress response are strictly related, indeed, formation of stress granules was also anticipated with the same kinetic of the IFN response.

Recently several authors have proposed a model in which SG induced by viral infection can play a role in the immune response. By studying the localization of RIG-I during TBEV infection we found that this antiviral protein is first localizing to viral replication sites and then is recruited to SG, suggesting a role for this viral induced SG in the IFN response. Finally, by studying the activation status of RIG-I during the infection we collected evidences that RIG-I is early activated (8 h p.i.) but that this early activation might not be sufficient to induce a full IFN response.

Taken together these data suggest that TBEV is able to evade both the stress and the interferon responses, which appear to be strictly interconnected, and that the UPR may play a critical and unexpected role in the delayed activation of both.

List of Publications:

The stress granule component TIA-1 binds Tick-Borne Encephalitis Virus RNA and is recruited to perinuclear sites of viral replication to inhibit viral translation

*Albornoz A, **Carletti T**, Corazza G, Marcello A*

Journal of Virology

2014 June; 88(12):6611-22

Persistent viremia and urine shedding of Tick-Borne Encephalitis Virus in an infected immunosuppressed patient from a new epidemic cluster in North-Eastern Italy

*Caracciolo I, Bassetti M, Paladini G, Luzzati R, Santon D, Merelli M, De Sabbata Giovanni, **Carletti T**, Marcello A, D'Agaro P.*

Journal of Clinical Virology

2015 Aug; 69:48-51

Throughout my thesis I was supported and helped by many people.

First of all, I want to thank Dr. Alessandro Marcello for welcoming me to the lab four years ago. Alessandro allowed me to work on this and several other projects, he has always been open to discussions and ready to guide me. He gave me the possibility to grow and start my scientific career. I will always be extremely grateful.

I would also like to thank Prof. Daniel Ruzek for accepting to be my examiner and for the enthusiasm he has demonstrated in accepting this role.

I am grateful to all the current and previous members of the Molecular Virology Laboratory for their help and support. In particular I want to acknowledge Mia and Vale that supported me during the hardest moments while writing the thesis. Thanks to Ambra, Khalid, Laura, Marylene and Marco, for the talks, coffees and laughs that make our group special.

Thanks to Nadja that always supported me, even when she didn't agree with me, knowing that it was important to me. Together with Cardo you became my family in Trieste.

I want to especially thank my parents and my sister for their unconditional support and for always believing in me.

Finally, the biggest thank you goes to Poto. With your constant support, encouragement and presence in my life you make me feel loved and never alone in this adventure.

And yes, thanks also to you, my little boy… you helped me make this possible!

1 INTRODUCTION

1.1 Family Flaviviridae

Flaviviridae is a large family of enveloped, positive single-stranded RNA viruses, that share similarities in virion morphology, genome organization and replication strategy. The Flaviviridae family consists of four different genera (Brett D Lindenbach, Thiel, and Rice 2007):

- *Flavivirus* (from the Latin *flavus, yellow*) is the largest genus in the family, consisting of more than 70 members. Flaviviruses are also called arboviruses, arthropod-borne viruses, because they are mostly transmitted by mosquitoes or ticks. This family includes important human and animal pathogens such as Dengue viruses (DV), Yellow Fever virus (YFV), West Nile virus (WNV), Zika virus (ZIKV) and Tick-Borne Encephalitis virus (TBEV).
- *Pestivirus* (from the Latin *pestis, plague*) are animal pathogens of major economic importance for the livestock industry. They include Bovine Viral Diarrhea virus (BVDV), classical swine fever virus (CSFV) and border disease virus (BDV) of sheep.
- *Hepacivirus* (from the Greek *hepar, hepatos, liver*) include Hepatitis C virus (HCV) and GB virus B (GBV-B). Hepaciviruses share many features in common with the pestiviruses, including genome organization, a similar mechanism of translational control and limited sequence relatedness.
- *Pegivirus* (from pe, persistent; g, GB or G) is a new genus of the Flaviviridae family (Stapleton et al. 2011) that includes GB-like viruses based on phylogenetic relationships, genome organization and pathogenic features: GBV-A, GBV-C and GBV-D.

In figure 1.1 a simplified phylogenetic tree of the family Flaviviridae is shown.

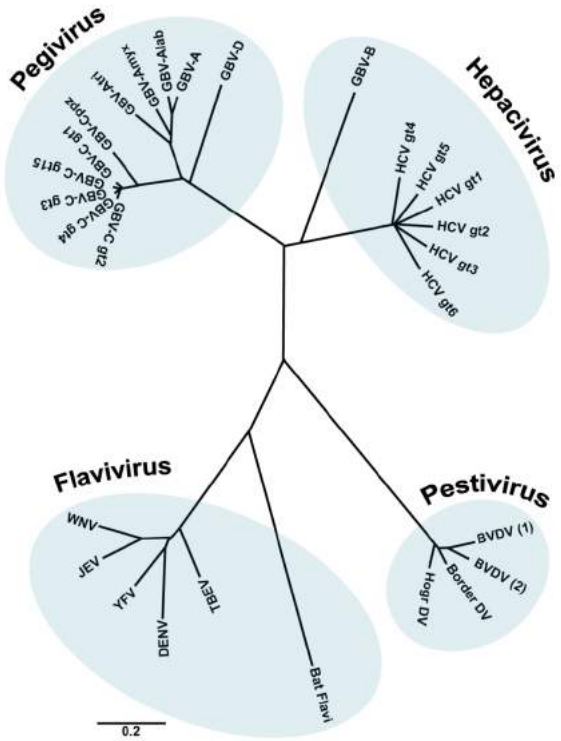

Figure 1.1 - Family Flaviviridae. Phylogenetic tree based on the analysis of aligned conserved motifs of the RNA dependent RNA polymerase (RdRp). Shown are selected members of the family. A distance scale corresponding to amino acid substitutions per position is shown. Figure from (Romero-Brey and Bartenschlager 2014).

1.2 Genus Flavivirus

The genus Flavivirus consist of more than 70 viruses that are transmitted to humans through the bite of arthropod vectors. According to the arthropode, Flaviviruses can be divided in three clusters:

- mosquito-borne: include Yellow Fever virus, Dengue virus, Japanese Encephalitis virus, West Nile virus and Zika virus;
- tick-borne: the most important member is Tick-Borne Encephalitis virus;
- nonvector-borne (i.e., for which no arthropod vectors are known): include Entebbe bat virus, Modoc virus and Rio Bravo virus (Brett D Lindenbach, Thiel, and Rice 2007).

Many of the Flaviviruses are human pathogens and can cause a variety of diseases, including biphasic fever, encephalitis, haemorrhagic fever, flaccid paralysis and

jaundice (Gould and Solomon 2008). Interestingly, recent reports suggest that Zika virus infection of pregnant women might correlate with microcephaly in foetuses (Mlakar et al. 2016).

Flaviviruses are highly prevalent in the developing world. Many factors as urbanization, transportation and changes in land use but also natural factors, such as genetic change in the virus, host-vector relationships, bird migration and climate changes have lead to the spread of viruses to new geographic area (J. S. Mackenzie, Gubler, and Petersen 2004).

Although a large number of humans are infected annually, there are no available antiviral therapies and only a limited number of vaccines are available, including inactivated TBEV and JEV.

1.3 Flavivirus life cycle and genome structure

1.3.1 Binding and entry

Mature virions are small, ≈ 50 nm, and contain a 30 nm electron dense core surrounded by a lipid envelope. The surface of the virus contains two viral proteins: E (envelope) and M (membrane). E glycoprotein is the major antigenic determinant and mediates binding of the virus to the host membrane receptor and fusion during virus entry.

Flaviviruses can utilize multiple receptors for different cell types and in different host species (Brett D Lindenbach, Thiel, and Rice 2007). Infection of dendritic cells (DC) is particularly important because these intradermal cells are the primary targets of Flavivirus infections. The entry occurs through receptor-mediated endocytosis with formation of clathrin-coated pits. Viruses subsequently traffic to a prelysosomal endocytic compartment where low pH induces fusion between the virus and host cell membranes to release the viral nucleocapsid.

1.3.2 Genome Structure

Flavivirus genome consists of a single, positive-strand RNA of approximately 11 kb, with a 5’ type I cap ($m7GpppAmpN_2$). Unlike cellular messenger RNA (mRNA), Flavivirus genomes lack the 3’ polyadenylate tail (Wengler, Wengler, and Gross 1978). The genome encode a single long open reading frame (ORF) flanked by a 100 bp 5’

noncoding region (NCR) or untraslated region (UTR) and a 400-700 bp 3' NCR (or UTR) (Markoff 2003).

Despite the lack of sequence conservation at the 5' NCR, common secondary structures in this region called 5'-stem loop (5' SL) have been show to be conserved among different Flaviviruses. These structures are functionally important as cis-acting regulatory elements for genome amplification, translation or packaging (Lindenbach, Thiel, and Rice 2007).

The 3' NCR exhibit great sequence variability as well, but show similar patterns of conserved sequences and structures. The most conserved structure is a long 3' stem-loop (3' SL) that is enhancing both viral translation and replication (Holden and Harris 2004). A 25 nucleotides region is located just upstream of the 3' SL called cyclization sequence (3' CS). This sequence is highly conserved among Flaviviruses and was found to be complementary with a sequence in the beginning of the capsid gene, more than 10 kbp upstream (5' CS) (Alvarez et al. 2005). The complementarity between these cyclization sequences was shown to be essential for Flavivirus replication (Khromykh et al. 2001). Moreover, during flaviviral replication, the cellular 5'-3' exoribonuclease XRN1 digests viral genomes but stalls at secondary RNA structures at the beginning of the 3' UTR resulting in a 0.3-0.5 kb RNA fragment called subgenomic flavivirus RNA (sfRNA) (Pijlman et al. 2008). It has been demonstrated that the sfRNA regulates multiple cellular pathways to facilitate flaviviral pathogenicity (Roby et al. 2014).

Figure 1.2 shows a schematic representation of the Flaviviruses genome structure.

Figure 1.2 - Flavivirus genome organization. The Flavivirus genome is a positive ssRNA of approximately 11 kb, which is capped at the 5' and do not contain the polyA tail typical of cellular mRNA. It contains a single open reading frame with the structural and non-structural protein (coloured in green and red respectively), flanked by a 5' and 3' untranslated region (UTR). Simplified RNA secondary and tertiary structures within UTRs are also indicated: SL, stem loop; CS, cyclization sequence.

1.3.3 Translation and polyprotein processing

Translation of the viral genome is cap dependent and initiates by ribosomal scanning. The translation is performed by the host cell machinery and produces a single large polyprotein precursor of approximately 3400 amino acids in length. This precursor is a multi-transmembrane domain protein localized on the membrane of the endoplasmic reticulum. The polyprotein is co- and post-translationally cleaved by the cellular enzymes signalase and Furin and by the viral NS2B-NS3 protease into ten proteins: the three structural proteins named capsid (C), envelope (E) and pre-membrane (prM) that form the virion particle, and the seven non-structural proteins named non-structural protein 1 NS1, NS2A, NS2B, NS3, NS4A, NS4B, NS5 that are involved in viral replication, virus assembly and immune response evasion (Lindenbach, Thiel, and Rice 2007) (Figure 1.3).

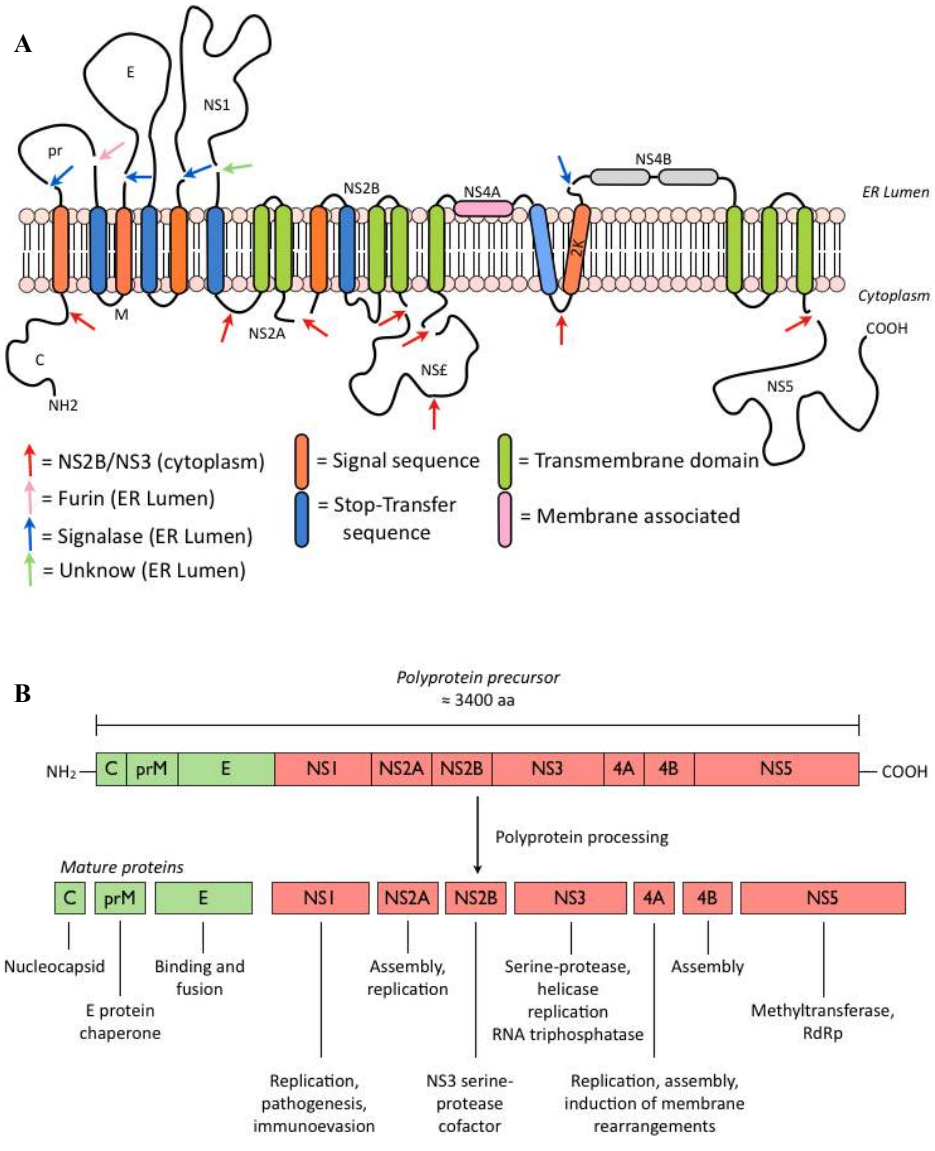

Figure 1.3 - Flavivirus Polyprotein. A) Flavivirus genome encodes for a multi-transmembrane protein localized on the membrane of the ER. The polyprotein is co- and post-translationally cleaved by the NS2B/NS3 viral protease and by cellular enzymes located in the ER lumen. B) Schematic representation of Flavivirus polyprotein and processing. The Polyprotein precursor and the putative functions of the viral proteins during infection are described. C, capsid; prM, pre-membrane protein; E, envelope; RdRp, RNA-dependent RNA polymerase.

1.3.4 Features of the structural proteins

C Protein

The capsid protein, also named core, is a structural component of the virion forming the nucleocapsid and is essential during the assembly of viral particles ensuring specific encapsidation of the viral genome (Ferlenghi et al. 2001). Capsid is a highly basic protein of approximately 11 kDa. Although the sequence identity of capsid protein among the genus is very low, the structural organization is highly conserved for all Flaviviruses: charged residues are clustered at the N- and C- terminal region, whereas the internal region is hydrophobic. C protein folds into a dimer with each monomer containing four alpha helices. The region rich in basic residues interacts with the viral RNA during the assembly of the virion, whereas the hydrophobic region interacts with the membrane (Ma et al. 2004). Nascent C (anchC) contains a C-terminal hydrophobic domain of about 20 amino acids that anchor the protein to the ER membrane and serve as signal peptide for the translocation of the prM protein to the ER lumen (Lobigs 1993). During maturation this domain is cleaved by the viral serine protease NS2B-NS3 (Amberg et al. 1994).

prM protein

prM is a 26 kDa protein precursor of the structural protein M. As mentioned above, prM is translocated into the lumen of the ER by the signal peptide of the C protein. The N-terminal region of prM contains a variable number of N-linked glycosilation sites and six conserved cysteine residues while the C-terminal region, in mature virions, contains a short ectodomain (41 aa) that contains two membrane spanning domains (Chambers et al. 1990).

During the maturation, occurring in the secretory pathway, the Golgi-resident protease Furin, or a related enzyme, cuts prM in the fragments pr, that is released, and M, that remains anchored to the membrane. prM has a crucial role for the formation of mature and infectious virions. Indeed, it acts as chaperone assisting the folding of E protein and preventing its acid-catalyzed rearrangements that could occur in the secretory pathway (Guirakhoo, Bolin, and Roehrig 1992; Brett D Lindenbach, Thiel, and Rice 2007).

E protein

The E protein has an important role in several stage of viral life cycle being involved in receptor binding, membrane fusion and virus assembly processes. Moreover, E protein is the main target of neutralizing antibodies (Stiasny and Heinz 2006; Kaufmann and Rossmann 2011).

Although the aminoacid sequence identity is low (≤ 40%), the structural features of E protein are conserved among different Flaviviruses. E is a 53 kDa type I membrane protein composed by two transmembrane domains and a N-terminal ectodomain connected one to each other by a α-helical stem region. E protein on the viral surface is forming sets of three head-to-tail homodimers that are tightly associated and parallel to the viral membrane (Kaufmann and Rossmann 2011). The ectodomain has three distinct structurally defined domains: DI, DII and DIII connected by flexible junctions capable of hinge-like motions, this flexibility is important during membrane fusion and transition from immature to mature virion (Stiasny and Heinz 2006). DI is the central β-barrel domain that carries an N-linked carbohydrate side chain and that participates in the conformational changes induced by endosomal acidification during cell entry. DII has an elongated structure and provides most of the intersubunit contacts, and is so called dimerization domains. Moreover it contains a hydrophobic fusion loop at its tip that is indispensable for virus-cell membrane fusion. DIII is the immunoglobuline-like C-terminal domain and appears to be involved in receptor binding (Stiasny and Heinz 2006; Bressanelli et al. 2004; Rey et al. 1995).

When exposed to low pH in the endosomal compartments, E protein dimers undergo major rearrangements: from a pre-fusion homodimeric array, to a fusion-active homotrimers (Kaufmann and Rossmann 2011).

1.3.5 Features of the non-structural proteins

NS1

The Non-Structural protein 1 is 46 kDa glycoprotein that is translocated into the ER lumen during polyprotein synthesis. At the N-terminal region of NS1 the junction E/NS1 is cut by a host signal peptidase while at the N terminal, the junction NS1/NS2A is cut by an ER-resident host enzyme that is still unknown. NS1 contains two or three N-linked glycosylation sites and 12 conserved cysteine residues that form disulphide bonds. Newly synthesized NS1 appears as monomer but it has been shown that around 30 minutes after synthesis NS1 forms highly stable homodimers and acquires an affinity for membranes.

NS1 is found intracellularly, on cell surface and, as soluble form, can also be secreted by mammalian cells (Brett D Lindenbach, Thiel, and Rice 2007). Intracellular NS1 is important for RNA replication and mutation of the N-linked glycosylation sites can lead to dramatic defects in RNA replication and virus production (Muylaert et al. 1996).

The function of extracellular forms of NS1 is not yet clear. It has been shown that Flavivirus NS1 has a direct immune evasion function antagonizing complement activation (Avirutnan et al. 2010)and that high levels of NS1 soluble form in the serum of DV-infected patients correlate with severe disease, suggesting that extracellular NS1 is implicated in viral pathogenesis (Avirutnan et al. 2010). A recent report demonstrated that NS1 of all DENV serotype is able to induce endothelial barrier dysfunctions, causing increased permeability of human endothelial cell monolayer in vitro. In the same paper, they show that these reactions could be blocked by NS1 immune polyclonal mouse serum or monoclonal antibody against NS1, suggesting NS1 as a new potential target for DENV therapeutics and vaccines (Beatty et al. 2015).

NS2A

NS2A is a 22 kDa hydrophobic membrane-associated protein. The N-terminal is generated by the cleavage of an unknown ER-resident host enzyme at the junction NS1/NS2A, whereas, the cytosolic C-terminal is generated by the cutting of the viral serine protease NS2B-NS3 (Brett D Lindenbach, Thiel, and Rice 2007). The viral protease cleaves also at an internal site in NS2A generating a C-terminally truncated form named NS2Aα (Nestorowicz, Chambers, and Rice 1994). Mutation study at the

NS2Aα cleavage site provided the evidences that NS2A is involved in virus assembly and release (Kümmerer and Rice 2002). Moreover, it has been demonstrated that NS2A also acts as interferon (IFN) antagonist inhibiting the IFN-α/β-signalling pathway (Muñoz-Jordan et al. 2003).

NS2B

NS2B is also a small, 14 kDa, membrane-associated protein with a central hydrophilic domain and two terminal hydrophobic helices. It has been shown that NS2B forms a stable complex with NS3 and acts as cofactor for NS2B-NS3 serine protease.

The hydrophilic region strongly interacts with the NS3 protease whereas the two hydrophobic domains are responsible for membrane association of the NS2B-NS3 complex (Falgout et al. 1991). Consistently with his role as cofactor of the viral protease, NS2B strongly influences the secondary structure of NS3, by stabilizing the N and C-terminal domains and completing substrate-binding site (Erbel et al. 2006).

NS3

The NS3 is a large, 70 kDa, multifunctional protein, containing several activities for polyprotein processing and RNA replication. The N-terminal of the protein is the catalytic domain of the NS2B-NS3 serine protease complex (NS3pro) (Chambers et al. 1990) and cleaves the NS2A/NS2B, NS2B/NS3, NS3/NS4A and NS4B/NS5 junctions but also generates the C-termini of mature capsid protein and NS4A and can cleave at an internal site of NS2A and NS3. NS3pro is a trypsin-like serine protease and, as mentioned above, it works in association with NS2B cofactor that is contributing with a β-strand to form a chymotrypsin-like fold (Erbel et al. 2006). The protease contains the characteristic catalytic triad (Asp-His-Ser) and a highly specific substrate recognition sequence conserved in all Flavivirus. The cleavage site consist of two basic residues followed by an amino acid with a short side chain (Chambers et al. 1990).

The C-terminal portion (NS3hel) shows significant homology to supergroup 2 RNA helicases and performs different activities including nucleoside triphosphatase (NTPase), RNA triphosphatase (RTPase) and helicase activities. NS3hel is a member of the DEAH/D box family of RNA helicases and its activity is thought to be involved in initiation of RNA synthesis by unwinding the secondary structures present at the 3‘UTR of the Flavivirus genomes, to facilitate polymerase processivity during elongation, or to

separate double-stranded RNA (dsRNA) intermediates generated during viral replication (Warrener et al. 1993; Brett D Lindenbach, Thiel, and Rice 2007). The NS3 RTPase dephosphorylates the 5' end of genome RNA and is therefore involved, together with the NS5 methyltransferase (MTase) domain, in capping the viral RNA (Wengler and Wengler 1993). It is also thought that NS3 can have a role in inducing apoptosis through activation of caspase-8. Whether this is the normal pathway for Flavivirus-induced cell killing requires further study (Ramanathan et al. 2006).

NS4A

NS4A is a small hydrophobic protein of about 16 kDa. As mentioned above, its interaction with the NS1 protein is required for efficient RNA amplification (B D Lindenbach and Rice 1999) and its role in RNA replication is supported by the co-localization of this protein with replication complexes (J M Mackenzie et al. 1998).

The maturation of the NS4A protein involves first the cutting, by the viral serine protease NS2B-NS3, at a site just upstream of the 2K internal signal peptide and then a cut at the 2K-NS4B junction by the signal peptidase (Brett D Lindenbach, Thiel, and Rice 2007). Overexpression studies show that regulated NS4A/2K/4B cleavage is necessary for induction of membrane rearrangements by NS4A (Miller, Sparacio, and Bartenschlager 2006).

NS4B

The non structural protein 4B of Flavivirus is also a small, 27 kDa, hydrophobic protein capable to associate to the ER membrane independently of the 2K signal peptide and co-localize with NS3 and dsRNA in viral replication complex (Miller, Sparacio, and Bartenschlager 2006).

As noted for the NS2A protein, DENV NS4A and NS4B have been shown to block the IFN signalling pathway. NS4B has the strongest antagonist effect which requires a proper processing of the protein by the protease NS2B-NS3 (Muñoz-Jordan et al. 2003; Munoz-Jordan et al. 2005).

NS5

NS5 is at the C terminus of the viral polyprotein and is the largest, 103 kDa, and most conserved flaviviral protein. NS5 is a multifunctional protein with two main enzymatic activities: the N-terminal domain has a methyltransferase (MTase) activity

whereas the C-terminal contains the RNA-dependent RNA polymerase (RdRp) domain (Brett D Lindenbach, Thiel, and Rice 2007). A study on the purified N-terminal domain of NS5 of DENV-2 shows that this domain is capable to transfer methyl groups from S-adenosyl-methionine (SAM) to capped RNA substrates. The same report shows that this domain presents structural similarity with other MTase and binds guanosine triphosphate (GTP) with high specificity (Egloff et al. 2002). The C-terminus of NS5 contains significant homology to RdRPs of other positive-strand RNA virus and its polymerase activity has been confirmed using recombinant NS5 (Guyatt, Westaway, and Khromykh 2001).

NS5 localizes to sites of viral replication complex (RC), associated with the dsRNA template located in induced membranes (Jason M Mackenzie, Kenney, and Westaway 2007).

In addition to MTase and polymerase activities, a new role of for NS5 as an IFN antagonist has recently emerged: study on DENV, TBEV and JEV demonstrated that NS5 antagonizes IFN signalling by inhibiting the Janus kinase-signal transducer and activator of transcription (JAK-STAT) transduction pathway (Ashour et al. 2009; Best et al. 2005; Lin et al. 2006).

1.3.6 RNA Replication and membrane compartments

After translation of the genomic input RNA, the NS5 RdRP synthesizes a genome-length minus strand RNA, which then serves as a template for the synthesis of additional plus strand RNA (Brett D Lindenbach, Thiel, and Rice 2007). Flaviviral RNA synthesis is asymmetric: the positive strand RNA is produced ten times more than the negative strand (Chu and Westaway 1985). The newly synthesized positive strand RNA can be subsequently used for several purposes: for further translation of viral proteins, for synthesis of additional negative strand RNA, or to be incorporated into new viral particles. Hence, the viral RNA genome has three different functions: translation, replication and association with nascent viral particles. Flavivirus replication occurs in close association with virus-induced membrane structures of the rough ER, predominantly in the perinuclear region. These membrane structures may serve as a scaffold for anchoring the replication complex (RC), or to limit the diffusion of viral/host proteins and viral RNA increasing the concentration of components required for RNA synthesis (Miller and Krijnse-Locker 2008). In addition, it has also been suggested that these membrane structures may serves to hide the replication

intermediate dsRNA from the host cellular surveillance (Fernandez-Garcia et al. 2009; Miorin et al. 2013). Composition and three-dimensional organization of these compartments have been recently characterized (Miorin et al. 2008; Miller and Krijnse-Locker 2008; Welsch et al. 2009; Gillespie et al. 2010; Miorin et al. 2013): earliest event leading to the formation of the RC is the proliferation of the ER membranes, followed by the appearance of smooth membrane structures around the time of early logarithmic virus production. These structures are clusters of about 100 nm vesicles, called vesicles packets (VPs). Afterwards other structures are formed: convoluted membranes (CM) and paracrystalline arrays (PC). Three-dimensional EM tomography studies have also showed that VPs, CM and PC are all part of a single ER-derived membrane network. Moreover, dsRNA, NS5, NS2B-NS3 immunolabelling of cryosections prepared from Flavivirus infected cells revealed that VPs are the sites of RNA replication, whereas CM and PC are possibly the sites of protein translation and proteolytic cleavage (Figures 1.4a and 1.4b).

More recently, electron tomography analyses of TBEV infected human neurons were performed (Bílý et al. 2015). The authors demonstrated that TBEV induces vesicles and cisterns containing tubule-like structures (Figure 1.4c and 1.4d). Moreover, they proved that vesicles containing TBEV are associated with cellular microtubules to be transported in infected neurons (Figure 1.4e, 1.4f and 1.4g). This pioneer study reveals important steps of the neuronal injury caused by TBEV infection.

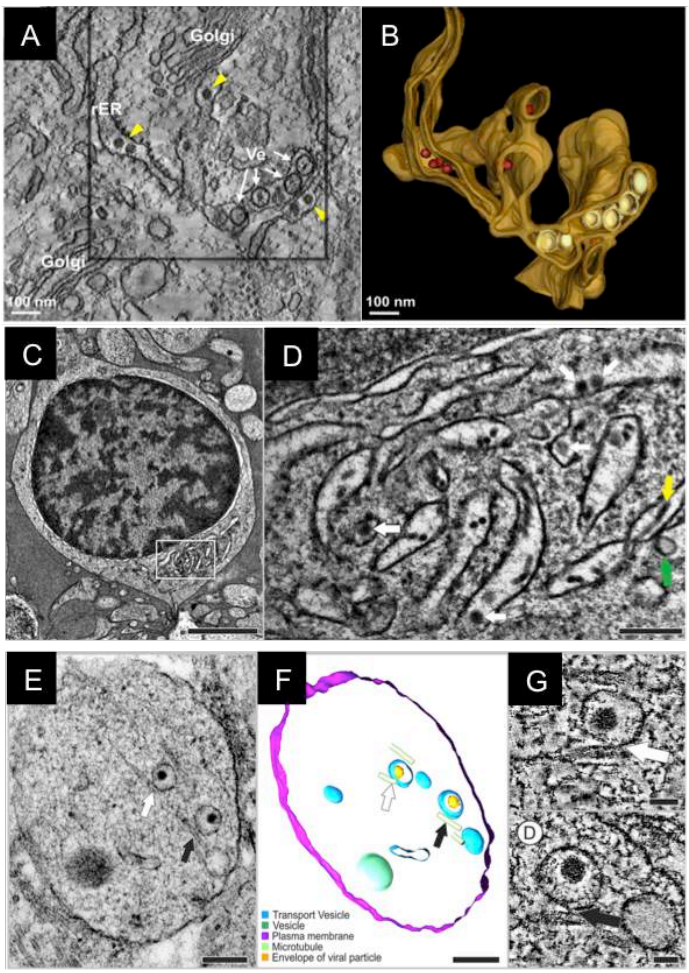

Figure 1.4 - Ultrastructure of TBEV-induced membrane alterations. (A) Electron Tomography of BHK-21 cells infected with TBEV. Vesicles (Ve) and virions (yellow arrowheads) were observed in the lumen of the rough ER. (B) 3D reconstruction of the tomogram displaying the TBEV-induced vesicles (in light yellow) in the lumen of the ER (in light brown), as well as virions (in dark red). Figure A and B are adapted from Miorin et al. 2013. (C) Human neurons infected with TBEV for 3 days displaying RER rearrangements. (D) Detail of the boxed region in (C) shows the RER containing viral particles, virus-induced vesicles (green arrow), and tubule-like structures (yellow arrow). (E) Two vacuoles that accommodated TBEV particles in a neuronal extension at 12 days after infection. Arrows indicate connections between vacuoles and microtubules. (F) 3D model. (G) Details of the connection. Figures C-G are adapted from Bílý et al. 2015.

1.3.7 Virion assembly and maturation

Virion assembly occurs in association with ER membranes, then budding occurs in the lumen of the ER and virions are transported via the secretory pathway and released at the cell surface (Jason M Mackenzie and Westaway 2001). At the earlier step E and prM proteins are associated as heterodimers through their C-terminal transmembrane anchors. The highly basic C protein interacts with the RNA viral genome in the cytoplasm and forms the nucleocapsid precursor that acquires an envelope by budding into the ER lumen. The maturation of the virus occurs in the trans-Golgi network (TGN) and includes the glycan modification of E and prM and the cleavage, by the host enzyme Furin, of prM. This cleavage renders the mature virion ready for acid-catalysed rearrangements of E required for productive entry (Figure 1.5) (Mukhopadhyay, Kuhn, and Rossmann 2005; Lindenbach, Thiel and Rice 2007).

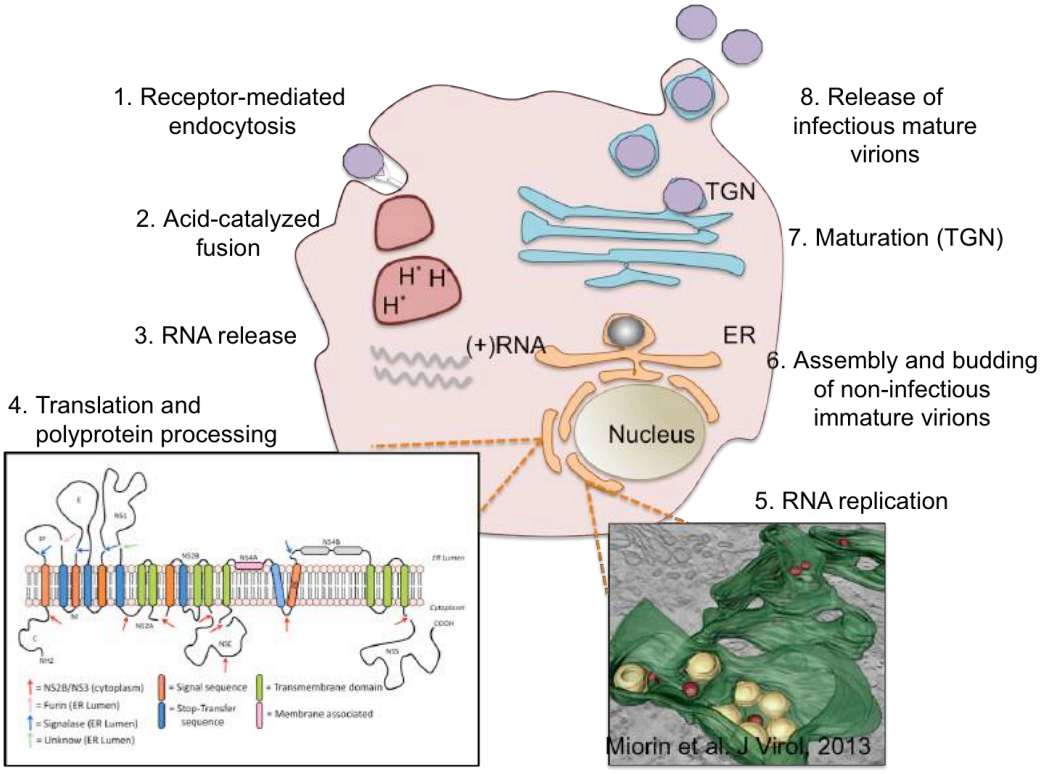

Figure 1.5 - Flavivirus Life Cycle. Flaviviruses are internalized by receptor-mediated endocytosis and trafficked to early endosomes, where the acidic environment induces fusion between the virus and the host membrane resulting in genome release. The genome is then translated and replicated. Packaging of newly synthesized RNA genomes occurs on the surface of the ER. The immature virions are transported to the trans-Golgi where Furin-mediated cleavage of prM to M generates mature infectious particles that are released by exocytosis.

1.4 Pathogenesis of Flavivirus

The major human pathologies caused by Flaviviruses can be grouped into encephalitis and haemorrhagic diseases. Interestingly, recent reports suggest that Zika virus infection of pregnant women might correlate with microcephaly in foetuses (Mlakar et al. 2016).

The host cells targeted by flaviviruses include monocytes, macrophages and dendritic cells (DC). After the inoculation of the virus in the host by the bite of an infected mosquito or tick, the virus undergoes replication in the local tissues. The host cells targeted by flaviviruses include monocytes, macrophages and dendritic cells (DC). Then the virus migrates to the lymph nodes where it further replicates in monocyte resulting in a primary viremia. From the lymphoid system the virus can spread into the body of the host and infect peripheral tissues like the spleen or kidneys. After this peripheral amplification the virus can enter the circulation and cross the blood-brain barrier (BBB) and enters the central nervous system (CNS) (King et al. 2007; Ye et al. 2013).

Human infections are usually asymptomatic. A low percentage (probably lower than 1%) of individuals shows clinical signs of infection, with symptoms ranging from general malaise to mild fever and headache and these individuals recover without sequelae. In some cases the symptoms can be more severe and the patients develop encephalitis and haemorrhagic disease. Children and the elderly, as well as those with debilitating chronic illness or immunosuppression (Caracciolo et al. 2015; Chmelík, Chrdle, and Ruzek 2016) are statistically at greatest risk of disease and death.

1.5 Immune response to Flavivirus

To detect, contain and clear viral infection, mammalian cells have evolved two self-defence mechanisms: innate immune response and the acquired immune response. The innate immune response offer the first protection against pathogens and is mediated by germline-encoded pattern recognition receptors (PRRs) that senses viral RNA, as retinoic acid-inducible gene I (RIG-I), Toll-like receptors 3 and 7 (TLR3 and TLR7) and melanoma differentiation associated gene 5 (MDA5). Acquired immunity is instead implicated in pathogens clearance during the late phase of infection and involves lymphocytes T and B expressing antigen-specific receptors.

The innate immune response to viral infection involves two phases: in the early phase PRRs detect specific pathogen-associated molecular patterns (PAMPs) triggering cytokine production including pro-inflammatory cytokines and type I interferons (IFNs), whereas in the late phase occur the IFN signalling that induce the expression of the interferon stimulated genes (ISGs) (Yoneyama and Fujita 2009).

1.5.1 RIG-I like receptors

The RIG-I like receptors (RLRs) belong to the DExD/H-box helicases family and sense viral RNA in the cytoplasm of infected cells. The RLR family is composed of three members: the retinoic acid-inducible gene I product RIG-I, melanoma differentiation-associated antigen 5 (MDA-5) and laboratory of genetics and physiology 2 (LPG2) (Kang et al. 2002; Yoneyama et al. 2005). RLRs are expressed in most cells of the human organism where they play a crucial role in antiviral responses, except in pDCs where for this function the TLRs are indispensable (Kato et al. 2005).

All RLRs proteins share structural and functional similarities. Their primary structure can be divided into three basic domains: the N-terminal domain consisting of two tandem caspase activation and recruitment domain (CARD), the central DExD/H box RNA helicase domain that hydrolyse ATP and bind and unwind RNA and a C-terminal repressor domain (RD) (Figure 1.6). The CARD domain of RIG-I and MDA5 is essential for the interaction with the CARD domain of IPS-1, also called MAVS, and thus for the downstream signalling. LGP2 lacks the CARD domains and therefore is unable to signal through MAVS (Yoneyama et al. 2005). However, it has been proved that LGP2 acts as a positive regulator of RIG-I and MDA5 viral sensing (Satoh et al. 2010).

Figure 1.6 – Schematic representation of the RLRs and their adaptor IPS-1. Key structural domains involved in signaling are shown. The RLRs consist of CARD (caspase activation and recruitment domain) domain; ATPase containing DEAD box helicase (DEAD helicase); and a C-terminal domain (CTD) that in RIG-I and LGP2 but not MDA5 encodes a repressor domain (RD) involved in autoregulation. LGP2 lacks the N-terminal CARDs. IPS-1 consists of a homologous CARD, a proline-rich region (Pro), and a transmembrane domain (TM) on its C terminus. Figure from Loo and Gale 2011.

1.5.2 Retinoic acid-inducible gene I (RIG-I)

RIG-I was originally identified as activator of IRF-regulated reporter gene expression when co-transfected with PolyI:C (PIC) (Yoneyama et al. 2004). In particular, Yoneyama and colleagues demonstrated that the CARD domains are responsible for the downstream signalling cascade. Further studies have identified that the C-terminal domain contains a ssRNA/dsRNA binding sites that when unbound functions as a repressor domain (RD), inhibiting RIG-I activation in the absence of viral stimulation (Saito et al. 2007).

It has been demonstrated that RIG-I binds preferentially RNA sequences marked with a 5'-ppp end (Hornung et al. 2006). Subsequently, next-generation sequencing of RNA derived from RIG-I-bound RNA complexes isolated from influenza virus-infected cells confirmed that RIG-I associates preferentially with short 5'ppp-RNA sequence motifs and RNA containing dsRNA regions but that full-length genomes of RNA viruses are not bound by RIG-I (Baum, Sachidanandam, and Garcia-Sastre 2010). More recently it has been also demonstrated that RIG-I is capable to react to incoming viral nucleocapsid containing 5'ppp dsRNA structures of negative-strand RNA virus (Weber et al. 2013). This last observation suggests that RIG-I can recognize a wider set of viral RNA structures than what it was thought before.

In the absence of an RNA ligand RIG-I is held in a closed conformation in which the CARD domain function is repressed due to interaction between the CTD and the helicase region. When viral infection produces short dsRNA or 5'ppp-RNA, these oligonucleotides bind the CTD in the presence of ATP and RIG-I changes its conformation and unmasks the CARD domains. CARD is able to interact with other CARD domains to form the RIG-I oligomers (Takahasi et al. 2008), or to the CARD domain of its adaptor protein IPS-1 and start the signaling cascade that induce IFN production (Figure 1.7).

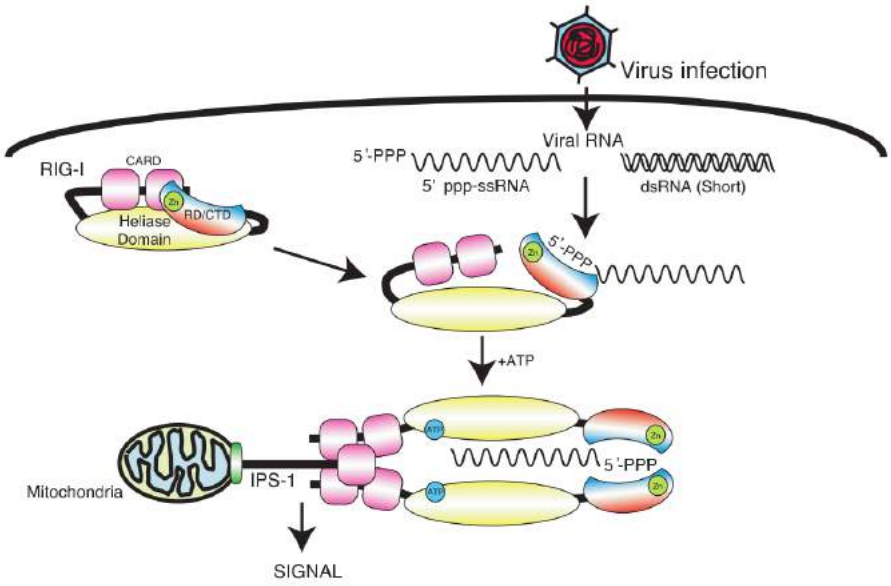

Figure 1.7 – RIG-I activation and conformational changes. In absence of viral infection, RIG-I is inactivated by intramolecular interaction between C-terminal repressor domain (RD) and caspase recruitment domain (CARD) or linker region of helicase domain. When viral RNA is released in the cytoplasm of infected cells, RIG-I selectively detects these non-self-RNAs via the C-terminal domain (CTD) and induces ATP-dependent conformational change to form a dimer or an oligomer, which allows CARD to interact with the downstream adapter protein IPS-1. Figure from Yoneyama and Fujita 2009.

1.5.3 RIG-I signalling pathway

Upon activation, RIG-I, but also MDA5, interacts with its adaptor protein IPS-1 (interferon-β promoter stimulator 1), also called mitochondrial antiviral signalling (MAVS), virus-induced signalling adaptor (VISA) and CARD adapter inducing IFN-β (Cardif). The interaction occurs through the association of the CARD domains. Indeed,

IPS-1 contains a N-terminal single CARD domain and a proline-rich region (PRR) and a transmembrane domain (TM) at its C-terminal end that localize the protein on the outer membrane of mitochondria, suggesting a critical function of mitochondria as a platform for RLR-mediated signalling (Figure 1.6) (Yoneyama and Fujita 2009). The interaction leads to the recruitment of downstream signalling molecules. In particular, IPS-1 associates with the tumor necrosis factor (TNF) receptor-associated factor (TRAF) 3 leading to TBK1 and inhibitor of kB kinase (IkB) ε (IKKε) activation and subsequent IRF3 phosphorylation. Alternatively, IPS-1 recruits the adaptor Fas-associated death domain (FADD) and the kinases receptor-interacting protein 1 (RIP1) in order to trigger the NF-kB pathway. Upon activation, IRF3 and NF-kB translocate to the nucleus to drive type I IFN transcription and subsequent induction of the antiviral state (Figure 1.8) (Yoneyama and Fujita 2009).

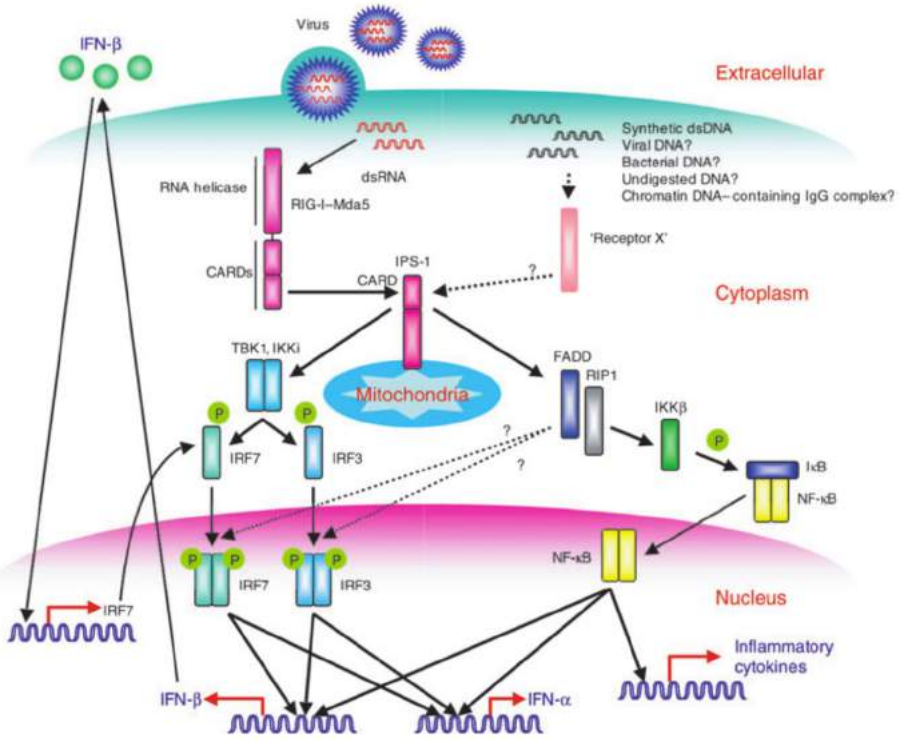

Figure 1.8 – RIG-I-like receptors signaling cascade. Signaling pathway triggered by RIG-I, Mda5 and DNA. Viruses entering the cytoplasm produce dsRNA during replication. RIG-I and Mda5 recognize dsRNA to initiate antiviral signaling. IPS-1 interacts with RIG-I and Mda5 via the CARD-like domain, followed by the activation of IRF3 and IRF7 via TBK1- and IKKi-dependent phosphorylation (P). IPS-1 also activates NF-|B via FADD- and RIP1-dependent pathways. These pathways coordinately activate type I interferon promoter. Synthetic dsDNA also activates an IPS-1-dependent pathway, although a receptor responsible for DNA recognition has not been identified. It is possible that such a putative sensor would recognize bacterial DNA, viral DNA, undigested DNA and chromatin DNA–containing immunoglobulin G (IgG) complexes. Figure from Kawai and Akira 2006.

1.5.4 Type I IFN system

Type I IFN is a critical cytokine for antiviral innate immunity (Samuel 2001). Since they are induced by viral infection, type I IFNs are also known as viral IFNs and include: IFN-α (produced mainly in leukocyte), IFN-β (produced mainly in fibroblast), and IFN-ϖ.

Most types of infected cells, in cell culture, are able to synthesize both IFN-α and IFN-β. The large number of type I IFN genes in humans include: 13 IFN-α genes, 1 IFN-β gene, and 1 IFN-ϖ gene. It is not known why there are so many IFN-α genes. A mice KO for IFN-β gene is highly susceptible to viral infection suggesting that IFN-α is not able to compensate the loss of IFN-β that has an essential role for antiviral response (Deonarain et al. 2000).

Once that the RLR-signalling pathway induce the expression of IFNα/β, a secondary signalling pathway is induced in an autocrine or paracrine manner and is called IFN receptor-mediated secondary signal. The receptor-mediated secondary signal starts from the interaction of the expressed IFNs with the heterodimeric IFNα/β receptors (IFNAR), which are broadly expressed in the majority of cells. This interaction triggers the activation of the Jak-STAT transduction pathway that induce the expression of hundreds of IFN-inducible genes (ISGs), like double-stranded RNA-dependent protein kinase (PKR), 2'-5'-oligoadenylatesynthetase (2'-5'-OAS), adenosine deaminase and guanosine triphosphatase (GTPase) that all together establish a strong antiviral activity (Figure 1.9) (Yoneyama and Fujita 2009).

In addition to these mechanisms, to establish the antiviral state, type I IFNs have a role in the regulation of innate and adaptive immunity. It has been shown that IFNs regulate natural killer (NK) cells and cytotoxic T cells (CTLs) and also it has been shown to facilitate cross-presentation by DCs of viral antigens to $CD8^+$ T cells (Stetson and Medzhitov 2006).

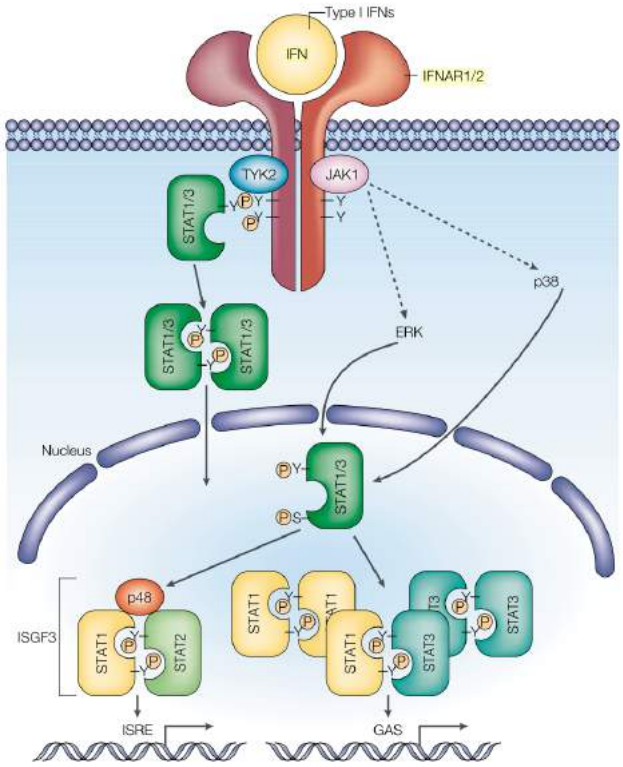

Figure 1.9 – IFNAR signaling cascade. Binding of type I IFN to the IFN-a/b receptor activate the JAK–STAT pathway. The activation of Tyk2 and Jak1 kinase results in the generation, phosphorylation and assembly of the trimeric ISGF3 transcription factor complex, which consists of a STAT1-STAT2 heterodimer and IRF9 (p48). This complex translocates to the nucleus, binds to IFN-stimulated response elements (ISRE) and induces ISGs production. Figure from Katze, He, and Gale 2002.

1.5.5 Evasion to the interferon system by viruses

To establish infection and replication in the hosts, Flaviviruses have evolved a variety of strategies to modulate the host's immune responses. These strategies can be summarised in five main activities, as reviewed in Ye et al. 2013:

- delaying PRR detection: it has been shown that during replication TBEV form intracellular membrane structures in order to hide viral dsRNA and delay IFN production (Overby et al. 2010; Miorin et al. 2012; Miorin et al. 2013);
- inhibiting the transcription of IFN genes: it has been shown that during WNV (Wilson et al. 2008) and TBEV infection (Miorin et al. 2012; Overby et al. 2010), IRF3 nuclear translocation is inefficient;

- suppressing IFN signalling: several non-structural proteins of flaviviruses have been shown to suppress the activity of downstream molecular key component of the IFN receptor-mediated secondary signal, for example by inhibiting the phosphorylation and the subsequent nuclear translocation of STAT1, suggesting a common mechanism for mosquito-borne flaviviruses (Munoz-Jordan et al. 2005);
- directly affecting the function of antiviral ISGs: for example the 2'-O-methylation of the 5' cap of WNV RNA modulates the effect of IFIT that during infection interact with eIF3 and limits the translation of viral mRNA (Daffis et al. 2010).
- regulating antiviral responses through the sfRNA. The sfRNA of DENV-2 has been shown to bind and prevent TRIM25 deubiquitination which is critical for RIG-I-induced type I interferon expression (Manokaran et al. 2015).

1.6 Stress Response to viral infection

1.6.1 Integrated Stress Response

The Integrated Stress Response (ISR) is a signalling program common to all eukaryotes that enable cellular adaptation to several type of cellular stress, like hypoxia, nutrient deprivation, ER stress or viral infection (Harding et al. 2003).

The ISR is designed to limit global translation and it is characterized by the phosphorylation of the initiation of translation factor eIF2α at Ser51. This phosphorylation is performed by four different kinases that are activated by different stress:

- PERK, a transmembrane protein of the ER, is sensing the stress of the ER due to accumulation of unfolded proteins. PERK is also a key regulator of the unfolded protein response (see section 1.7.3);
- GCN2 (general control non-derepressible 2), senses low amino acids levels by binding to uncharged tRNAs;
- HRI (heme-regulated inhibitor kinase), is mainly expressed in erythrocytes and is activated by heme deficiency;

- PKR (double stranded RNA activated protein kinase) is ubiquitously expressed and is activated by sensing dsRNA, playing an important role in antiviral immunity.

Upon activation, all four kinases phosphorylate eIF2α leading to an inhibition of translation of cellular mRNAs that are redirected from polysomes to discrete cytoplasmic foci known as stress granules (SG).

1.6.2 Stress Granules

Stress granules, as well as processing bodies (PB), are ribonucleoprotein granules found in the cytoplasm of cells in response to many types of environmental stress such as oxidative stress, heat shock, or viral infection. SG and PB are dynamically connected to regulate the translation repression and decay of host mRNA (Anderson and Kedersha 2006).

Upon activation of one of the cellular kinases involved in the integrated stress response the α subunit of the eukaryotic translation initiation factor 2 (eIF2α) is phosphorylated, a modification that blocks the eIF2-GTP-Met-tRNAi^{Met} ternary complex that in normal condition load tRNAi^{Met} onto the small ribosomal subunit to initiate protein synthesis. When eIF2α is phosphorylated the GTP/GDP exchange factor eIF2B is not able to convert the ternary complex in the active form, inhibiting the protein translation. In this case, an eIF2/eIF5-deficient stalled 48S preinitiation complex is formed and together with the associated mRNAs, the T-cell restricted intracellular antigen-1 (TIA-1) and TIA-1 related protein (TIAR) gives rise to the formation of SG complex which in turn results in global protein synthesis inhibition (Kimball et al. 2001; N. Kedersha et al. 2002) (Figure 1.10).

Recent studies have further demonstrated that SGs are composed also by other translation factors like eIF3, eIF4G and eIF4E as well as the polyA binding protein (PABP) and HuR and G3BP1 among others (Kedersha et al. 1999; Kedersha et al. 2002; Tourrière et al. 2003).

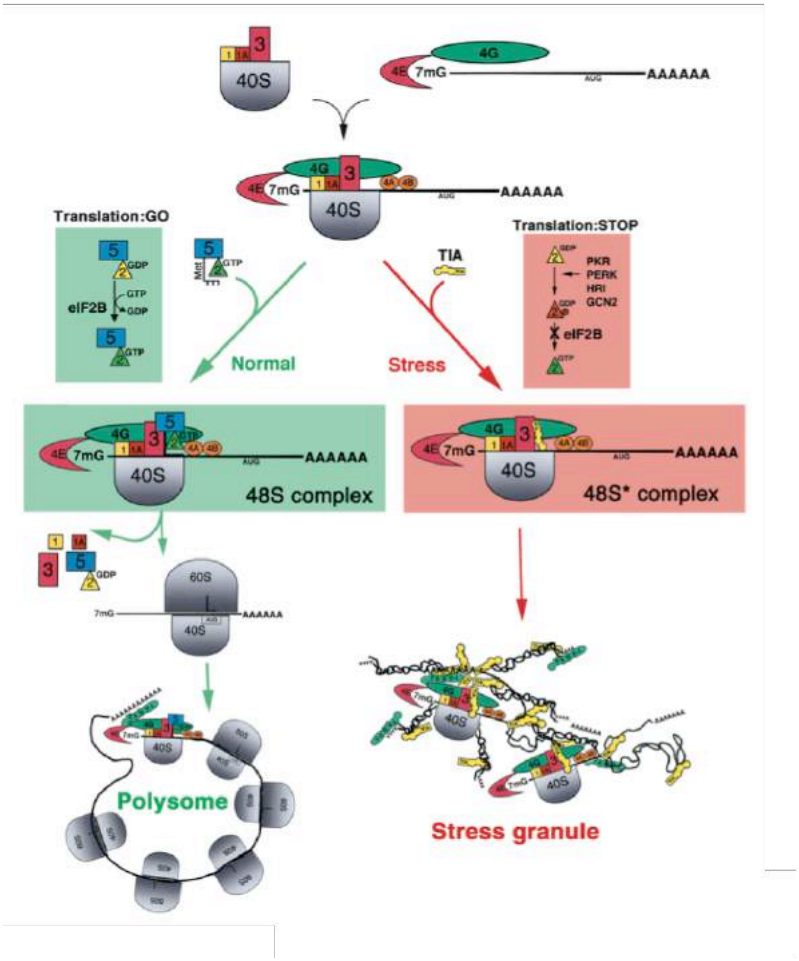

Figure 1.10 - Stress Granules assembly. In the absence of stress, eIF2B promotes the charging of the eIF2-GTP-tRNA^{Met} ternary complex by exchanging GDP for GTP. When the eIF2-GTP-tRNA^{Met} ternary complex is available, a canonical 48S preinitiation complex is assembled at the 5' end of capped transcripts and ribosomal scanning begins (left part of the figure). Upon recognition of the initiation codon by the anticodon of tRNAMet, eIF5 promotes GTP hydrolysis, and early initiation factors are displaced by the 60S ribosomal subunit. As additional ribosomes are added to the transcript, the mRNA is converted into a polysome. In stressed cells, phosphorylation of eIF2α by PKR, PERK, HRI or GCN2 converts eIF2 into a competitive antagonist of eIF2B. Under these conditions TIA-1 is included in a non-canonical eIF2/eIF5-deficient 48S* preinitiation complex that is translationally silent. TIA-1 self-aggregation then promotes the accumulation of these complexes at discrete cytoplasmic foci known as stress granules. Blue square, eIF5; green triangle, eIF2 bound to GTP; yellow triangle, eIF2 bound to GDP; red triangle, phospho-eIF2 bound to GDP. Picture from (Anderson and Kedersha 2002).

1.6.3 Stress Granules and Flaviviruses

Several viruses can manipulate the cellular components of the SG and regulate their formation, indeed, translational shutoff of cellular proteins is a common strategy to benefit viral protein translation, a process that gives the advantage to the virus to replicate faster and to avoid the production of antiviral cellular protein, but at the same time could be disadvantageous for example for RNA viruses that exploit the cellular translation machinery for their replication.

It is known that some viruses induce the formation of SG, for example Respiratory Syncytial virus (RSV), whereas other viruses, for example WNV as well as Rotavirus among others, do not induce SG formation (Emara and Brinton 2007; Lindquist et al. 2010).

Regarding flaviviruses, it has been demonstrated that T-cell restricted intracellular antigen-1 (TIA-1) and TIA-1 related protein (TIAR), both key proteins in stress granules assembly, interact with the 3'SL of WNV complementary minus-strand RNA that is the site of initiation of RNA synthesis. By binding to this structure the proteins facilitate the viral replication, indeed the authors measured a reduced WNV RNA amplification in TIAR knockout fibroblasts (Li et al. 2002). Another report shows that during WNV and DENV infection, both TIA-1 and TIAR are sequestered, at different time of infection, at sites of viral replication and thus SG formation is reduced, suggesting that these viruses interferes with SG assembly by hijacking the cellular localization of SG proteins (Emara and Brinton 2007). Furthermore, a recent study shows that JEV core protein recruits several SG-associated proteins, including G3BP1 and USP10, through an interaction with Caprin-1, another RNA binding protein involved in SG assembly (Katoh et al. 2013). In the same study, Katoh and colleagues, demonstrated that a mutant JEV carrying a core protein incapable of binding to Caprin-1 exhibited lower propagation in vitro and lower pathogenicity in mice than the wild-type JEV, suggesting that inhibition of SG formation by the core protein is crucial to antagonize host defence (Katoh et al. 2013). All together these results suggest a common strategy of flaviviruses to prevent the inhibition of viral mRNA translation and to enhance RNA synthesis.

Due to these evidences it has always been wrongly assumed that Flaviviruses belongs to that group of viruses unable to trigger SG formation. Recently, the group of Brinton reinterpreted their own data, this time looking at G3BP1 as a marker for SG, showing that natural WNV genotypes, such as Eg101, induces SG less efficiently than

the lineage 2/1 chimeric WNV infectious clone W956IC, which produces high levels of early viral RNA (Courtney et al. 2012). More recently we have demonstrated (Albornoz et al. 2014) that, in agreement with Emara and colleagues studies, TIA-1 and TIAR proteins are recruited to sites of TBEV replication, binding the viral RNA and inhibiting its translation, but also that TBEV is able to trigger the formation of SG containing other SG markers as G3BP1, eIF3 and eIF4B. Moreover, in 2012, the group of Bartenschlager demonstrated that HCV infection is able to induce oscillatory formation of SG in Huh7 cells stimulated with IFNα (Ruggieri et al. 2012).

Taken together all these evidences suggest that flaviviruses are indeed capable of inducing SG formation in infected cells.

1.6.4 Antiviral-Stress Granules

As mentioned above, viral infection can trigger the integrated stress response through activation of the kinase PKR that by phosphorylating the initiation of translation factor eIF2α is inducing formation of SG and the subsequent global inhibition of translation. Depending on both the virus and the host cell, different pattern of SG formation have been observed during infection: stable SG formation, no SG formation, transient SG formation and oscillating SG formation as reviewed in Onomoto et al. 2014.

In some cases have been demonstrated that viruses are able to inhibit SG formation. For example the NS1 protein of Influenza A virus (IAV) has been shown to inhibit eIF2α phosphorylation by blocking PKR activation (Onomoto et al. 2012). In the case of JEV infection, SG formation is inhibited by direct interaction of the viral Core protein with Caprin1, a component of SG (Katoh et al. 2013). These data leads to the hypothesis that SG have an antiviral role and for this reason viruses have developed strategies to suppress their formation. Moreover, Onomoto and colleagues demonstrated that the RLRs MDA5 and RIG-I localizes to IAV-induced SG, together with PKR and viral RNA. Moreover they demonstrated that inhibition of SG formation during IAV infection, by silencing of the G3BP1 SG protein, reduce the expression of IFN-β. Their pioneer work suggests that these viral-induced SG, that they termed antiviral SG (avSG), may act as a platform for viral RNA sensing and activation of IFN response (Onomoto et al. 2012).

In figure 1.11 is shown the model that Onomoto and colleagues proposed for avSG.

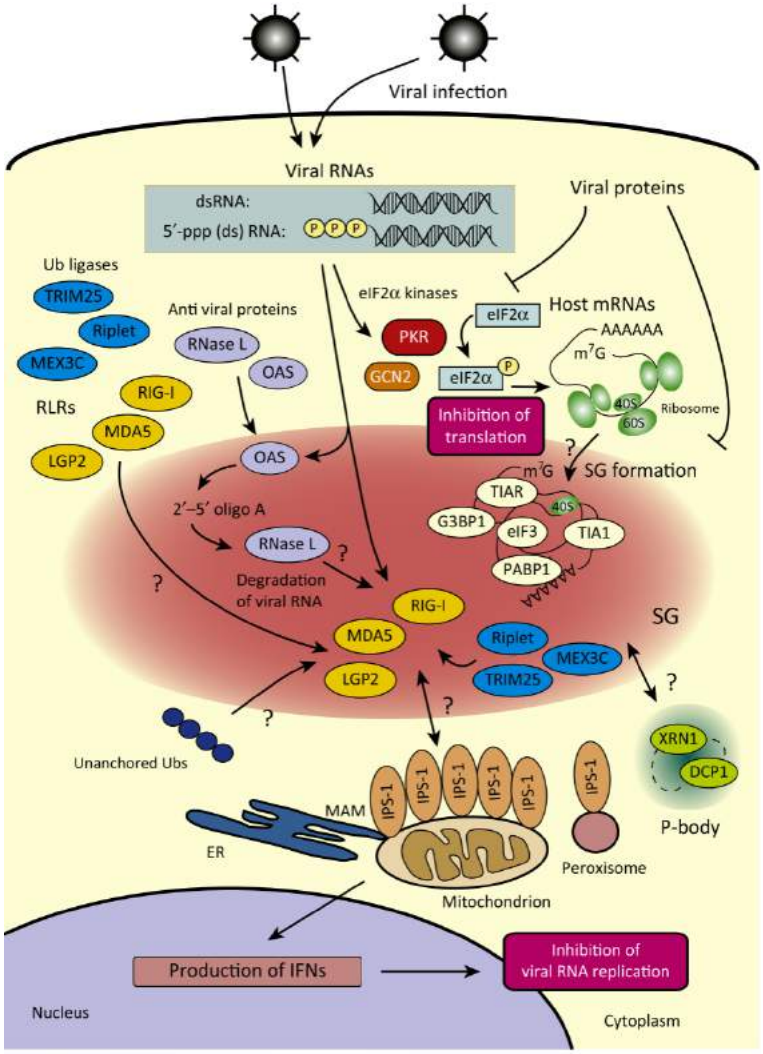

Figure 1.11 - A model for antiviral function of stress granules. In virus-infected cells, viral RNAs activate PKR that by phosphorylation of eIF2α initiate the assembly of SG. eIF2α phosphorylation blocks translation of cellular mRNAs that are accumulated in SG or transferred to P-bodies for degradation. Viral RNAs are also recognized by RLRs, which are recruited to SGs with several signaling molecules including antiviral proteins and ubiquitin ligases. The OAS–RNase L pathway cleaves viral RNAs, and the cleaved RNAs may act as ligands for RLRs. IPS-1, which is localized on mitochondria and/or MAM (Mitochondria-Associated ER Membranes), forms prion-like aggregates, interacts with RLRs on SGs, and activates IFN-inducing signaling. Areas that require further investigation are highlighted with question marks. Figure from Onomoto et al. 2014.

1.7 The Unfolded Protein Response

Intracellular perturbations caused by a variety of stressors, like hypoxia, glucose deprivation, defective calcium regulation and viral infection, can induce endoplasmic reticulum (ER) stress, leading to accumulation of misfolded proteins into its lumen (Kaufman 2002; Chakrabarti, Chen, and Varner 2011). Normally, cells ensure a proper protein folding using combination of chaperons, foldases and lectins, but when ER stress is affecting the folding process, two are the possible cellular response: degradation of the incorrectly folded proteins trough the ER Associated Degradation pathway (ERAD) or activation of the Unfolded Protein Response (UPR) (Chakrabarti, Chen, and Varner 2011).

In mammalian cells, the UPR is a complex signalling program mediated by three ER transmembrane receptors:

- Activating transcription factor 6, ATF6;
- Inositol requiring kinase 1, IRE1;
- Double-stranded RNA-activated protein kinase (PKR)-like endoplasmic reticulum kinase, PERK.

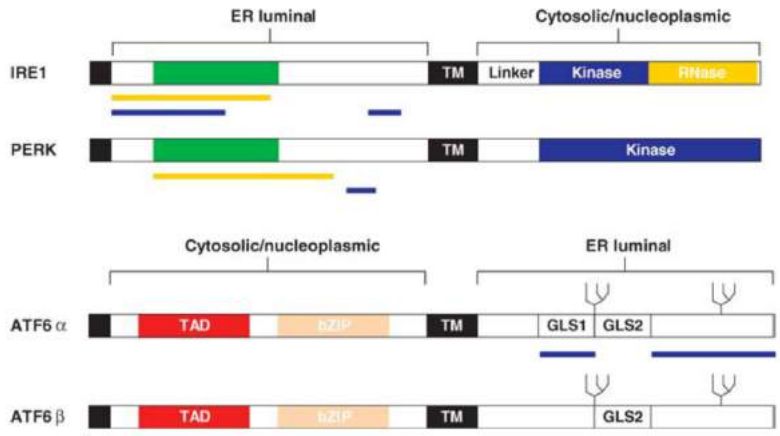

Figure 1.12 – Schematic representation of the structure of the ER stress sensors. Yellow bars represent regions sufficient for signal transduction or oligomerization. Purple bars represent regions interacting with BiP. The black boxes represent the signal peptides, and the green boxes depict the region of limited homology between IRE1 and PERK. Both IRE1 and PERK display a kinase domain in the cytosolic part (in blue). The RNase domain of IRE1 is indicated in yellow. bZIP, basic leucine zipper; GLS1 and GLS2, Golgi localization sequences 1 and 2; TAD, transcriptional activation domain; and TM, transmembrane domain. Figure from Schröder and Kaufman 2005.

UPR performs three functions: adaptation, alarm and apoptosis. Activation of the Unfolded Protein Response results in an initial adaptation, where the UPR tries to reestablish the normal protein folding processes by enhancing transcriptional synthesis of chaperones and enzymes required for protein folding. Simultaneously, translation is attenuated, to reduce the load of proteins at the ER level, and degradation of the misfolded proteins is increased. If these procedures of crisis containment fail, the UPR induces a cellular alarm that involves several signal transduction events that lead to the activation of an apoptosis program.

The three UPR pathways are regulated by the chaperone protein BiP (Binding immunoglobulin Protein), also known as HSPA5 or GRP78, a member of the HSP70 family. BiP is located in the ER lumen and binds newly synthesized proteins to help in their folding. This chaperon protein consists in an N-terminal ATPase domain and a C-terminal peptide-binding domain (Gething 1999). Unfolded or misfolded protein binding stimulates the N-terminal ATPase activity of BiP resulting in ATP hydrolysis that strengthens BiP affinity for the hydrophobic motifs of unfolded peptide (Gething 1999). Normally, BiP is bound to the transmembrane ER stress transducers PERK, ATF6 and IRE1, blocking their activation. However, in the presence of exposed hydrophobic residues BiP disassociates, allowing activation of these UPR regulatory proteins.

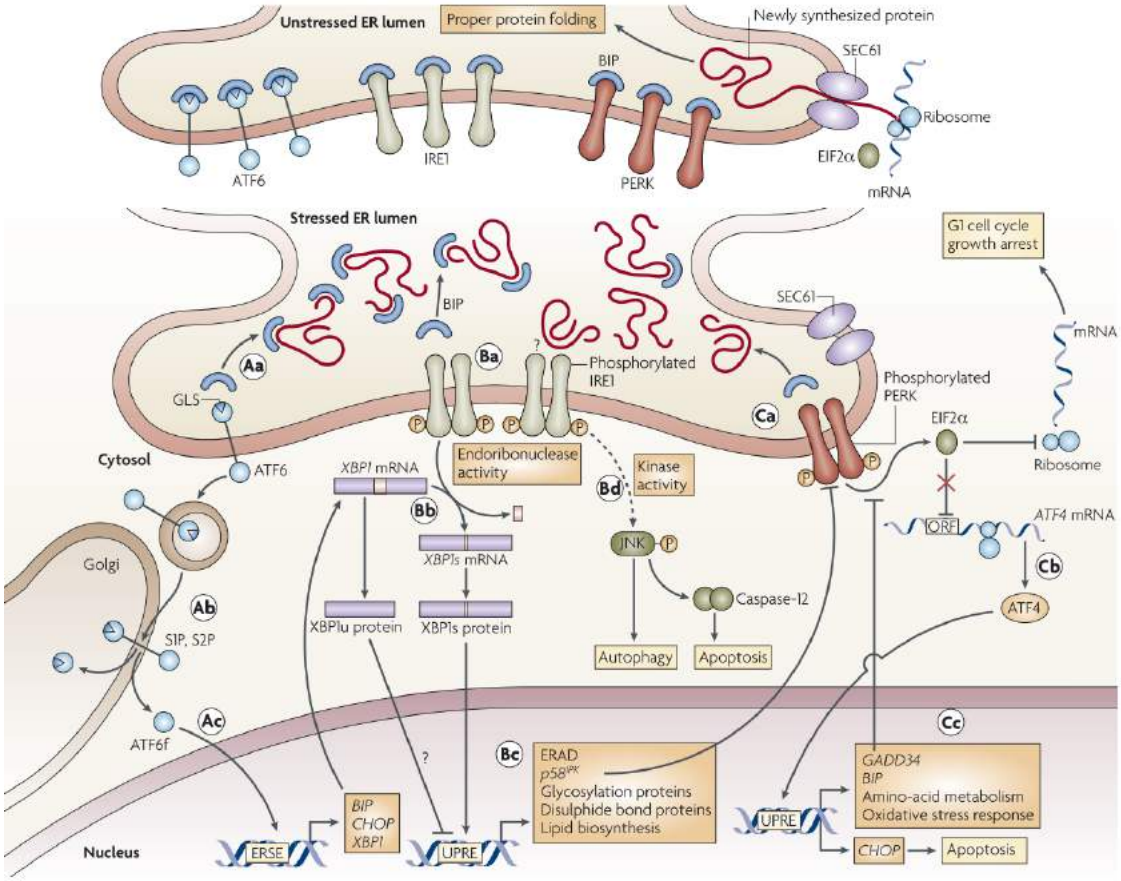

Figure 1.13 – Schematic representation of the three main UPR pathways. In the presence of unfolded polypeptides BiP dissociates from the UPR sensors PERK, ATF6 and IRE1 causing their activation. Through phosphorylation or proteolytic cleavage of the three sensors are activated, leading to phosphorylation of elF2α (impairing translation), splicing of Xbp1 and translocation of resulting transcription factors to the nucleus to boost transcription of UPR genes. Picture from Todd, Lee, and Glimcher 2008.

1.7.1 ATF6

ATF6 is a 90 kDa type II transmembrane protein encoding a basic leucine zipper (bZIP) transcription factor in its cytosolic domain. Two homologous proteins, ATF6α and ATF6β exist in mammals. The ER-luminal domain of ATF6 contains two independent and redundant Golgi localization sequences, GLS1 and GLS2, which are masked by the binding of BiP (Figure 1.12) (Schröder and Kaufman 2005). Following BiP dissociation, ATF6 is transported to the Golgi where the proteases S1P and S2P remove the luminal and the transmembrane domain, respectively. The resulting 50 kDa N-terminal cytoplasmic fragment (ATF6f) is a DNA-binding protein that translocates to

the nucleus where it activates the transcription of UPR target (Figure 1.13) (Chen, Shen, and Prywes 2002). Although ATF6α participates in the induction of various UPR target genes, ATF6β seems to have a minimal role in the UPR. The main targets of ATF6f are the ERSE (ER stress response element) which control the expression of ER-localized molecular chaperons like BiP, PDI and GRP94 and XBP1, providing a feed-forward strategy to augment the IRE1 axis of the UPR. Moreover, ATF6f can form heterodimers with XBP1 that can bind to the cis-acting UPRE (Unfolding Protein Response Elements), located in the promoters of several components of the ERAD system (Walter and Ron 2011; Todd, Lee, and Glimcher 2008).

1.7.2 IRE1

IRE1 is a 110 kDa type I ER transmembrane protein that exists in 2 isoforms, IRE1α and IRE1β. While IRE1α is ubiquitously expressed, IRE1β expression is limited to gut epithelial cells. Among the UPR regulators, IRE1 is the most conserved and the only one presents in lower eukaryotes. IRE1 consists in an ER-luminal dimerization and cytosolic serine/threonine kinase and endoribonuclease domains (Figure 1.12) (Schröder and Kaufman 2005). After BiP dissociation, IRE1 oligomerize and trans-phosphorylate other IRE1 molecules in the complex. It has been demonstrated that activation of IRE1 can occurs also by direct binding of unfolded proteins by a peptide-binding pocket present in the luminal domain of the transmembrane protein (Walter and Ron 2011).

The IRE1-mediated kinase activity has yet to be fully elucidated. Activated IRE1 bind to the tumor-necrosis factor (TNF)-receptor-associated factor 2 (TRAF2) that promotes activation of JUN N-terminal kinase 1 (ASK1) through apoptosis signal-regulating kinase 1 (ASK1), allowing cells to initiate autophagy or promoting apoptosis (Todd, Lee, and Glimcher 2008) (Figure 1.13).

The IRE1 endoribonuclease activity is better understood. Activated IRE1 performs a non-conventional cytoplasmic splicing, excising a 26-nucleotide sequence from XBP1 (X-box-binding protein 1) mRNA (Yoshida et al. 2001). This splicing event causes a shift in the reading frame of XBP1 mRNA generating a new longer protein called XBP1s (spliced form) that possess a transcriptional trans-activation domain in its C-terminal region. Once translated, XBP1s translocates to the nucleus where it binds to UPR elements (UPRE) on the promoter of several UPR target genes encoding for

enzymes involved in protein folding or disposal, as ER-associated degradation (ERAD) protein EDEM-1 and ER-localised chaperons such as DNAJB9 and DNAJC3 (Figure 1.13). Moreover, it has been demonstrated that XBP1s regulates lipid biosynthesis and ER biogenesis (Sriburi et al. 2004; Todd, Lee, and Glimcher 2008), indeed, its overexpression is sufficient to induce phospholipids biosynthesis and trigger the expansion of the ER.

The specific splicing of XBP1 mRNA was considered the only RNase activity of IRE1α but it has then been shown that IRE1 can mediates the rapid degradation of a specific subset of mRNAs that are targeted to the ER for translation and that localize in proximity to IRE1. This activity was termed Regulated IRE1-Dependent Decay (RIDD) and thought to help relieves ER stress by diminishing protein translation (Hollien and Weissman 2006). Moreover it has been shown that IRE1 through its RIDD activity is involved in the cellular immune response. Indeed, the exonuclease domain of IRE1 shows similar catalytic mechanisms of the protein RNaseL, which is able to produce RNA fragments that activate RIG-I. A recent report (Cho et al. 2013) showed that exposure of human intestinal cell lines with cholera toxins induces activation of RIDD activity that produce mRNA fragments that are then recognized by RIG-I leading to induction of the IFN response and production of inflammatory cytokine.

1.7.3 PERK

PERK is a 125 kDa type I transmembrane protein with an ER-luminal stress sensor domain and a cytosolic protein kinase domain (Figure 1.12). The PERK branch of the UPR transduces both pro-survival and pro-apoptotic signals but its main function is to modulate translation. Dissociation of BiP from the luminal domain initiates trans-phosphorylation of the kinase domain at T981 of other PERK molecules, promoting PERK oligomerization (Todd, Lee, and Glimcher 2008). The kinase domain of PERK phosphorylates also the α subunit of the eukaryotic translation initiation factor-2 (eIF2α) at Ser51, causing a global inhibition of translation, thus reducing also the amount of newly synthesized proteins (Harding et al. 1999; Harding et al. 2000). Interestingly, some mRNAs that contain an internal ribosome entry site (IRES) sequence in the 5' untraslated regions bypass the P-eIF2α translational block (Schröder and Kaufman 2005). The most known one encodes the transcription factor ATF4 that binds to UPR elements inducing the transcription of pro-survival genes involved in

amino-acid metabolism and oxidative stress response but also of pro-apoptotic genes as CHOP that lead to a controlled cell death if the stressed cells are not able to restore their homeostasis (Figure 1.13). Another direct target of ATF4 is the co-factor GADD34, which role is to recruits the serine/threonine-protein phosphatase PP1 to dephosphorylate the translation initiation factor eIF2α, thereby reversing the shut-off of protein synthesis initiated by stress-inducible kinases and facilitating recovery of cells (Novoa et al. 2001).

1.7.4 The Unfolded Protein Response in Flavivirus infections

As largely discussed previously the UPR is a cellular homeostatic response to an ER stress and it can be triggered also by viral infections. Increasing evidences suggest an intimate relationship between virus and the UPR. Indeed, if on one hand, the host activates the UPR in an attempt to restrict virus infection, on the other hand, the virus can manipulates the UPR to facilitate its own replication.

Since Flavivirus infection induce ER-derived membrane structures where it takes place the viral replication, is not surprising that Flavivirus infection induce ER stress and consequently activation of the UPR.

Several studies on members of the Flaviviridae family have documented the activation of one or more arms of the UPR. For instance, in OR6 cells, a genome-length HCV RNA replication system in Huh7 cells, all the three UPR signalling pathways are activated compared to control cells OR6c from which HCV genome had been removed by treatment with IFNα (Shinohara et al. 2013). In DENV infected cells the activation of the UPR arms follows a time dependent mechanism, with PERK activation and eIF2α phosphorylation during early stages of infection that rapidly switched off and with IRE1 and ATF6 upregulation occurring at later stages of the replication cycle (Peña and Harris 2011). Also for WNV, it has been shown that UPR is activated upon infection. Indeed Medigeshi and colleagues demonstrated ATF6 and IRE1 upregulation, as well as eIF2α phosphorylation and induction of CHOP and GADD34 (Medigeshi et al. 2007). More recently, it has been described that infection with WNV Kunjin (WNV_{KUN}), an attenuated strain of WNV, is activating only the ATF6 and IRE1 arms of the UPR and that the virus might regulate PERK activation to facilitate viral replication and preventing CHOP transcription (Ambrose and Mackenzie 2011). These data indicate a high variability in the stress responses induced by different flaviviruses. Also

TBEV has been shown to induce XBP1 splicing and ATF6 cleavage and nuclear translocation. In the same study they demonstrated that by inhibiting the UPR TBEV replication is impaired suggesting that the virus could manipulate this response to facilitate the infection (C. Yu, Achazi, and Niedrig 2013).

Finally, increasing evidences support an intersection between the UPR and inflammation, in particular the production of pro-inflammatory cytokines and type I IFN (Smith et al. 2008). These studies suggest that upon viral infection the UPR might serves as an intracellular "danger signal" alerting the cell about the infection and working in a synergic way together with the IFN response.

2 MATERIALS AND METHODS

2.1 Materials

2.1.1 Cells

Bacteria

- **MAX Efficiency DH10B Competent Cells** (Invitrogen – cat.num. 18297-010). Genotype: F^- mcrA Δ(mrr-hsdRMS-mcrBC) φ80lacZΔM15 ΔlacX74 recA1 endA1 araD139 Δ (ara, leu)7697 galU galK λ^- rpsL nupG /pMON14272 /pMON7124.
- **XL10-Gold Ultracompetent Cells** (Stratagene – cat.num. 200315). Genotype: Tet^r Δ(mcrA)183 Δ(mcrCB-hsdSMR-mrr)173 endA1 supE44 thi-1 recA1 gyrA96 relA1 lac Hte [F´ proAB $lacI^qZ\Delta M15$ Tn10 (Tet^r) Amy (Kanr)].
- **MAX Efficiency Stbl2 Competent Cells** (Invitrogen – cat.num. 10268-019). Genotype: F^- mcrA Δ(mcrBC-hsdRMS-mrr) recA1 endA1lon gyrA96 thi supE44 relA1 λ^- Δ(lac-proAB).

Mammalian Cells

- U2OS: Human osteosarcoma cell line (ECACC No. 92022711);
- Vero: African green monkey kidney (ECACC No. 84113001);
- U2OS_Flag-RIG-I: U2OS transduced with a lentivirus carrying Flag-RIG-I;
- U2OS_EGFP-ATF6: U2OS cells transfected with the plasmid p-EGFP-ATF6.

2.1.2 Media

Bacteria

- Luria-Bertani (LB) Medium: 10 g bacto-trypton, 5 g bacto-yeast extract, 10 g NaCl per 1 liter medium. Ampicillin was added at a concentration of 100 µg/ml. For hardening 1.5% agar-agar was added to the liquid medium.
- SOC Medium: Super Optimal Broth (SOB) medium (20 g bactotrypton, 5 g bacto-yeast extract, 0.5 g NaCl per 1 liter medium) was enriched with 20 mM glucose.

Mammalian Cells

- DMEM complete medium: Dulbecco's Modified Eagle Medium (Gibco – cat.num. 31885-023) supplemented with 10% fetal bovine serum (FBS) (Euroclone – cat.num. ECS0180L). For selection of stable cell lines Geneticin, also called G418 Sulfate (Invitrogen – 10131035), or Puromycine Dihydrochloride (Invitrogen – A1113803) were added at a concentration of 1.2 mg/ml and 1 μg/ml respectively.
- OptiMEM: Reduced-Serum Medium (Gibco – cat.num 31985-070)
- Cryo medium: for long-term storage cells were frozen in liquid nitrogen in 90% FBS, 10% DMSO.

2.1.3 Antibodies and antisera

Primary antibodies

Reactivity	Species	Subtype	Source	Comments
TBEV E	Rabbit	Polyclonal	The antibody was produced by our colleague Gianmarco Corazza whole serum not purified	1:100 IF 1:1000 WB
Human G3BP11	Mouse	IgG Monoclonal	BD transduction laboratories	1:100 IF
Human eIF3	Goat	Polyclonal	Santa Cruz	1:200 IF
Human eIF4B	Rabbit	Polyclonal	Abcam	1:100 IF
Human P-eIF2α (Ser51)	Rabbit	Polyclonal	Cell Signalling	1:500 WB
Human eIF2α	Rabbit	Polyclonal	Santa Cruz	1:100 WB
TBEV NS1	Mouse	IgG Monoclonal	Dr. Connie Schmaljohn (Iacono-Connors et al, 1996)	1:1000 WB
β-Actin-HRP	Mouse	IgG Monoclonal	Sigma	1:50000 WB
dsRNA J2	Mouse	IgG Monoclonal	English and Scientific Consulting	1:200, IF
TBEV prM	Rabbit	Polyclonal	Kindly provided by Dr. Heinz, Medicine University, Vienna	1:100 WB
Human PERK	Rabbit	Polyclonal	Santa Cruz	1:500 WB
Human P-PERK (T981)	Rabbit	Polyclonal	Santa Cruz	1:200 WB
Human β-Catenin	Mouse	IgG Monoclonal	BD Trunsduction Lab	1:2000 WB
Human PKR	Mouse	IgG Monoclonal	Santa Cruz	1:200 WB

Human P-PKR (T446)	Rabbit	IgG Monoclonal	Abcam	1:1000 WB
Human RIG-I (CTD)	Rabbit	Polyclonal	Kindly provided by Dr. Takashi Fujita, Kyoto University	1:100 IF
Human RIG-I (Alme-I)	Mouse	IgG Monoclonal	AdipoGen	1:500 WB
Flag	Mouse	IgG Monoclonal	Sigma-Aldrich	1:1000 WB
Flag	Rabbit	IgG Monoclonal	Sigma-Aldrich	1:100 IF

Table 2.1 Primary antibody used in this study.

Secondary antibodies

- Donkey, anti-mouse IgG, Alexa Fluor 488 (Molecular Probes); 1:500 for IF.
- Donkey anti-rabbit IgG, Alexa Fluor 594 (Molecular Probes); 1:500 for IF.
- Donkey, anti-goat IgG, Alexa Fluor 594 (Molecular Probes); 1:500 for IF.
- Donkey, anti-rabbit IgG, Alexa Fluor 488 (Molecular Probes); 1:500 for IF.
- Donkey anti-mouse IgG, Alexa Fluor 594 (Molecular Probes); 1:500 for IF.
- Goat polyclonal, anti-rabbit immunoglobulins/HRP (DakoCytomation); 1:10000 for WB.
- Rabbit polyclonal, anti-mouse immunoglobulins/HRP (DakoCytomation); 1:10000 for WB.

2.1.4 Vectors

Plasmid	Relevant characteristics	References
pEGFP-ATF6	Expressing EGFP-ATF6, Geneticine Resistance gene	32955, Addgene Chen et al., 2002
psPAX2	Packaging Vector	12260, Addgene
pMDG.2	Encodes VSV-G Envelope	12259, Addgene
pWPI- NEO	Lentivector, Neomycin Resistance gene	D. Trono (EPFL)
pEF-BOS-Flag-RIG-I-N	Encodes Flag-RIG-I	Kindly provided by Dr. Takashi Fujita
pWPI-Flag-RIG-I	Lentivector expressing Flag-RIG-I	Produced in this study

Table 2.2 Cloning and expression vectors used in this study

2.1.5 Oligonucleotides

Name	Sequence (5' to 3')
TBEV 5'NCR Fw	GCGTTTGCTTCGGA
TBEV 5'NCR Rv	CTCTTTCGACACTCGTCGAGG
β-Actin Fw	CATGTGCAAGGCCGGCTTCG
β-Actin Rv	GAAGGTGTGGTGCCAGATTT
IFNβ Fw	AGGACAGGATGAACTTTGAC
IFNβ Rv	TGATAGACATTAGCCAGGAG
IFIT2 Fw	ACGTCAGCTGAAGGGAAACA
IFIT2 Rv	TGTTCTCACTCATGGTTGCAGT
IFIT3 Fw	TGCAGGTCTCAAGCCGTTAG
IFIT3 Rv	GACCTCACTCATGACTGCCC
IL8 Fw	CAGAGACAGCAGAGCACACA
IL8 Rv	GGCAAAACTGCACCTTCACA
OASL Fw	TACCAGCAGTATGTGAAAGCCA
OASL Rv	GGTGAAGCCTTCGTCCAACA
CHOP Fw	TAAAGATGAGCGGGTGGCAG
CHOP Rv	CTGCCATCTCTGCAGTTGGA
XBP1s Fw	CTGAGTCCGCAGCAGGTG
XBP1s Rv	GGCTGGTAAGGAACTGGGTC
XBP1tot Fw	CCGGAGCTGGGTATCTCAAAT
XBP1tot Rv	CCGTATCCACAGTCACTGTAAGCA
XBP1u Fw	AGCCAAGGGGAATGAAGTGAGG
DNAJC3 Fw	CGTTTGCGTTCACAAGCACT
DNAJC3 Rv	CCCGAACTTCACTGAGGGAC
DNAJB9 Fw	TGGGGAAGCGTTTCGTGTAG
DNAJB9 Rv	CTAATATCCTGCACCCTCCGAC
EDEM1 Fw	AGGACCAAGGGGGAAAGTCT
EDEM1 Rv	GTACACGATTGCAGTTGGAGC
BiP Fw	CCCGAGAACACGGTCTTTGA
BiP Rv	TCAACCACCTTGAACGGCAA
GADD34 Fw	CCCAGAAACCCCTACTCATGAT
GADD34 Rv	CTCGGAGAAGCGCACCTTT
XmaI-FlagRIGI Fw	TCCC*CCCGGG*ATGGATTATAAGGATGATGATGATAAAGG
SpeI-FlagRIGI Rv	ATACG*ACGCGT*TCATTTGGACATTTCTGCTGG

Table 2.3 Sequence of oligonucleotides used in this study. The restriction sites contained in the primer sequence are indicated in italic letters.

2.2 General Procedures

2.2.1 Cell culture

Monolayers of cells were grown at 37°C, 5% CO_2 in DMEM complete medium. Cells were passaged after treatment with 0.05% Trypsin – 0.02 % EDTA and seeded at the appropriate dilution.

2.2.2 Plasmid construction

pWPI-Flag-RIG-I is a lentiviral protein expression vector created with pWPI-Neo cloning vector. pWPI cloning plasmid was digested with XmaI and SpeI restriction enzymes. Insert was created by PCR amplification using PFU DNA Polymerase (Promega – cat.num M7745) and PCR Nucleotide Mix (Promega – cat.num M0202L) from the pEF-BOS-Flag-RIG-I plasmid. For the reaction the primers Xmai-FlagRIGI Fw and SpeI-FlagRIGI Rv were used and PCR was performed under the following thermal cycling conditions: 94 °C 5 min, 94 °C 30 sec – 64 °C 30 sec – 72 °C 2.5 min for 35 cycles, and 72°C 2 min.

After purification with the QIAquick PCR Purification Kit (Promega – cat.num 28104) the PCR product was digested with XmaI and SpeI restriction enzymes. Both linearized vector and digested PCR product were run on a 1% agarose gel to evaluate size and integrity. After gel extraction with the QIAquick Gel Extraction Kit (Qiagen – cat.num 28704), PCR digested product was ligated over-night (O/N) at 16°C using T4 DNA Ligase enzyme (New England Biolabs – cat.num M0202S) into the linearized pWPI-Neo vector.

2.2.3 Plasmid transformation

XL10-Gold Ultracompetent cells (Agilent Technologies) were used for transformation of all parental and produced plasmids. Briefly, cells were incubated with plasmids on ice for 30 min. Afterwards, they were heat-shocked at 42°C for 40 sec, and left on ice for 2 min more. Then, SOC medium was added into cells, and cells were incubated at 37°C for 1 h. Finally, cells were plated onto LB agar with the desired antibiotic and grew over-night (O/N) at 37°C.

Selected colonies were picked and inoculated into 3 ml of LB medium containing the desired antibiotic. After 12-15 hours bacteria were lysed and plasmid DNAs were extracted using GenElute Plasmid Miniprep Kit (Sigma-Adrich – cat.num PLN350). Extracted plasmids were controlled by restriction enzyme digestion assay and sequencing.

2.2.4 Production of infectious Lentiviral particles

Lentiviral (LV) particles were produced in HEK 293T cells using calcium phosphate transfection method. Briefly, 2 x 10^6 HEK 293T cells were plated in 10 cm dishes one day prior to transfection. The following mix was prepared in 450 µl of sterile dH2O:

- 5 µg pWPI-Flag-RIG-I expression plasmid,
- 3.75 µg psPAX2 packaging plasmid
- 1.25 µg pMD2.G envelope plasmid

50 µl of sterile 2.5 M $CaCl_2$ was added to each tube.

This mixture was incubated for 5 min at room temperature and then added dropwise to 500 µl sterile 2X HBS (Hepes Buffered Saline: 50 mM HEPES pH 7.05, 280 mM NaCl, 1.5 mM Na_2HPO_4) by gently vortexing and incubated at room temperature (r.t.) for 30 min. The transfection mixture was added dropwise to the cells and incubated O/N.

The day after, the media was changed to remove the transfection reagent and replaced with fresh DMEM + 10% FBS. Cells were then incubated at 37 °C, 5% CO_2 for 24 h. Following day, media containing the lentiviral particles were collected and centrifuged at 2250 rpm (Eppendorf Centrifuge 5804R) for 10 min at 4 °C to pellet any HEK-293T cells that were accidentally collected during harvesting. The surnatant was filtered with 0.45 µm sterile filters. The filtered lentiviral stocks were aliquoted and kept at -80 °C until needed for transduction experiments.

2.2.5 Transduction of target cells with purified Lentiviruses

In order to produce stable cell lines expressing the chimeric protein Flag-RIG-I, 1.5 x 10^5 U2OS cells were prepared in 3 ml of DMEM + 10% FBS and were incubated together with 1 ml of lentiviral particles additioned with 1 µl (150 ng/ml) of Polybrene (hexadimethrine bromide, Sigma Aldrich – cat.num 107689). Cells were plated in 6 cm dishes and incubated at 37 °C. Two days after, medium was replaced with fresh DMEM + 10 % FBS additioned with 1.2 mg/ml Neomycin and cells were kept under selection for one week. Expression of the chimeric protein was evaluated by WB analyses.

2.2.6 Transfection of U2OS cells with Lipofectamine LTX

Plasmid DNAs were delivered into U2OS cells using Lipofectamine LTX (Invitrogen) according to the manufacturer's instructions.

2.2.7 Flow cytometry analysis

For the analysis of EGFP-ATF6 expression, after transfection and selection, cell monolayers were treated with 0.05 % Trypsin – 0.02 % EDTA to prepare single cells suspensions. Cells were then washed twice with PBS (Phosphate Buffered Saline), resuspended with 500 µl PBS and analyzed immediately by flow cytometry using a FACSCalibur apparatus (Becton Dickinson) and the Cell Quest Pro software.

2.2.8 Indirect Immunofluorescence (IF) analysis

In general, cells were seeded onto microscope coverslips and supplied with complete growth medium. For IF analysis cells were washed three times with PBS and fixed in 3.7 % paraformaldehyde (PFA) solution (3.7% PFA in PHEM buffer: 60 mM PIPES, 25 mM HEPES, 10 mM EGTA, 2 mM $MgCl_2$) for 15 minutes at room temperature. Thereafter, cells were again washed three times with PBS containing CaCl2 and MgCl2 (PBS+S) and incubated 5 minutes with 100 mM Glycine in PBS+S in order to saturate excesses of PFA and to stop the fixation reaction. Cells were permeabilized for 5 minutes with 0.1 % Triton X-100 in PBS and washed three times, 5 min each. Before incubation with antibodies, a blocking step was performed at 37°C for 30 minutes with 1 % bovine serum albumin (BSA, Roche – cat.num 10735078001) and 0.1 % Tween 20

(Sigma Aldrich – cat.num P2287-500ML). Primary antibodies were diluted to the desired concentration in blocking solution to prevent aspecific binding of the antibodies. After one hour incubation at 37°C, or overnight incubation at 4°C, coverslips were rinsed three times with PBS+S 0.1 % Tween 20 (washing solution) and incubated with secondary antibodies for 1 hour at 37°C. Coverslips were finally washed three times with washing solution and mounted on slides using Vectashield mounting medium with addition of DAPI (Vector Laboratories – cat.num H-1200).

In order to detect endogenous RIG-I intracellular localization, U2OS cells were fixed and permeabilized as previously described. The blocking was instead performed at 37°C for 1 hour with PBS, 0.5 % BSA and 0.04 % Tween 20 following Dr. Takashi Fujita protocol (Onomoto et al. 2012). Cells were next incubated O/N at 4°C with the anti RIG-I antibody diluted in the blocking solution described above, washed twice for 20 minutes at room temperature with PBS 0.04 % Tween 20 and finally incubated with the secondary antibody for 1 hour at 37°C with the same blocking solution used before. After two washes at room temperature for 20 minutes, coverslips were mounted on slides as already described.

2.2.9 Imaging of fixed cells

Fluorescent images of fixed cells were captured with the Zeiss LSM 510 META confocal microscope (Carl Zeiss Microimaging, Inc.).

The LSM 510 META confocal microscope was equipped with a 63X Plan-Apo/1.4 NA Oil objective and with a 40X Plan-Neo/1.3 NA Oil objective. The pinhole of the microscope was adjusted to get an optical slice of less than 1.0 μm for any wavelength acquired. The fluorophore Alexa488 as well as EGFP-ATF6 protein were excited with 488 nm line of the Argon Laser, while the fluorophore Alexa594 was excited with the HeNe Laser 543 nm. Their emissions were collected using the appropriate filters.

Co-localization analyses of RIG-I and TBEV signals were performed with ImageJ software.

2.2.10 Real-time quantitative reverse transcription PCR (qRT-PCR)

Total cellular RNA was extracted by using Isol-RNA Lysis Reagent (5Prime – cat.num 2302700) according to the manufacturer's instructions, treated with DNase I (Life Technologies – cat.num 18060-015) and then quantified.

500 ng of extracted RNA was used as a template to synthesize cDNA using 150 ng Random Primers (Life Technologies – cat.num 8190-011) and M-MLV Reverse Transcriptase (Life Technologies – cat.num 28025-013) according to manufacturer's protocol.

Quantitative Real-time PCR (qRT-PCR) using KAPA SYBR FAST qPCR Master Mix (KapaBiosystem - cat. num. KK4607) was performed from cDNA samples. Signals of inducible cellular mRNAs or viral RNAs were normalized to the β-Actin mRNA signal. The sequences of oligonucleotides used for this analysis are reported in table 1.3.

Amplification and detection were carried out on a CFX96 Real Time System (Bio-Rad).

2.2.11 PstI digestion of Xbp1 splicing forms

Total RNA samples were reverse transcribed as described in previous paragraph.

Amplicon spanning Xbp1 splicing site was synthesized using the primers Xbp1u_Fw and Xbp1s_Rv (table 2.3) under the following thermal cycling conditions: 94 °C 5 min, 95 °C 30 sec – 60 °C 30 sec – 72 °C 30 sec for 35 cycles, and 72°C 2 min. PCR products were purified with the QIAquick PCR Purification Kit (Promega – cat.num 28104) and subsequently digested with the restriction enzyme PstI (NewEngland BioLabs – cat.num R0140S). Finally the digested amplicons were run on a 2% Agarose gel.

2.2.12 Cell Lysis

Depending on the type of analyses required cells were lysed in different lysis buffer:

- Laemmli Buffer (50 mM Tris-Cl pH 6.8, 2% SDS, 10% glycerol, 100 mM DTT, 0.1% bromophenol blue);
- RIPA buffer (50 mM Tris HCl pH8, 150 mM NaCl, 1% NP-40, 0.5% Sodium Deoxycholate, 0.1% SDS additioned with Proteinase Inhibitors (Roche - 11836170001) and Phosphatase Inhibitors: Sodium Fluoride and Sodium Orthovanadate;
- Native Lyses Buffer: 0.5% Triton-X100 in PBS

2.2.13 Trypsin digestion of infected samples

To assay the conformation of RIG-I, cells were lysed in native lysis buffer, 0.5% Triton X-100 in PBS, and incubated on ice for 10 min. Then, samples were sonified at 4 °C for 10 min and centrifuged at 4 °C for 10 min at 10000 g. Aliquots of 30 μg of total protein were digested for 10 min with 0.3 μg of Sequencing Grade Modified Trypsine (Promeca – cat.num V511A) at 37 °C. Reaction was stopped by adding Laemmli buffer and heating the samples at 95 °C for 10 min. Samples were subjected to 10% SDS-PAGE and western blot analysis using mouse monoclonal anti-RIG-I antibody (ALME-1). Staining of the blot with 0.1% Ponceau S in 5% acetic acid served as a loading control.

2.2.14 SDS PAGE

Whole cell lysates were resolved by SDS–PolyAcrylamide Gel Electrophoresis (SDS-PAGE) at the appropriate acrylamide percentages. Initially, the protein lysates were boiled at 95°C for 10 min, and centrifuged for 1min at RT at 1000g, and subsequently loaded into the acrylamide gel.

Gels were run in SDS electrophoresis buffer (25 mM Tris, 190 mM glycine, 0.1% SDS), initially at 90 V into the stacking gel and later at 140 V into the running gel.

2.2.15 Native PAGE

To investigate the oligomerization of RIG-I, 50 μg of sonified cell lysate in native buffer (50mMTris-HCl [pH 6.8], 10% glycerol, 0.1% bromphenol blue) was loaded onto a nondenaturing 8% polyacrylamide gel. Proteins were separated by electrophoresis with 50 mM Tris-NaOH (pH 9.0), 384 mM glycin as anode buffer and 50 mM Tris (pH 8.3), 384 mM glycin, 1% sodium deoxycholate as cathode buffer. Western blot analysis was performed using anti-RIG-I (ALME-1) antibody.

2.2.16 Western blot analysis

For Western blotting, nitrocellulose membrane (GE Healthcare – cat.num 10600015) was used and membranes were blocked for 1 hour in 4% milk followed by incubation with the appropriate primary antibodies diluted in 4% milk / 0,5% Tween-20 at 4°C O/N. After three washing with TBS 0.5% Tween-20 secondary antibodies conjugated with HRP (DakoCytomation – cat.num P0447/8) were diluted in 4% milk / 0,5% Tween-20 and incubated for 1 hour. Blots were developed using Immobilon Western Chemiluminescent HRP Substrate (Millipore – coat.num WBKLS0500) according to manufacturer's instructions.

2.2.17 Whole-genome transcriptome analysis

U2OS cells were seeded into 10-cm dishes. Next day, cells were infected, or mock infected, with TBEV at a MOI of 5. After 1 hour cells were washed with PBS and sample corresponding to 0 hours post infection (h p.i.) was lysed in Isol-RNA lysis buffer. For all other samples DMEM containing 5% decomplemented (Heat inactivation: 56°C for 30 minutes) FBS was added. Other RNA samples were collected at 10 and 24 h p.i.

Total RNA was extracted. Integrity and concentration of total RNA were measured with denaturing agarose gel electrophoresis and nanodrop, respectively. Three independent experiments were performed.

Total RNA samples were sent to the company (IGA Technology Services, Udine, Italy). RNA integrity number (R.I.N.) was measured. RNA samples were run with HiSeq 2000 sequencing system (Illumina). An average of 25 millions reads were

performed for each sample. Afterwards, the company performed alignment and expression analysis.

Raw data were analyzed by Dr. Danilo Licastro (CBM, Trieste, Italy). Briefly, bioconductor packages DESeq2 version 1.4.5. and EdgeR version 3.6.2 in the framework of R software version 3.1.0 were used to perform differential gene expression analysis of RNA-seq data. Both packages are based on the negative binomial distribution (NB) to model the gene reads counts and shrinkage estimator to estimate the per-gene NB dispersion parameters. Specifically, rounded gene counts were used as input and the per-gene NB dispersion parameter was estimated using the function DESeq for DESeq2 while, for edgeR the function calcNormFactors with the default parameters was used. To detect outlier data after normalization, R packages arrayQualityMetrix were used and before testing differential gene expression all genes with normalized counts below 14 were eliminated to improve testing power while maintaining type I error rates. Estimated p- values for each gene were adjusted using the Benjamini-Hochberg method. Genes with adjusted $P<0.05$ and absolute Logarithmic base 2 fold change > 1 were selected.

From the analyses 437 resulted up-regulated and 318 down-regulated.

Finally, some of the down-regulated and up-regulated genes were validated by q-PCR analysis in order to prove the accuracy of the whole-genome transcriptome analysis.

2.2.18 Ingenuity pathway analysis

Significantly changed genes (up-regulated, down-regulated, or both) were analyzed by using online bioinformatics tool Ingenuity Pathway Analysis (Qiagen). Settings for the analysis as following: direct relationships were included with experimentally observed or highly predicted confidence from human species. Canonical pathways, diseases and disorders, and molecular and cellular functions were analyzed.

2.3 Working with viruses

2.3.1 Preparation of TBEV stocks

TBEV strain Neudoerfl was used for these studies.

Viral stocks were prepared by infection of Vero cells at the low multiplicity of infection of 0.1. After cytopathic effect (CPE) was observed, cell culture supernatant was collected, clarified by centrifugation, supplemented with 20 % FBS, and stored in aliquots at -80°C.

Viral titres were determined by using a plaque-forming assay.

2.3.2 Plaque Assay

Vero cells were seeded into 24-well plates till monolayer was formed.

Cells were infected the day after with a 10-fold serial dilution of TBEV in a total volume of 200 µl of serum-free medium. After 1 hour incubation at 37°C with 5% CO_2, the inoculum was removed and a 500 µl overlay containing 1 volume of 6% carboxymethyl cellulose (CMC) to 1 volume of maintenance medium (DMEM supplemented with 4 % decomplemented FBS) was added. The plates were incubated for 5 days before fixation with 4 % PFA dissolved in PBS. Infected cells were stained adding 300 µl of 1% crystal violet solution in 80% methanol / 20% PBS. After 30 minutes the staining solution was removed and cells were washed 3-4 times with water. Viral titres were determined by counting number of plaques formed and multiplying it for the dilution factor.

2.3.3 TBEV infection of cells

For standard infection assays, U2OS cells were seeded in a 12 well plate at an appropriate confluency.

24 hours later, cells were infected at the appropriate moltiplicity of infection (MOI) by adding 400 µl of virus stock properly diluted in serum-free medium. After 1 hour incubation at 37°C with 5 % CO_2, the inoculum was replaced with maintenance medium (DMEM supplemented with 4 % decomplemented FBS).

The moment in which the virus is replaced with normal medium is considered time zero, 0 hours post infection (0 h p.i.). Cells were then harvested at the appropriate time points.

2.3.4 Tunicamycin treatment of cells

U2OS cells were plated in 12 well plates and 24 hours later were infected with TBEV at a MOI of 1. After one hour, cells were washed with PBS and medium was changed with complete medium (untreated samples) or medium containing 1 μg/ml Tunicamycin (TM) (Sigma – cat.num. T7765-1MG). Control cells, mock infected and not treated with TM were also used. Cells were then harvested at the appropriate time points.

3 RESULTS

3.1 TBEV induce formation of Stress Granules

Stress granules (SG) are dynamic aggregates of non-translating mRNAs in conjunction with translation pre-initiation complexes and several RNA binding proteins, including: the polyA binding protein, T-cell restricted intracellular antigen 1 (TIA-1), TIA-1-related protein (TIA-R) and RasGAP SH3-domain binding protein 1 (G3BP1). Cells react to various stresses by activating cellular kinases that phosphorylate the eukaryotic initiation of translation factor 2α (eIF2α), thereby rendering eIF2α inactive and inducing a stop in translation with consequent formation of SG. Among the stresses that can cause formation of SG there is infection with a wide variety of viruses. Until some years ago it was accepted the idea that Flaviviruses, like West Nile Virus and Dengue Virus, were not able to induce formation of SG (Emara and Brinton 2007). More recently it has been demonstrated that HCV was able to induce oscillating SG (Ruggieri et al. 2012). In our recent work (Albornoz et al. 2014) we found that TBEV is able to induce SG formation.

In figure 3.1 U2OS cells were infected with TBEV with a MOI of 1 and fixed for immunofluorescence analysis (IF) at 24 hours post infection (h p.i.). IF was performed using anti-TBEV and anti-G3BP1 antibodies to mark infected cells and the SG marker G3BP1, respectively. The same analysis was made on mock infected cells. Since we observed that G3BP1 was recruited to cytoplasmic granules only upon TBEV infection, we wished to understand if TBEV-induced granules are *bona-fide* stress granules.

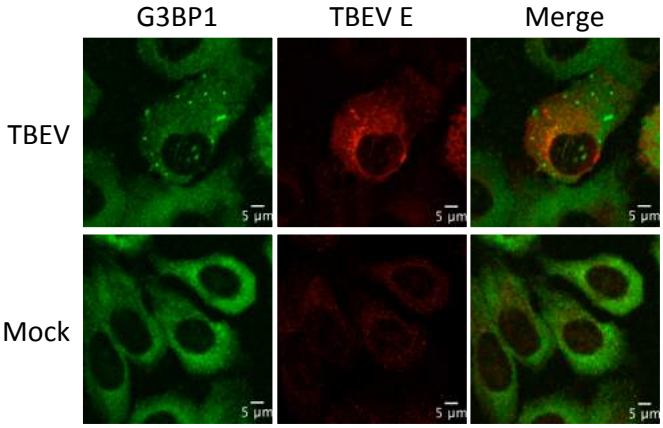

Figure 3.1 – TBEV infection induces formation of stress granules. U2OS cells were either mock infected or infected with TBEV at a MOI of 1. At 24 hours post infection cells were fixed and immunostained with an anti-G3BP11 antibody to detect stress granules and an anti-TBEV antibody to evidence viral replication. Scale bar: 5 μm.

Therefore we performed additional immunofluorescence analysis on TBEV infected U2OS cells (MOI=1) fixed at 24 h p.i. As shown in figure 3.2, G3BP1 co-localize in SG upon infection together with eIF3 (Figure 3.2a) and eIF4B (Figure 3.2b) that are typical marker of stress granules.

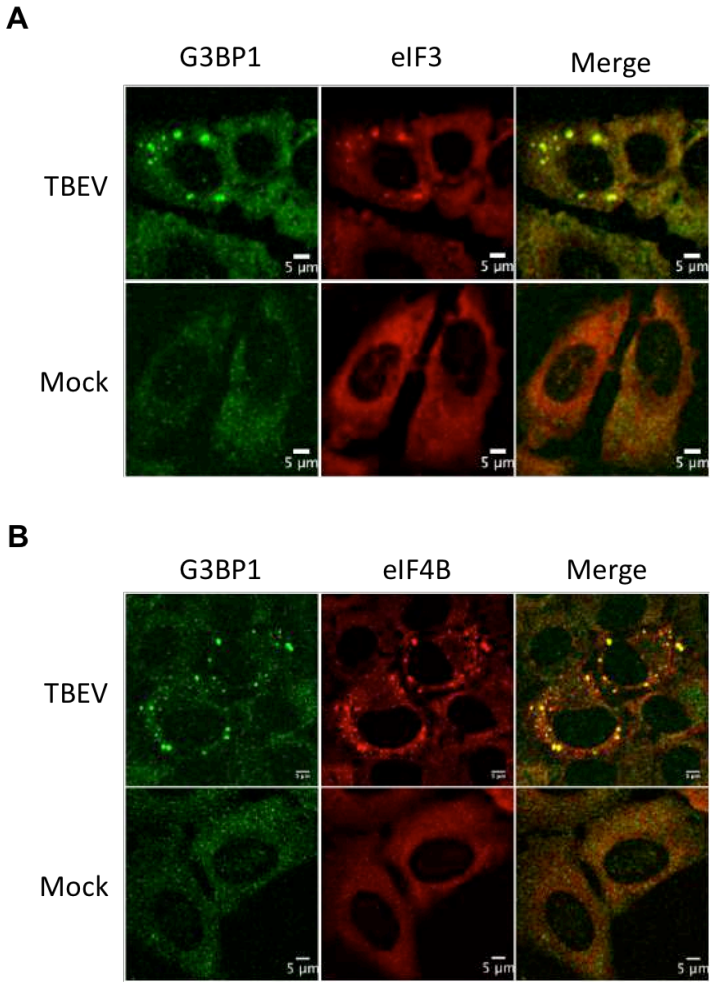

Figure 3.2 - Characterization of TBEV-induced stress granules. U2OS cells were either mock infected or infected with TBEV at a MOI of 1. At 24 hours post infection cells were fixed and immunostained for G3BP1 and eIF3 (A) or G3BP1 and eIF4B (B) to detect stress granules. Scale bar: 5 µm.

As already described in the introduction, the very first step triggering the formation of SG in stressed cells is the phosphorylation of the initiation of translation factor eIF2α by several serine/threonine kinases, depending on the type of stress.

Knowing that TBEV is able to induce SG formation, we wanted to study the phosphorylation status of eIF2α upon infection. To this end, lysates of U2OS mock cells, U2OS TBEV infected and U2OS heat shocked cells were used for WB analysis.

We were able to demonstrate that in infected cells eIF2α is phosphorylated (P-eIF2α) as much as in heat-shocked cells (positive control), confirming the activation of stress response upon TBEV infection (Figure 3.3). We also have to notice that a small portion of eIF2 α is phosphorylated even in mock cells but that this amount is probably not sufficient to trigger the formation of SG and the inhibition of translation. To exclude that the increased amount of P-eIF2α was due to an increased expression of eIF2α in infected cells we also performed a WB analysis using the anti-eIF2α antibody. As control of infection the anti TBEV NS1 antibody was also used. Anti-β-Actin antibody was used for the loading control.

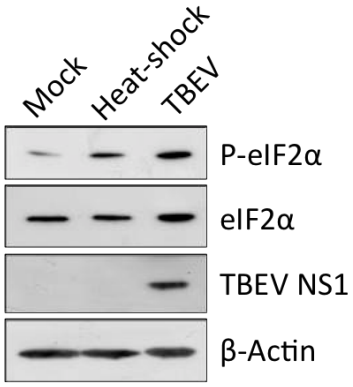

Figure 3.3 - eIF2α is phosphorylated upon TBEV infection. U2OS cells were either mock infected, heat shocked for 40 minutes at 45°C or infected with TBEV at a MOI of 1 for 24 hours. The cell lysates were immunoblotted for total eIF2a and phosphorylated eIF2a (P-eIF2a). Loading control (b-actin) and infection control (NS1) are also shown.

3.1.1 Stress granules are formed in TBEV infected cells starting from 16 h p.i.

So far we know that TBEV infection of U2OS cells is able to induce the activation of a stress response and the formation of stress granules at 24 h p.i.

However, it would be more interesting and informative to study the kinetics of viral replication and of the cellular responses following infection in order to understand better the possible crosstalk between cellular responses, molecules responsible of

triggering these responses and, not less important, possible escaping routes of viruses from these cellular responses.

In order to study the kinetic of stress granules formation during TBEV infection U2OS cells were infected at a MOI of 1 and fixed at different time-points: 0, 4, 8, 12, 16 and 24 h p.i. Immunofluorescence analysis was performed using the anti-dsRNA antibody, detecting an intermediate of TBEV replication, and the anti-eIF3 antibody as marker of SG. As it is possible to observe in figure 3.4, TBEV dsRNA becomes detectable at very early time of infection, starting from 4 h p.i. with a typical perinuclear localization that corresponds to the endoplasmic reticulum (ER) (Miorin et al. 2013). By analysis of the eIF3 staining it is possible to observe that SG are formed much later, starting from 16 h p.i. highlighting a delay of this response with respect to viral replication. Indeed, while virus replication is detectable as early as 4 h p.i. SG are visible only after 16 hours.

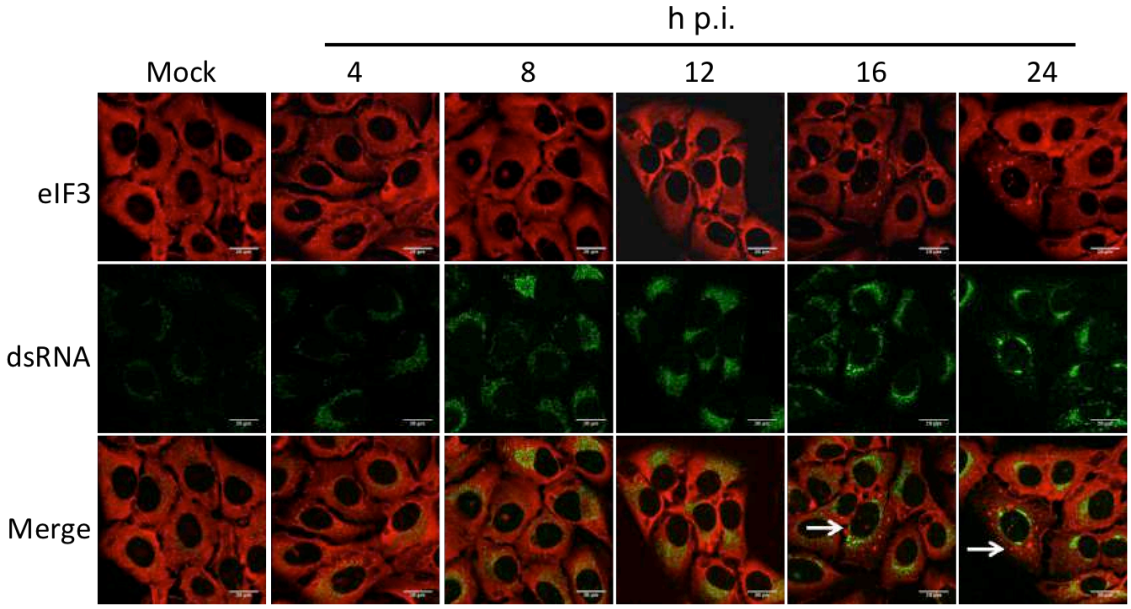

Figure 3.4 – Formation of stress granules occurs after16 hours post infection. U2OS cells were either mock infected or infected with TBEV at a MOI of 1. At 4, 8, 12, 16 and 24 hours post infection (h p.i.) cells were fixed and immunostained with the eIF3 antibody to detect stress granules and with the anti-dsRNA antibody to evidence viral replication. White arrows indicate cells containing stress granules. Scale bar: 20 μm.

3.2 IFN-β expression is delayed during TBEV infection with the same kinetic of stress granules formation.

The observed kinetic of SG formation was reminiscent of a previous observation about the IFN-β response (Miorin et al. 2012).

Therefore, Another time-course experiment was performed on U2OS cells infected with TBEV at a MOI of 1, but this time protein samples and cell supernatant were collected at 0, 4, 8, 10, 12, 14, 16 and 24 h post infection in order to perform respectively WB analysis and Plaque Assays.

As we can see from figure 3.5a, WB analysis reveals that viral proteins, in this case stained with anti-prM antibody, were detectable starting from 12 h p.i. Anti-β-Actin was used as loading control. From the Plaque Assay we could determine that production of infectious viral particles starting already at 10 h p.i (Fig. 3.5b). The lack of detection of prM by WB at earlier time points is due to the sensitivity of the antibody and of the test itself.

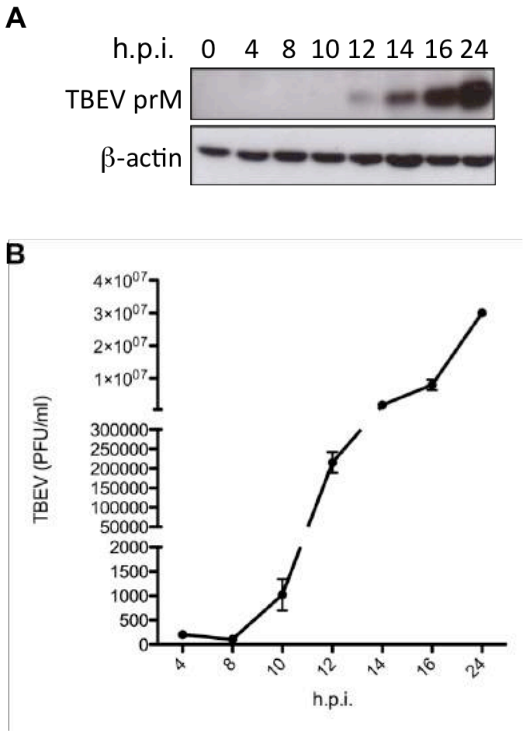

Figure 3.5 - Pattern recognition receptor agonists are present in infected cells from early time after infection. A) U2OS cells were infected with TBEV at a MOI of 1. At different time during infection cell lysates were collected and immunoblotted for prM. Loading control β-actin is also shown. (B) U2OS cells were infected with TBEV at a MOI of 1. At different time during infection cell supernatants were collected and Plaque Assays using these samples were performed. Data were averaged from two independent experiments and are represented as mean ± standard deviation.

From this final experiment we could conclude that both the stress response and the interferon response are activated later following TBEV infection.

During the same time course experiment of figure 3.5 RNA samples from infected cells were also collected. Total RNA was extracted and retro-transcribed. qRT-PCR for TBEV RNA and IFN-β mRNA were performed. As we can see from figure 3.6, black line, a first increased of TBEV RNA (≅ 80 fold) was measurable at 10 h p.i. followed by an exponential increase till the end of the time course (≅ 180000 fold at 24 h p.i.). This confirms that TBEV is replicating from early time of infection.

We could detect IFN-β mRNA levels only after 16 hours post infection as expected from previous data (Miorin et al., 2012).

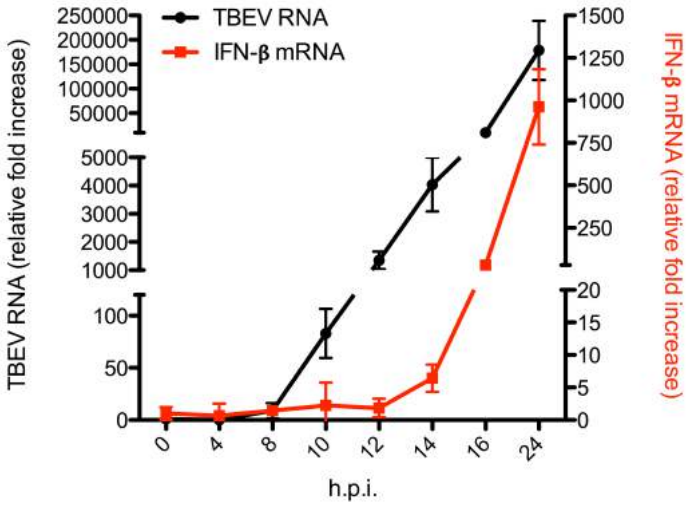

Figure 3.6 - IFN-β mRNA induction is delayed during TBEV replication. U2OS cells were infected with TBEV at a MOI of 1. At different time during infection cell lysates were collected and total RNA was isolated and retro-transcribed. qRT-PCR analysis for TBEV RNA levels (black line) and for IFN-b mRNA (red line) were performed. Expression levels are expressed as fold increase relative to 0 hours post infection (h p.i.). Data were averaged from two independent experiments and are represented as mean ± standard deviation.

3.3 The unfolded protein response is activated upon TBEV infection

In order to investigate the cellular events that lead to the stress and IFN responses in infected cells we applied an unbiased approach by analyzing differential transcription.

We identified two critical points: at 10 h p.i. when virus is actively replicating in the cells but no IFN is activated, and 24 h p.i. when the full response is clearly activated.

3.3.1 Whole-genome transcriptome analysis

U2OS cells were plated in 10 cm dish. The day after cells were infected, or mock infected, with TBEV at a MOI of 5. After one hour cells were washed with PBS and medium was replaced. This moment of infection correspond to 0 h p.i. RNA samples were collected at 10 and 24 h p.i. both for TBEV and mock infected cells. The experiment was performed in triplicate. A simplified scheme of the experiment is shown in figure 3.7.

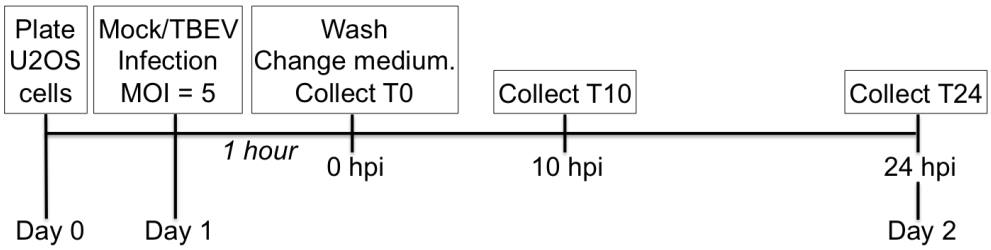

Figure 3.7 - RNAseq analysis: schematic drawing of the experimental approach. U2OS cells were plated at day 0. 24 hours later cells were either infected with TBEV at a MOI of 5 or mock infected. After 1 hour cells were washed and medium was changed. At this time the samples correspondent to 0 hpi (T0) were collected. At 10 hpi RNA samples for T10 were collected. At 24 hpi T24 samples were collected. Total RNA from the samples were extracted and sent for sequencing.

After the extraction, the quality of total RNA was evaluated by running an RNA gel electrophoresis (Figure 3.8a). We were able to detect 2 sharp bands corresponding to 28S and 18S rRNA, indicating that the RNA samples were not degraded and of good quality.

qRT-PCR analysis for TBEV RNA and IFN-β mRNA was also performed. As we can see in figure 3.8b, also in this experiment we were able to demonstrate that while at 10 h p.i. the virus is already abundantly replicating (≅ 10 fold), the interferon response is still silent and that IFN-β is induced later during infection.

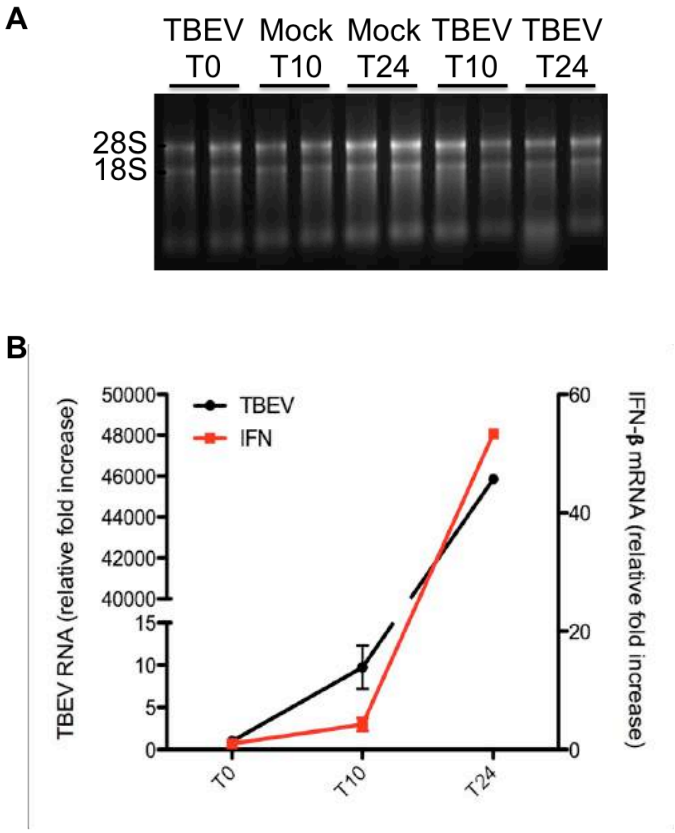

Figure 3.8 – Testing RNA quality and IFN-β and TBEV levels in samples for whole-genome transcriptome analysis. A) RNA gel electrophoresis was performed on TBEV or mock infected samples collected at 0, 10 and 24 hpi (T0, T10, T24). 2 mg of RNA were used. 28S and 18S rRNA are shown. Two different samples were tested. B) Total RNA extracted at 0, 10 and 24 hpi was retrotranscribed and TBEV RNA (black line) and IFN-β mRNA levels were tested by qRT-PCR analysis. Data were averaged from three independent experiments and are represented as mean ± standard deviation.

Three biological replicates for each condition were sent to an external company for high-throughput RNA-Seq analysis. Raw data were analysed with the help of Dr. Danilo Licastro (CBM, Trieste, Italy) that used bioinformatics tools as explained in materials and methods.

In figure 3.9 is reported a Volcano Plot representation of the statistical analysis. Significance is plotted versus fold-change on the y- and x-axes respectively: up-

regulated genes are shown in red (fold change ≥ 2), down-regulated genes are shown in green (fold change ≤ 2), the genes whose expression did not change between the two time of infection are shown in grey. The red line indicates the False Discovery Rate (FDR) of the analysis, 0.05.

As expected TBEV infection induced big changes in cell gene expression and in particular we can state that between 10 and 24 h p.i. cells undergo a critical reprogramming of gene expression, which will be further analyzed.

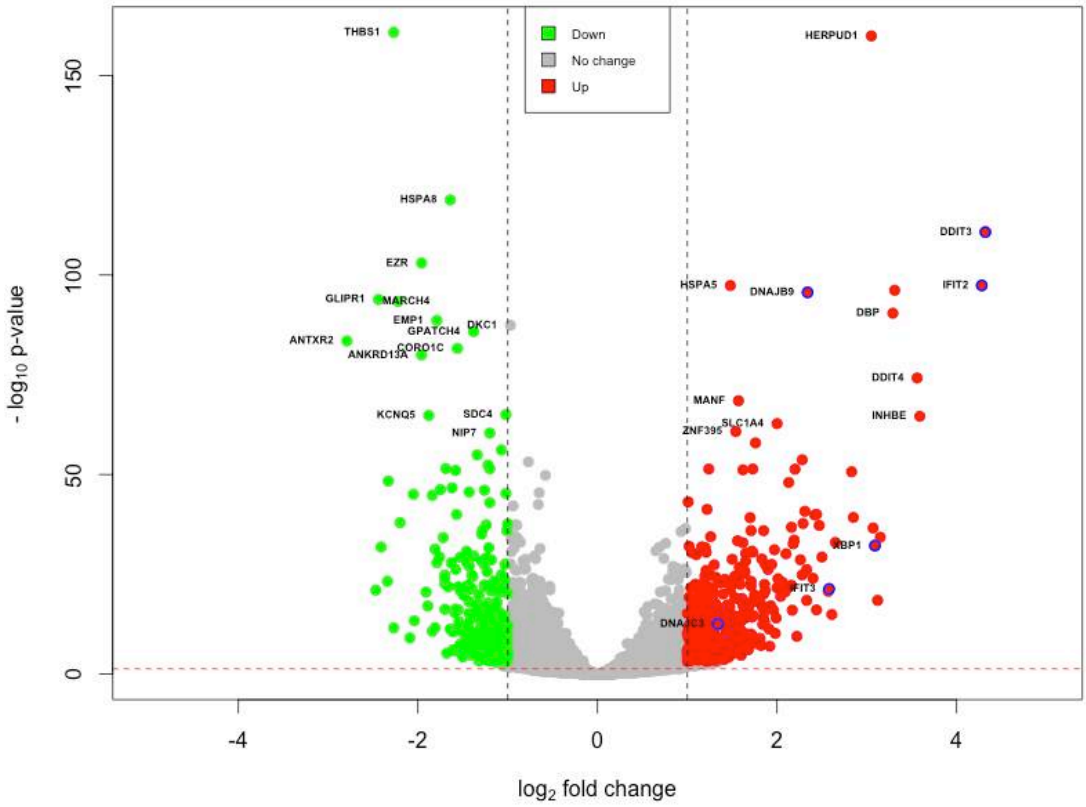

Figure 3.9 - Analysis of whole-genome transcriptome sequencing data. Raw data were analyzed and comparison of gene expression at T0 and T24 was performed. The Volcano Plot represents in green the downregulated genes and in red the upregulated genes. Genes belonging to the Unfolded Protein Response are circled in blue. Unaffected genes are shown in grey. FDR at 0.05, red dot line.

3.3.2 Ingenuity Pathway Analysis (IPA)

In order to understand which cellular pathways were mostly affected in our experiment, we analyzed our data with the Ingenuity Pathway Analysis software (IPA), a software for the functional analysis of omics data.

As we can see in the stacked bar chart of figure 3.10, many were the pathways affected by TBEV infection. For each pathway, the percentage of genes belonging to the pathway and affected in the analysis are reported in bold. In particular, in red is indicated the amount of up-regualted genes, in green the down-regulated and in grey the unchanged molecules. The significance is indicated by the yellow line, reported as logarithmic P-value.

The most significantly affected pathway was the Unfolded Protein Response, followed by the Adipogenesis pathway, CDK5 signalling and the Endoplasmic Reticulum Stress Pathway.

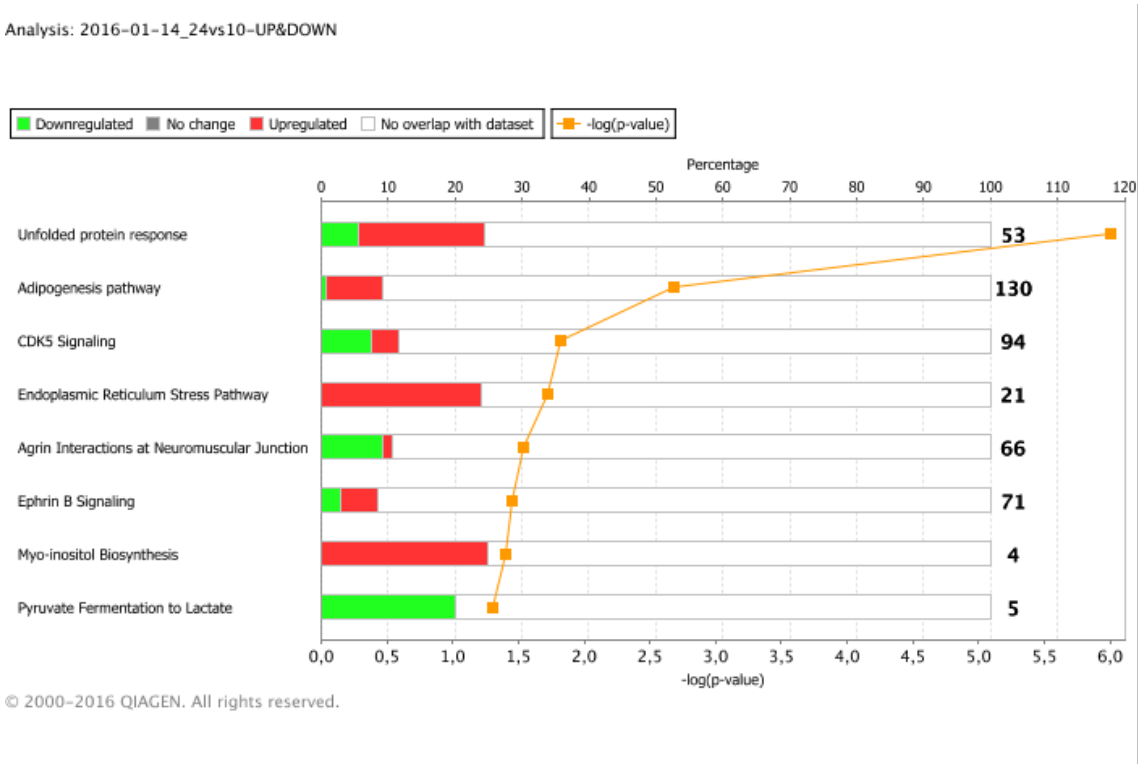

Figure 3.10 - Ingenuity Pathway Analysis of the top upregulated pathways of whole-genome transcriptome sequencing data. Data were analysed with Ingenuity Pathway Analysis (IPA) software. In the stacked bar chart are reported the main affected pathway resulted from the analysis. Percentage of genes belonging to the pathway and affected in the analysis are reported in bold. Upregualted (red), down-regulated (green) and unchanged molecules (grey) are indicated for each pathway affected. Significance is indicated by the orange line.

By a more detailed analysis of our subset of data, it was possible to identify which were the up-regulated genes whose products are involved in the UPR. In figure 3.11 is reported a schematic view of the Unfolded Protein Response where in red are highlighted the up-regulated components resulting from the RNA-seq analysis. It is evident that the majority of genes resulting from our analysis and overlapping the pathway are mainly upregulated, like, for example, the chaperonine BiP, the UPR key regulator PERK, the transcription factor XBP1s, the apoptosis regulator protein CHOP and other chaperons like DNAJC3 (also called P58IPK) and DNAJB9 (a member of the Heat Shock Protein 40 family). It is also interesting to notice that only few genes of this pathway are downregulated, i.e. HSPA8, a member of the Heat Shock Protein 70 family, involved in folding of nascent proteins, and KAI1, an apoptosis regulator.

During our studies we will mainly focus on the up-regulated genes of the Unfolded Protein Response and of the Endoplasmic Reticulum Stress Pathway but it might be interesting for future studies the understand of how the virus is able to inhibit the expression of HSPA8 and KAI1.

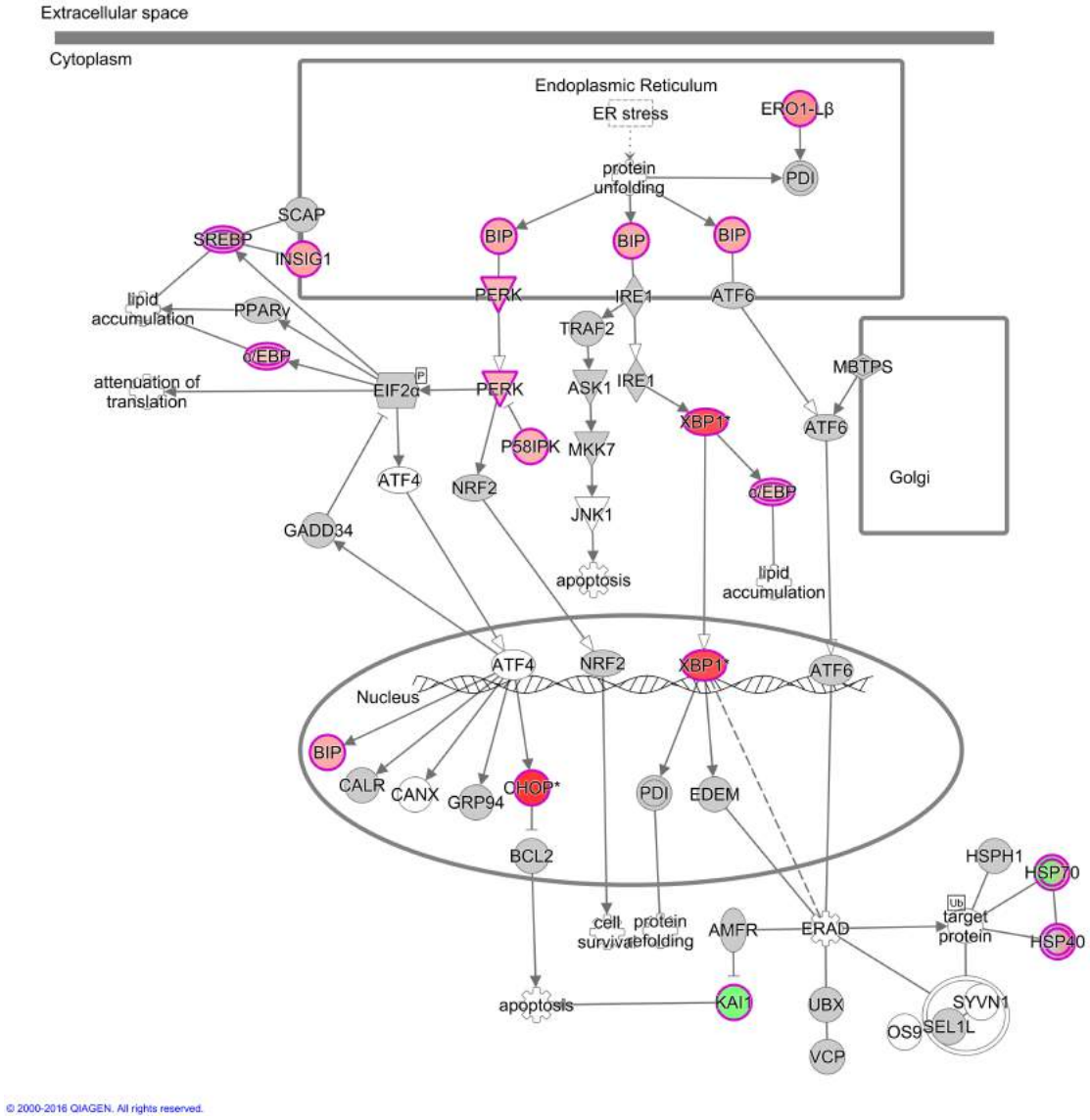

Figure 3.11 - – Ingenuity Pathway Analysis of the Unfolded Protein Response pathway. Interactive diagram of the canonical pathway Unfolded Protein Response. Highlited in pink the molecules from the dataset that overlap the pathway. Molecules are filled with different shades of red if upregulated, or green if downregulated. Double bordered molecules indicate groups or complexes that have members overlapping the dataset and may be differentially regulated. In grey, molecules that do not meet the analysis criteria. White, molecules that do not overlap with the dataset.

3.3.3 Validation of transcriptome analysis

Next, we wanted to validate the transcriptome analysis data by qRT-PCR of 9 selected genes in an independent experiment.

U2OS cells were infected with TBEV at a MOI of 1 and RNA samples were collected at 0 and 24 h p.i. Even if the normalization, as well as the time points analysed, were not the same of the RNA-Seq experiment, we were still able to demonstrate that UPR genes as CHOP (called DDIT3 in the VolcanoPlot), XBP1s, DNAJC3, DNAJB9 and EDEM1 were up-regulated at 24 h p.i. confirming the activation of the UPR during TBEV infection (Figure 3.12). Differences in the fold change are attributable to the different condition of the two experiments.

We also tested expression of some Interferon Stimulated Genes (ISG), i.e. IFIT2, IFIT3, IL8 and OASL that were up-regulate in the RNA-Seq analysis. For IL8 and OASL we were able to demonstrate their activation in the same independent experiment described above, while for IFIT2 and IFIT3 we were not able to show any induction. Several set of primers and several PCR conditions were tested but we never succeeded in demonstrating an increment of their expression. Since several published papers demonstrate that IFIT2 and IFIT3 are induced upon infection with Flaviviruses the failure of our tests could be related to the sets of primers chosen, or due to a discrepancy between the splicing variants of the 2 genes and the ones amplified by PCR (Figure 3.12).

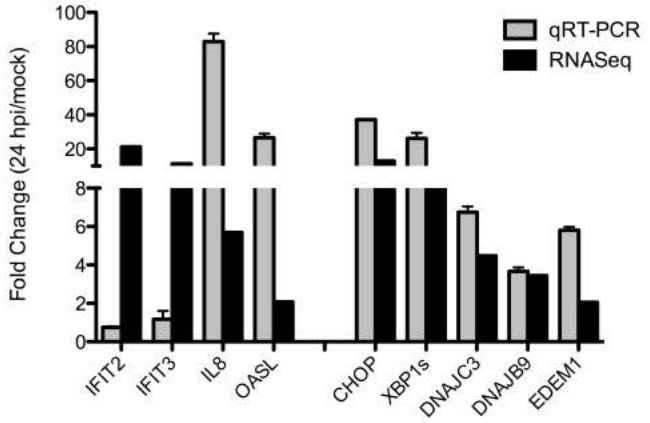

Figure 3.12 – Validation of whole-genome transcriptome. A total of 9 genes (4 belonging to immune response and 5 to UPR) were chosen among the most up-regulated of the analysis and their expression was analysed in an independent experiment where U2OS cells were infected with TBEV at a MOI of 1 and RNA samples were collected at 24 hpi. Expression levels resulting from qRT-PCR analysis (grey bars) are compared with RNAseq analysis (black bars). Data were averaged from two independent experiments and are represented as mean ± standard deviation.

3.4 Unfolded protein response is activated early during TBEV infection

From the RNA-Seq analysis we found that one of the main cellular responses activated during TBEV infection in U2OS cells is the Unfolded Protein Response (UPR).

The unfolded protein response is a cellular homeostatic response to endoplasmic reticulum stress. It is activated in response to accumulation of unfolded or misfolded proteins in the ER and has three main functions: inhibit protein translation, produce molecular chaperons to promote protein folding, degrade misfolded proteins. If the ER stress is too severe and prolonged, the UPR starts a signaling cascade leading to apoptosis.

Controversial studies have been published about the role of UPR during infection: on one hand the host activate the UPR in an attempt to restrict virus infection, on the other hand the virus could be able to exploit and manipulate the UPR for its benefit. Moreover the UPR has been proposed to augment the anti-viral response suggesting a synergic relationship between the PRR and the UPR.

Previous work (Peña and Harris 2011; Ambrose and Mackenzie 2011; C. Yu, Achazi, and Niedrig 2013) already demonstrated that the UPR is activated during

infection with different flaviviruses and that viruses are able to manipulate this pathway in order to favor cell survival or promote apoptosis, but no particular focus was posed on the role of UPR in inducing the IFN response.

In order to understand if in the case of TBEV the unfolded protein response is a possible trigger of the delayed IFN response we first investigated at what time during infection the UPR is activated.

3.4.1 Activation of ATF6 during TBEV infection occurs at early time of infection.

ATF6, Activating Transcription Factor 6, is one of the three key regulators of the UPR. ATF6 is an ER transmembrane protein that once activated by the detaching of BiP from its luminal domain, translocate to the Trans-Golgi Network (TGN) where is cleaved by two proteases, S1P and S2P, leading to the release of its cytoplasmic domain. The cytoplasmic domain of ATF6 is a transcription factor able to induce expression of several UPR target gene like BiP, CHOP and XBP1 (Schröder and Kaufman 2005; Walter and Ron 2011).

The canonical readout for ATF6 activation are: proteolytic cleavage and nuclear translocation of the cleaved product. However, both require a good antibody that we did not have. Therefore, we took advantage of a construct in which EGFP reporter gene is fused to the N-terminal domain (the transcription factor domain) of ATF6 (Chen, Shen, and Prywes 2002).

U2OS cells were transfected with the plasmid and subsequently selected with the Neomycin antibiotic for 4 days. Efficiency of transfection and selection was tested. Even if the cells were kept under selection for several weeks we were able to measure by cytofluorimetry analysis only a 52% of cells expressing the chimeric protein (Figure 3.13).

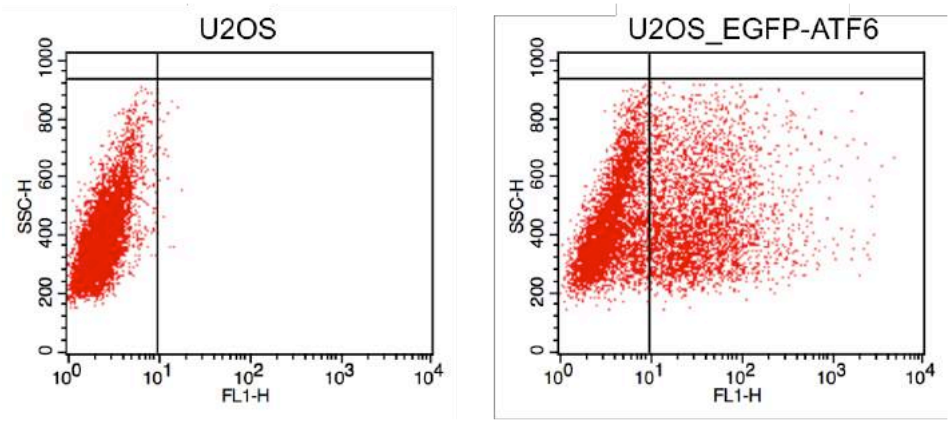

Figure 3.13 - Characterization of U2OS_EGFP-ATF6 cells. Cytofluorimetric analysis was conducted both in wild type U2OS (left) and in U2OS_EGFP-ATF6 cells (right). As shown in the graph, 52% of U2OS_EGFP-ATF6 were espressing EGFP-ATF6.

U2OS_EGFP-ATF6 cells were infected with TBEV at a MOI of 1 and samples for IF were collected at 0, 4, 8, 12, 16 and 24 h p.i. Anti-TBEV antibody was used to evaluate the infection. EGFP-ATF6 nuclear localization in mock cells was approximately 8%.

EGFP-ATF6 translocates in the nucleus of infected cells starting from 8 h p.i. The number of cells presenting nuclear localization of EGFP-ATF6 increases linearly with approximately 25% of infected cells presenting ATF6 positive nuclei (figure 3.14). This data suggests that ATF6 is slowly activated during infection starting from 8 h p.i.

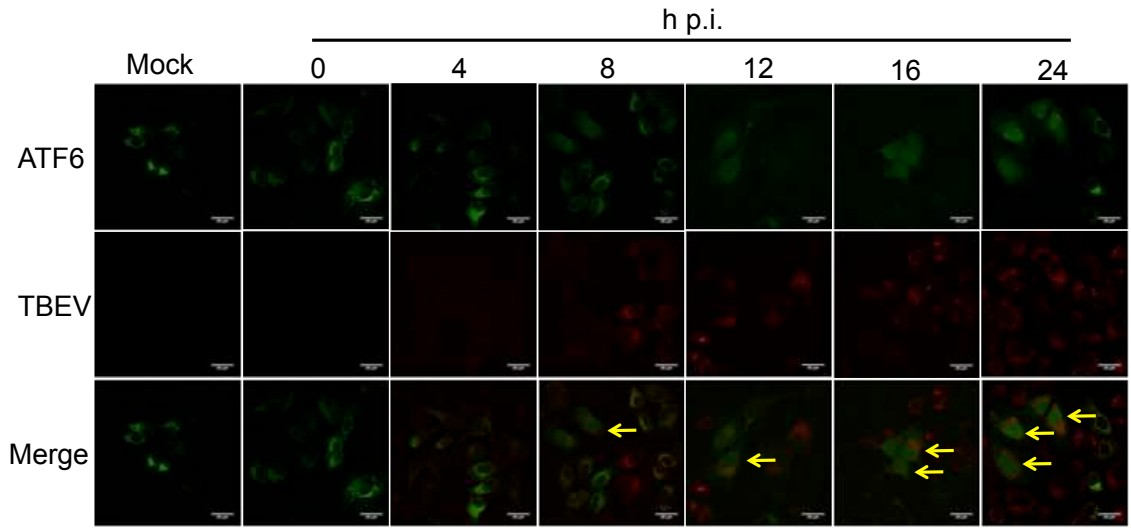

Figure 3.14 - ATF6 pathway is activated during TBEV infection starting from 8 hpi. U2OS_EGFP-ATF6 cells were either mock infected or infected with TBEV at a MOI of 1. Cells were fixed at different time after infection and immunostained with TBEV antibody to detect viral replication. EGFP-ATF6 nuclear localization was monitored to evidence activation of the protein. Yellow arrows indicate ATF6 nuclear localization. Scale bar: 35 μm.

To further study the activation of the ATF6 pathway we performed a qRT-PCR analysis of the genes BiP and XBP1 in samples of U2OS cells infected with TBEV at a MOI of 1 collected at different time points. Indeed, induction of these two genes is believed to be mainly activated by this arm of the UPR, although more recent finding suggest a more intricate regulation of these UPR markers also by the other UPR arms.

Surprisingly, our result demonstrates that both XBP1 (Figure 3.15a) and BiP (Figure 3.15b) have a slight increase in their expression at 14-16 h p.i. but that they are significantly induced only at 24 h p.i.

All together our studies about the activation of the ATF6 arm of the UPR suggest that nuclear translocation of ATF6 occurs as early as 8 h p.i. but that the gene expression induced by this arm might be differently regulated and activated only at later time of infection.

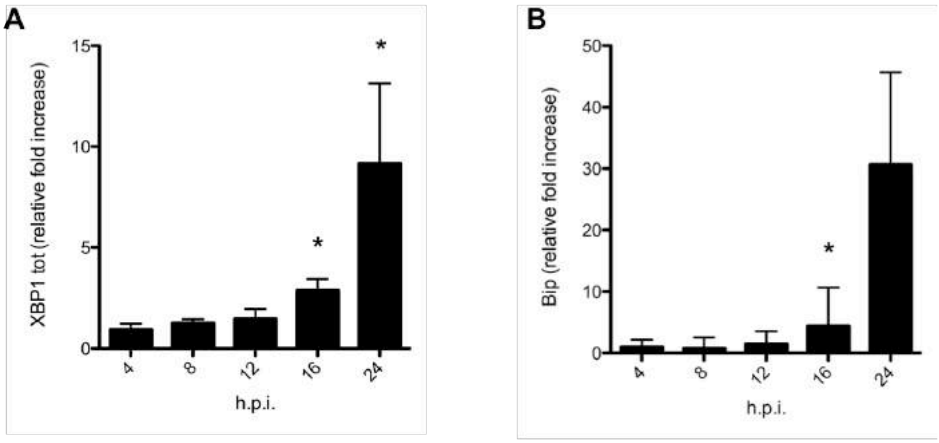

Figure 3.15 - XBP1 and BiP expression are induced at late time points during TBEV infection. U2OS cells were infected with TBEV at a MOI of 1. At different time during infection cell lysates were collected and total RNA was isolated and retro-transcribed. qRT-PCR analysis for XBP1 levels (A) and for BiP (B) were performed. Levels are expressed as fold increase relative to 0 hours post infection (h p.i.). Data were averaged from two independent experiments and are represented as mean ± standard deviation. Significant *p*-values were calculated with paired *t*-test (* = $p < 0.05$)

3.4.2 The IRE1 pathway is activated at 12 hours post infection

IRE1, Inositol-Requiring Enzyme 1, is an ER transmembrane protein containing an ER luminal dimerization domain and cytosolic kinase and RNase domains. IRE1 activation, due to the detachment of BiP from the luminal domain, induces the dimerization of the protein and consequent autophosphorylation of the dimer leading to

the activation of the RNase domain. This endoribonuclease activity initiates an unconventional splicing of the XBP1 mRNA, excising a 26 nt sequence and shifting the reading frame to produce a functional isoform of XBP1s which contains a C-terminal transactivation domain absent in the unspliced form (XBP1u). XBP1s is then translated and translocates into the nucleus where it induce the expression of many target genes involved in the Endoplasmic-Reticulum Associated protein Degradation (ERAD), chaperone proteins production and ER membrane biosynthesis.

To investigate the activation of the IRE1 pathway during TBEV infection, qRT-PCR for XBP1 spliced mRNA was performed in a time course experiment. As shown in figure 3.16 XBP1 splicing takes place starting from 12 h p.i. As already demonstrated earlier in figure 3.15a, XBP1 mRNA expression slightly increases only at later time points (16-24 h p.i.) confirming that the measured increase in XBP1s form is specifically due to IRE1 activation and not to a general increase of XBP1 transcription.

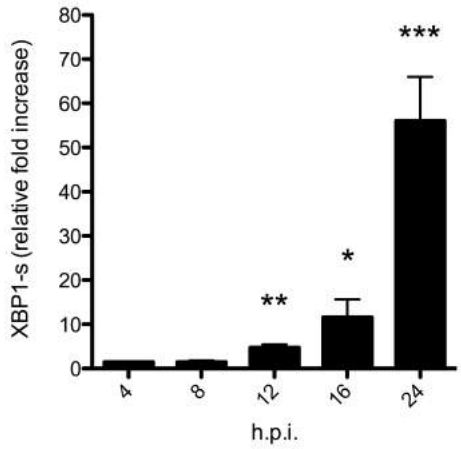

Figure 3.16 - XBP1 splicing occurs at 12 hours post infection. U2OS cells were infected with TBEV at a MOI of 1. At different time during infection cell lysates were collected and total RNA was isolated and retro-transcribed. qRT-PCR analysis for XBP1 spliced was performed. Expression levels are indicated as fold increase relative to 0 hours post infection (h p.i.). Data were averaged from two independent experiments and are represented as mean ± standard deviation. Significant *p*-value is calculated with paired *t*-test (* = $p < 0.05$; ** = $p < 0.01$; *** = $p < 0.001$).

Another method to evaluate splicing of XBP1 mRNA has been described in the work of (Hirota et al. 2006). A scheme of this procedure is reported in figure 3.17a. At the intron-exon junction, XBP1 mRNA contains the restriction site recognized by the enzyme PstI. This specific sequence is lost during the splicing of this mRNA. By PCR, a region of XBP1 mRNA containing the 26 nucleotides of the intron is amplified. The PCR product is then purified and digested with PstI. Finally, a 2% agarose gel is run in order to separate the different bands. The primer we choose for this test amplified a 255 bp amplicon of the unspliced XBP1 mRNA (XBP1u) and an amplicon of 229 bp of the spliced form. After digestion we would expect to obtain 2 different bands of 184 and 71 bp in the case of XBP1u-amplicon digestion and a unique band of 229 bp corresponding to XBP1s amplification product. In figure 3.17b is reported the result of this experiment. As we can see we always have the presence of a band of 255 bp probably indicating that the digestion with PstI was not 100% efficient. Nevertheless, the data obtained confirm the qRT-PCR results, i.e. IRE1 is activated at 12 h p.i. At 0 h p.i. as well as in mock infected samples, we only have XBP1u, correspondent to the 184 and 71bp bands. A little induction of splicing, corresponding to the appearance of the 229 bp band, occurs starting from 4 h p.i., but a significant increase occurred only at 12 h p.i. Starting from this time we can appreciate not only the increased signal of the band corresponding to XBP1s, 229 bp, but also a decreased signal of the 184 bp and 71 bp bands that almost disappear at 24 h p.i.

Altogether the data suggest that the IRE1 pathway of the UPR is activated early during infection, at 12 hours of infection or even earlier.

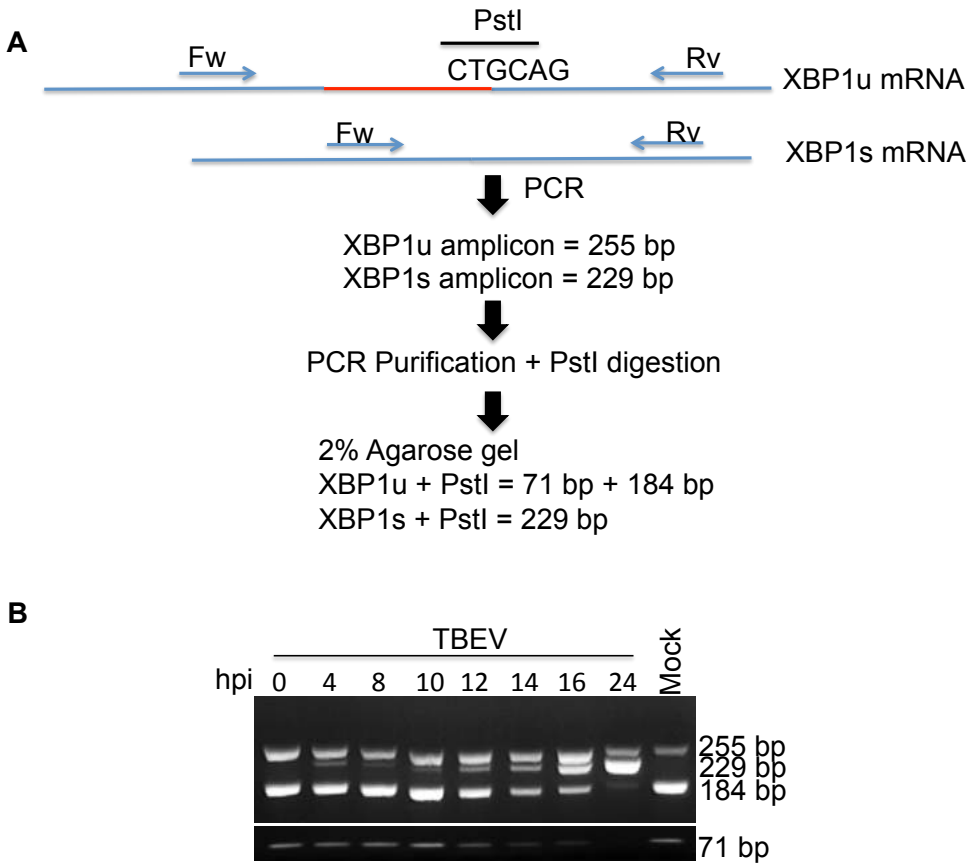

Figure 3.17 - XBP1 splicing analysis by PstI digestion. U2OS cells were infected with TBEV at a MOI of 1. At different time during infection cell lysates were collected and total RNA was isolated and retro-transcribed. A) Scheme of the analysis. By PCR amplicon spanning the intron (red) was amplified, purified and digested with PstI. B) 2% Agarose gel showing the products obtain by PCR and digestion. 255 bp, unspliced XBP1. 229 bp, spliced XBP1. 184+71 bp, unspliced XBP1 digested by PstI.

We then analyzed the expression of two genes downstream of XBP1s which resulted as upregulated in our RNA-Seq analysis, DNAJB9 and DNAJC3 (Lee, Iwakoshi, and Glimcher 2003). These are chaperones protein induced during ER stress that bind unfolded proteins in the lumen of the ER in order to contain the stress. Moreover, it has been demonstrated that DNAJC3 has an inhibitory effect on PERK activity (Yan et al. 2002), suggesting a negative feedback regulating the UPR.

Since we proved that XBP1 mRNA is spliced starting from 12 h p.i, it could be expected to see also early induction of these genes at 12 h p.i. but instead DNAJC3 (Figure 3.18a) is activated only at 24 h p.i. while DNAJB9 follow an upward trend, with a more significant increase at 24 h p.i. (Figure 3.18b).

Taken together these results demonstrate that the IRE1 pathway of the UPR is activated at 12 h p.i. an earlier time respect to activation of IFN response and SG formation.

Induction of genes regulated by the activation of this pathway might be delayed due to an unknown mechanism.

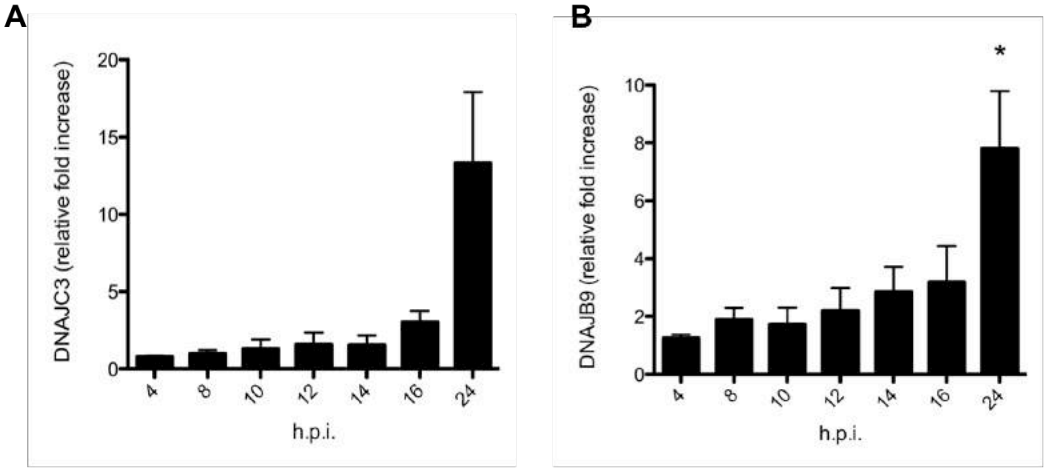

Figure 3.18 - DNAJC3 and DNAJB9 genes are induced during TBEV infection. U2OS cells were infected with TBEV at a MOI of 1. At different time during infection cell lysates were collected and total RNA was isolated and retro-transcribed. qRT-PCR analysis for DNAJC3 (A) and for DNAJB9 (B) were performed. Levels are expressed as fold increase relative to 0 hours post infection (h p.i.).Data were averaged from two independent experiments and are represented as mean ± standard deviation. Significant *p*-values were calculated with paired *t*-test (* = $p < 0.05$)

3.4.3 The PERK pathway of the UPR is activated at 12 h p.i.

At last, we studied activation of PERK during infection. PERK is the key protein of another branch of the UPR that is activated when BiP detach from its luminal domain to bind the unfolded proteins. When activated, PERK oligomerizes and phosphorylates itself and the initiation of translation factor eIF2α (Harding et al. 1999). As already mentioned above, eIF2α phosphorylation induces a block of translation. Selectively, cells hold the translation of those mRNA that are useful to recover from the stress, like heat-shock protein and chaperones. Moreover, phosphorylation of eIF2α induces the transcription of ATF4, a transcription factor that induces expression of UPR target genes like CHOP, involved in regulation of apoptosis, BiP and GADD34 that carry out

a negative feedback on this pathway regulating the activity of the phosphatase PP1 on eIF2α (Novoa et al. 2001).

WB analysis was performed with the anti-P-PERK antibody on samples obtained from a time course experiment of U2OS TBEV infected cells. As visible in figure 3.19, PERK is phosphorylated starting from 8h p.i. with a big increment of phosphorylation at 12-14 h p.i. Interestingly the level of phosphorylation is then decreased starting from 16 h p.i. As a control, a WB for PERK was also performed and no changes in total protein expression was evidenced. As loading control, an immunoblot with β-Catenin antibody was also performed.

The protein PERK is also a key regulator of the so called Integrated Stress Response (ISG), a cellular pathway regulated in cells by four different kinases that, depending on the stress, phosphorylate the initiation of translation factor that, as discussed previously, is able to induce formation of stress granules and inhibit cellular translation. The kinases involved in the activation of this response are: HRI, heme-regulated eIF2α kinase, that phosphorylates eIF2α in response to low levels of heme; GCN2, general control nonderepressible 2, activated when sensing aminoacid deprivation; PERK, Eukaryotic translation initiation factor 2-alpha kinase 3, described above and PKR, double-stranded RNA-activated protein kinase, that phosphorylates eIF2α upon recognition of viral RNA.

For our study we were particularly interested in understanding if the phosphorylation of eIF2α, and the subsequently formation of SG, during infection is due to PERK or PKR activity.

In figure 3.19 we report several WB of a time course experiment in which U2OS cells were infected with TBEV at a MOI of 1 and samples were collected at 0, 4, 8, 10, 12, 14, 16 and 24 h p.i. As controls anti-eIF2α and β-actin antibodies were used. Interestingly, when expression of P-PKR was analyzed, we found that phosphorylation, and subsequent activation, of this protein occurs at 16 h p.i. As controls PKR and β-Catenin antibodies were used as well as TBEV antibody as infection control.

These data suggest that both kinases are regulating the response during TBEV infection but in a time dependent manner. At early time of infection (8-12 h p.i.) eIF2α is phosphorylated by PERK and later during infection (from 16 h p.i.) PKR is responsible for the maintenance of the response.

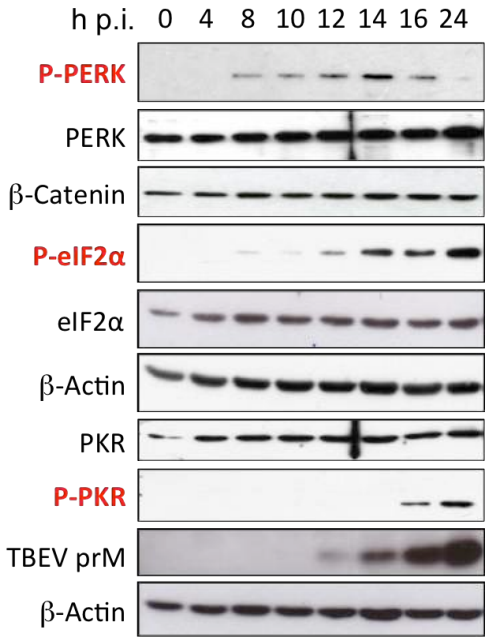

Figure 3.19 - eIF2a phosphorylation is regulated by both PERK and PKR during TBEV infection. U2OS cells were infected with TBEV at a MOI of 1. At different time during infection cell lysates were collected and immunoblotted for phosphorylated eIF2α (P-eIF2α), phosphorylated PERK (P-PERK) and phosphorylated PKR (P-PKR). Phosphorylated protein's blots are indicated in red. Immunoblot for total proteins eIF2α, PERK and PKR is also shown. and total PERK. Loading controls (b-Catenin and b-Actin) and infection control (prM) are also shown.

Since one of the most upregulated genes resulting from the RNA-Seq analysis was CHOP, a pro-apoptotic factor induced by ATF4 during stress, we performed a qRT-PCR analysis of its expression during TBEV infection. As we can see from figure 3.20a its expression is induced from 12 h p.i. This data is consistent with PERK activation.

Another direct target of ATF4 is the protein GADD34, which role is to recruit the serine/threonine-protein phosphatase PP1 to dephosphorylate the translation initiation factor eIF2α, thereby reversing the shut-off of protein synthesis initiated by stress-inducible kinases and facilitating recovery of cells. As we can see from figure 3.20b its expression is induced only at 24 hours post infection.

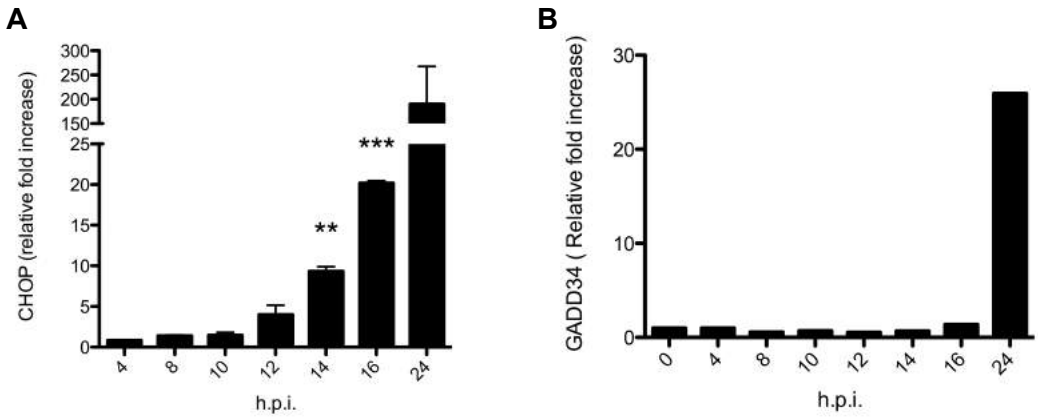

Figure 3.20 - CHOP and GADD34 genes are induced during TBEV infection. U2OS cells were infected with TBEV at a MOI of 1. At different time during infection cell lysates were collected and total RNA was isolated and retro-transcribed. qRT-PCR analysis for CHOP (A) and for GADD34 (B) were performed. Levels are expressed as fold increase relative to 0 hours post infection (h p.i.). Data for CHOP expression were averaged from two independent experiments and are represented as mean ± standard deviation. Significant *p*-value is calculated with paired *t*-test (** = $p < 0.01$; *** = $p < 0.001$). GADD34 expression levels are calculated from one single experiment and no statistical analyses were performed..

3.5 Early activation of the Unfolded Protein Response during TBEV infection trigger the IFN response

Recent reports have proposed a possible link between SG and IFN-β induction during viral infection (Onomoto et al. 2012) and indicate these cytoplasmic structures as platforms in which viral RNA and antiviral proteins interact and initiate the IFN response. Moreover, it has also been proved that UPR is able to induce IFN-β expression, as well as production of other cytokines, and that might play a key role in immune response during pathogens infection (Smith et al. 2008).

So far, our data demonstrate a clear involvement of UPR during TBEV infection and suggest a time-dependent regulation of eIF2α phosphorylation, and subsequent formation of SG and inhibition of translation, by the two cellular kinases PERK and PKR.

For these reasons we wanted to study if the UPR can actually be the cellular trigger for SG formation at 16 h p.i. and, more important, for IFN-β induction.

To answer these questions we performed a time course experiment with TBEV infected cells in which the UPR was activated earlier during infection by using Tunicamycin. Tunicamycin (TM) is a strong inducer of the unfolded protein response and its activity consist in inhibiting the glycosylation of newly synthesized glycoproteins.

A schematic representation of the experiment is reported in figure 3.21.

U2OS cells were plated in 12 well plates and 24 hours later were infected with TBEV at a MOI of 1. Mock-infected cells were also used. After one hour, cells were washed with PBS and medium was changed with complete medium (untreated samples) or medium containing 1 μg/ml Tunicamycin. Control cells, mock infected and not treated with TM were also used. Samples for RNA, immunofluorescence, WB and Plaque Assay were collected at 0, 4, 8, 12 and 24 h p.i.

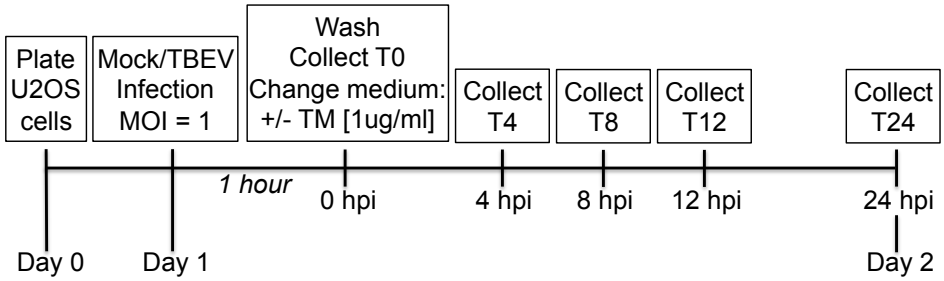

Figure 3.21 - TBEV infection in UPR preactivated cells: schematic drawing of experimental approach. U2OS cells were either infected with TBEV at a MOI of 1 or mock infected. After 1 hour cells were washed. At this time the samples correspondent to 0 hpi were collected. Medium additioned or not with 1 ug/ml Tunicamycin (TM) was added to the cells. At different time during infection RNA and protein samples as well as cell surnatants were collected and also samples were fixed for IF.

In order to verify the activation of the UPR by TM in our experiment we performed qRT-PCR analysis to detect splicing of XBP1. As we can see from figure 3.22a the combination of TBEV infection and treatment with TM (white bars) is inducing XBP1 splicing as early as 4 h p.i. while TBEV infection alone (black bars) induce this splicing only at 12 h p.i.. XBP1 total mRNA was also analyzed (Figure 3.22b) and we were able to see that its expression is increased early upon treatment with TM (4-8 h p.i.) but upon only infection is induced at later time point (24 h p.i.), as previously demonstrated.

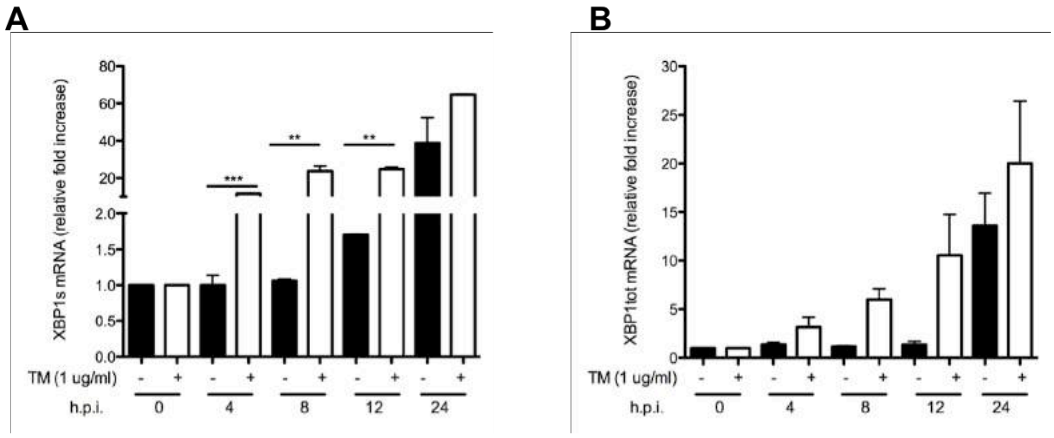

Figure 3.22 - XBP1 splicing is anticipated during TBEV infection in cells treated with tunicamycin. U2OS cells were infected with TBEV at a MOI of 1 and treated (white bars) or mock treated (black bars) with 1 mg/ml tunicamycin (TM). At different time during infection cell lysates were collected and total RNA was isolated and retro-transcribed. qRT-PCR analysis for XBP1s (A) and for XBP1 (B) were performed. Levels are expressed as fold increase relative to 0 hours post infection (h.p.i.). Data were averaged from two independent experiments and are represented as mean ± standard deviation. Significant *p*-value is calculated with paired *t*-test (** = $p < 0.01$; *** = $p < 0.001$).

Once established that the treatment with TM was anticipating the activation of the UPR in TBEV infected cells, we studied viral replication in cells infected and treated with the drug.

In figure 3.23a are reported the viral titers for samples treated (white bars) and not treated (black bars) with TM at different time point of infection. It is evident that early activation of the UPR, affect drastically TBEV replication.

In the graph of figure 3.23b we report qRT-PCR results for viral RNA. These data demonstrate that earlier UPR activation affects viral replication also at the level of RNA from earlier time of infection (8 h p.i.).

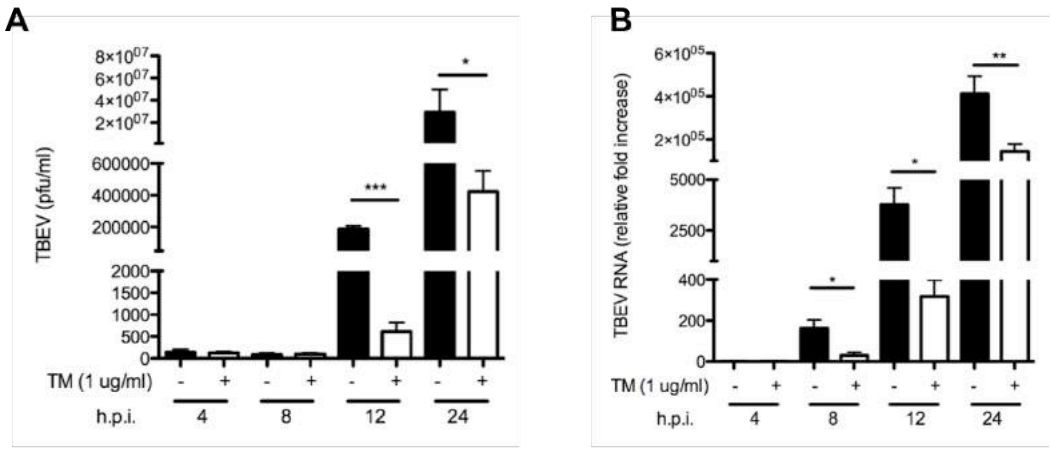

Figure 3.23 - TBEV replication is affected by early activation of the unfolded protein response. U2OS cells were infected with TBEV at a MOI of 1 and treated or mock treated with 1 mg/ml Tunicamycin (TM). At different time during infection cell supernatants and cell lysates were collected. Black bars show results of infected cells, white bars show results of TM treated and infected cells. A) Plaque assay analysis determining viral concentration (PFU/ml) during time. B) qRT-PCR analysis for TBEV RNA. Levels are expressed as fold increase relative to 0 hours post infection (h.p.i.). Data were averaged from two independent experiments and are represented as mean ± standard deviation. Significant *p*-value is calculated with paired *t*-test (* = $p < 0.05$; ** = $p < 0.01$; *** = $p < 0.001$).

As already mentioned before and in the introduction, activation of UPR itself can be sufficient to induce the IFN response (Smith et al. 2008). We tested this possibility in U2OS cells, not infected and treated with TM.

In figure 3.24a we report the qRT-PCR results for IFN-β mRNA expression upon treatment with tunicamycin (white bars) compare to mock-treated cells (black bars). As we can see, UPR activation was able to induce a little IFN-β mRNA expression starting from 8 hours of treatment, with a total of 7 fold increase after 24 hours. In untreated cells (black bars) IFN-β mRNA levels do not increase over the time.

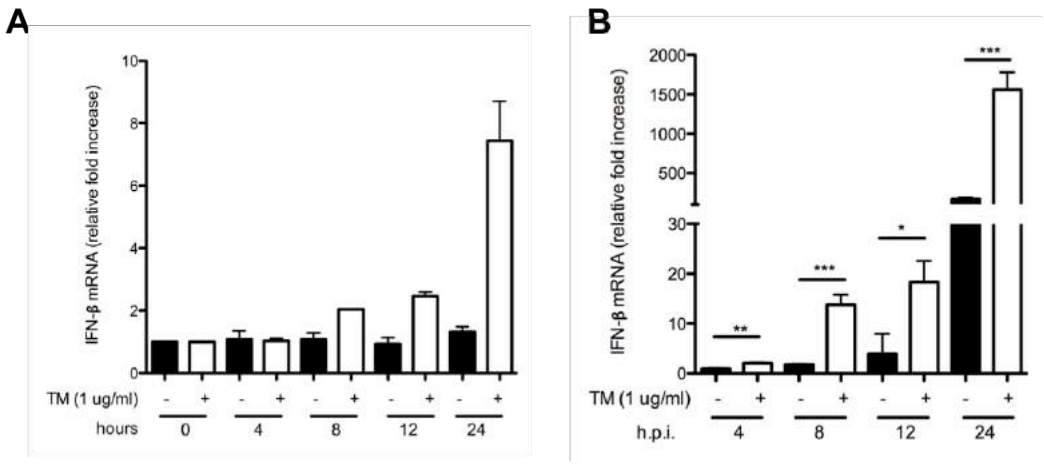

Figure 3.24 - IFN-β mRNA expression is induced by tunicamycin treatment and is affected during TBEV replication in UPR activated cells. A) U2OS cells were treated (white bars) or mock treated (black bars) with 1 mg/ml Tunicamycin (TM) and at different time of treatement cell lysates were collected and total RNA was isolated and retro-transcribed. qRT-PCR analysis for IFN-β was performed. B) U2OS cells were infected with TBEV at a MOI of 1 and treated or mock treated with 1 mg/ml Tunicamycin (TM). At different time during infection cell lysates were collected and total RNA was isolated and retro-transcribed. qRT-PCR analysis for IFN-β was performed. Levels are expressed as fold increase relative to 0 hours post infection (h.p.i.). Data were averaged from two independent experiments and are represented as mean ± standard deviation. Significant *p*-value is calculated with paired *t*-test (* = $p < 0.05$; ** = $p < 0.01$; *** = $p < 0.001$).

Since we demonstrated that UPR activation can regulate expression of IFN-β in U2OS cells and that upon activation of UPR the virus is replicating less efficiently, we wanted to see if this effect on the TBEV could be due to a different activation of the IFN response during this experiment. In figure 3.24b are shown the qRT-PCR results for IFN-β.

As expected, in infected but not treated samples (black bars) IFN-β mRNA levels increase only at late time point (24 h p.i.). Intringuingly, in samples infected and treated with TM (white bars) we were able to demonstrate that IFN-β mRNA expression not only start much earlier (8 h p.i.) but also at 24 h p.i. is much more induced, 1500 fold compare to 170.

All these data together suggest that the early activation of the UPR drastically affect TBEV replication due to a synergetic effect of antiviral proteins and UPR activation on IFN response.

3.5.1 Early activation of the Unfolded Protein Response during TBEV infection triggers the formation of stress granules.

As previously discussed, SG appear to be linked to the IFN response during infection. Since we saw that upon earlier activation of the UPR during TBEV infection we have an anticipation of the IFN response (8 h p.i.), we also wanted to study at what time SG are formed in this experiment. Cells infected and treated, or mock-treated, with TM were fixed at different time point and IF was performed using the anti-TBEV antibody and the anti-eIF3 as a marker for SG.

While in TBEV infected cells SG are formed at late time point (in this experiment they are visible at 24 h p.i. since 16 hours time point was not collected) we were able to see that formation of SG started at 8 h p.i. in cells that were both infected and treated with TM (Figure 3.25). Moreover, we noticed that at 24 h p.i. a larger number of cells were presenting SG compared to cells that were only infected reflecting the data about IFN-β expression that in TM treated and infected cells was much higher than in TBEV only infected cells (Figure 3.24b).

One more time, the formation of SG and the induction of the IFN-β expression are strictly linked during TBEV replication, suggesting a role for these cytoplasmic granules in the IFN response of the cells to the infection.

As a control we also performed IF analysis of U2OS cells treated with TM for different time (4, 8, 12 and 24 hours). Also in this case anti-eIF3 antibody was used in order to detect formation of SG. Interestingly, no SG were detectable at this time of treatment suggesting that UPR activation by itself is not sufficient to induce formation of SG. This data might counteract our hypothesis since upon TM treatment of U2OS cells we assist to a slight induction of IFN-β expression, but we also have to consider that, indeed, the levels of IFN induced by TM treatment are extremely low compare to the levels we record upon TBEV infection and so also the formation of SG can be extremely reduced and thus not detectable.

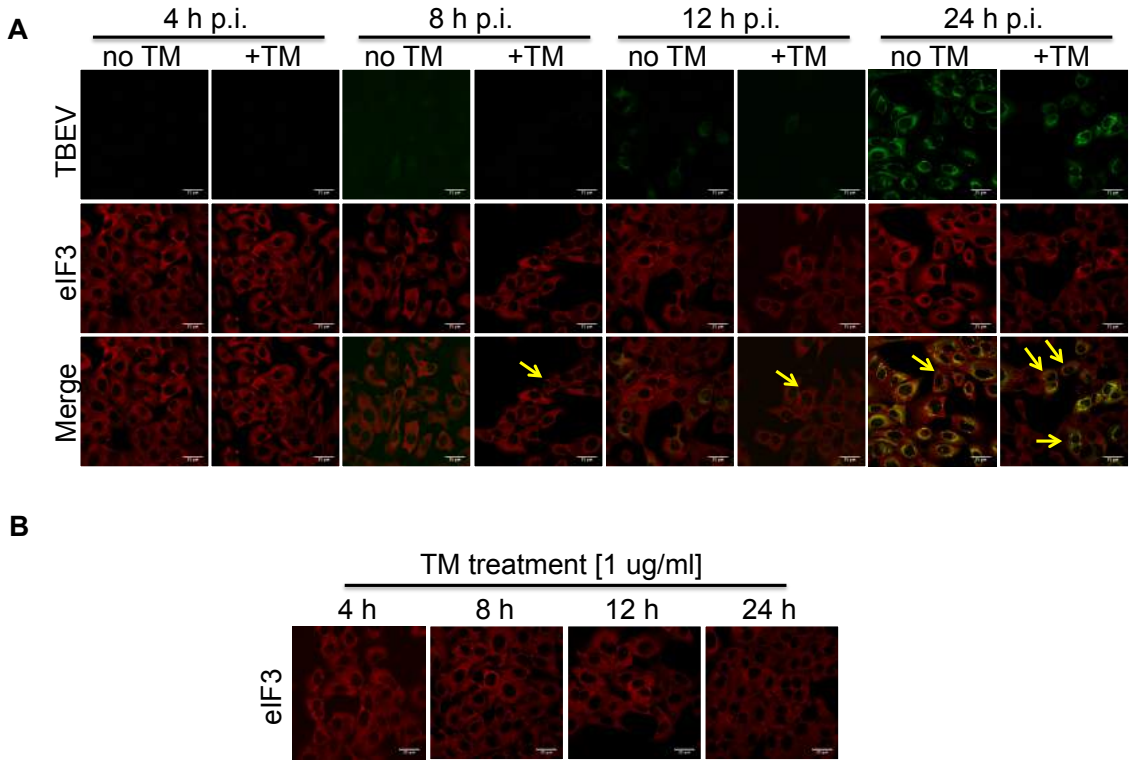

Figure 3.25 - Stress granules formation is induced earlier in UPR activated cells. A) U2OS cells were infected with TBEV at a MOI of 1 and treated or mock treated with 1 mg/ml Tunicamycin (TM). At different time during infection cell were fixed and immunostained with TBEV and eIF3 antibodies. Yellow arrows indicate cells containing SG. B) U2OS cells treated with 1 mg/ml Tunicamycin (TM) were fixed after different time of treatment and immunostained with eIF3 antibody. Scale bars represent 35 μm.

WB analyses were also performed for this experiment. From figure 3.26 is possible to appreciate how TM treatment drastically reduce the expression of TBEV proteins, indeed in infected cells TBEV protein E is detectable starting from 8 h p.i. but in cells that were both infected and treated with TM, the E protein of TBEV is detectable only from 12 h p.i. and at this time, as well as at 24 h p.i., its amount is drastically reduced. Anti-β-Actin antibody was used as loading control.

Afterwards we checked levels of phosphorylated eIF2α (P-eIF2α). In infected cells it is possible to detect P-eIF2α starting from 8-12 h p.i. and its level increase at 24 h p.i., confirming the data reported in figure 3.19.

In samples that were also treated with TM we assist to a rapid and strong phosphorylation of eIF2α, at 4 h p.i. that is then kept phosphorylated till 24 h p.i. where

is even possible to notice an increased in its level. As control anti-eIF2α and anti β-Actin antibodies were also used. The early and higher phosphorylation of eIF2α correlates with the early and more abundant formation of SG in these samples.

All these data together suggest a functional link between UPR and IFN response during TBEV infection. In particular, our experiments suggest that the Unfolded Protein Response could be responsible for the production of IFN-β and the formation of SG.

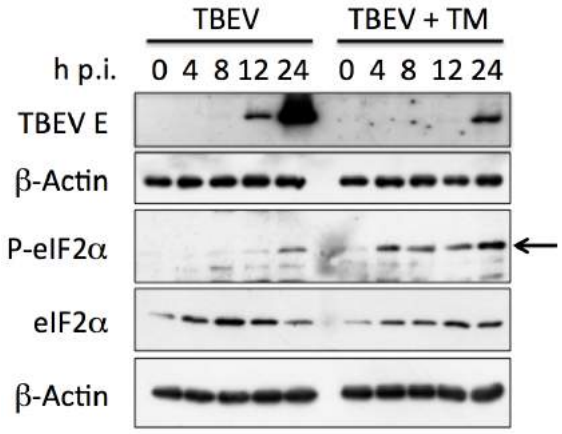

Figure 3.26 - Early activation of UPR affect viral replication and eIF2α phosphorylation. U2OS cells were infected with TBEV at a MOI of 1 and treated (TBEV + TM, right part) or mock treated (TBEV, left part) with 1 mg/ml Tunicamycin (TM). At different time during infection cell lysates were collected and immunoblotted for TBEV E protein (TBEV) and phosphorylated eIF2α (P- eIF2α). Immunoblot for total eIF2α and loading control (β-Actin) are also shown.

3.6 Localization study of the antiviral protein RIG-I during TBEV

So far we have evidence of a strict link between SG and the IFN response that are possibly both regulated by a synergic activity of the UPR with antiviral proteins belonging to the Pattern Recognition Receptors (PPR).

In the work of Onomoto (Onomoto et al. 2012), the authors described a new role for virus induced SG. In particular they characterized these cytoplasmic granules induced during influenza A virus (IAV) infection containing, not only the typical stress markers, like eIF3, but also antiviral proteins belonging to the PRR like RIG-I, MDA5, RNaseL, OAS and PKR as well as viral RNA, renaming them antiviral Stress Granules (avSG).

They also suggest that these specific avSG might work as a platform for recognition of viral RNA and induction of antiviral response.

In our group it has been previously demonstrated the essential role of the antiviral protein RIG-I in the induction of IFN response during TBEV infection (Miorin et al. 2012).

RIG-I, retinoic acid-inducible gene-I, is an antiviral protein belonging to the DExD/H box-containing RNA helicase family that has at its C-terminus a characteristic helicase domain responsible for the recognition of specific viral RNA. In particular, it has been shown that RIG-I can bind (5'-ppp)-containing viral RNA or short (≅ 30 bp) dsRNA (Hornung et al. 2006). The 11 kb TBEV genome contains a 5' Cap-1 structure (Brett D Lindenbach, Thiel, and Rice 2007) that is expected to mask the 5'-ppp structure necessary for RIG-I recognition. A possible modification of this 5' end, as well as the dsRNA replication intermediates or highly structured subgenomic fragments (sfRNA) produced during TBEV replication might be recognized by RIG-I during the first step of the antiviral response to TBEV infection. Moreover, in a recent work Weber and colleagues (Weber et al. 2013) demonstrate that RIG-I is capable to reacting to incoming viral nucleocapsid containing 5'ppp dsRNA structures of negative-strand RNA virus. This last observation suggests that RIG-I can recognize a wider set of viral RNA structures than what it was thought before.

3.6.1 RIG-I localize first with dsRNA in TBEV infected cells and later in stress granules.

In order to characterize the SG induced during TBEV infection U2OS cells were infected with a MOI of 1 and fixed for immunofluorescence analysis. G3BP1 antibody was used as marker of SG while RIG-I antibody was used to study the localization of this antiviral protein in infected cells.

As we can see from figure 3.27, at 24 h p.i. RIG-I localizes to SG marked by G3BP1. This data, for the first time, suggest a possible identification of TBEV induced SG as antiviral SG.

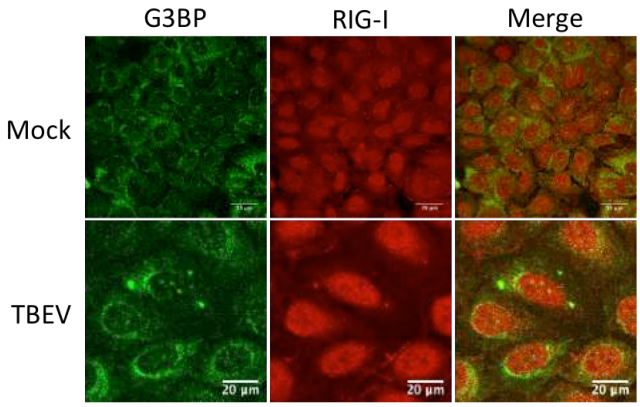

Figure 3.27 - RIG-I localize to TBEV induced stress granules. U2OS cells were either mock infected or infected with TBEV at a MOI of 1. At 24 hours post infection cells were fixed and immunostained with G3BP1 antibody to detect stress granules and RIG-I antibody to study localization of the antiviral protein. Scale bar: 20 μm.

Unfortunately, even if a more detailed characterization of these avSG induced by TBEV is required, all the antibodies in our hands for MDA5, PKR and P-eIF2α never worked in immunofluorescence experiments. Moreover, in this work we didn't have the possibility to perform RNA FISH analysis to analyze the presence of TBEV RNA in the avSG.

Since we have already demonstrated that SG formation during TBEV infection occurs at 16 h p.i. we wanted to investigate if RIG-I localization in avSG follow the same kinetic. For this purpose U2OS cells were infected with TBEV at a MOI of 1 and fixed for immunofluorescence analysis at 0, 4, 8, 10, 12, 14 and 16 h p.i. An antibody against dsRNA was used to study viral replication. From this experiment we were able to demonstrate that RIG-I localize to SG at 16 h p.i. (Figure 3.28), but more interestingly we found that at earlier time point (14 h p.i.) RIG-I is accumulating together with dsRNA in a perinuclear region, that we can assume to be the site of viral replication.

This is the first evidence of RIG-I localizing together with intermediates of TBEV replication. The different localization of RIG-I at 14 and 16 hours post infection might suggest that RIG-I is first recruited to viral replication sites while later translocate avSG.

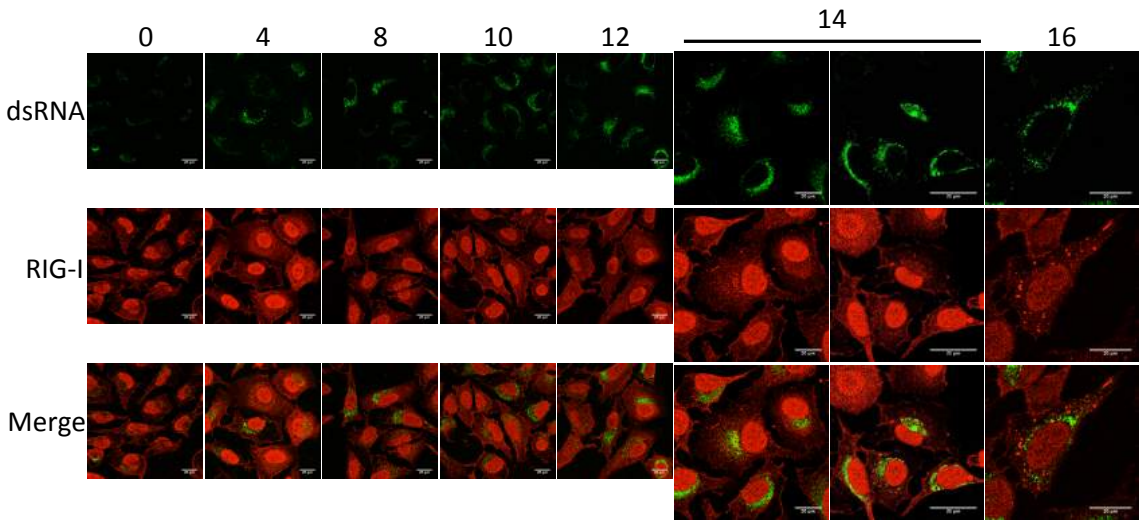

Figure 3.28 - During TBEV infection RIG-I localize first with TBEV dsRNA and lately in stress granules. U2OS cells were infected with TBEV at a MOI of 1. At 0, 4, 8, 12, 16 and 24 hours post infection (h.p.i.) cells were fixed and immunostained with dsRNA antibody to detect viral replication and RIG-I antibody to study localization of the antiviral protein during infection. Yellow arrows indicate colocalization of RIG-I with dsRNA. Scale bar: 20 μm.

3.6.2 Construction and characterization of U2OS_Flag-RIG-I cells

So far, the immunofluorescence analysis demonstrating RIG-I co-localization with dsRNA and SG were performed using an antibody recognizing specifically the C-terminal domain (CTD) of the protein RIG-I. This antibody required particular protocols to be used and sometimes showed aspecific signals. For these reasons we decided to produce a lentivector carrying the chimeric gene Flag-RIG-I (pWPI-Flag-RIG-I) to transduce U2OS cells in order to obtain cells stably expressing the chimeric protein Flag-RIG-I.

Details regarding the cloning method as well as the transduction protocol are reported in the Material and Methods section.

In figure 3.29a we show the results of a WB analysis of U2OS-Neo cells, control cells transduced with the empty lentivirus carrying only the resistance gene for neomycin, and U2OS_Flag-RIG-I cells, either infected or mock infected.

In the first blot we can appreciate how the expression of RIG-I is incresead in U2OS_Flag-RIG-I cells. For the second immunoblot an anti-Flag antibody was used to

evidence the expression of Flag-RIG-I protein in the engineered cells. Anti-TBEV and anti-β-actin antibodies were also used as controls.

We characterized these cells also by performing an IF analysis using anti-Flag and anti-RIG-I antibodies. From the analyses (Figure 3.29b) is clear that not all the cells express the chimeric protein but that in those cells expressing the chimeric protein, Flag-RIG-I has the same distribution as the endogenous one.

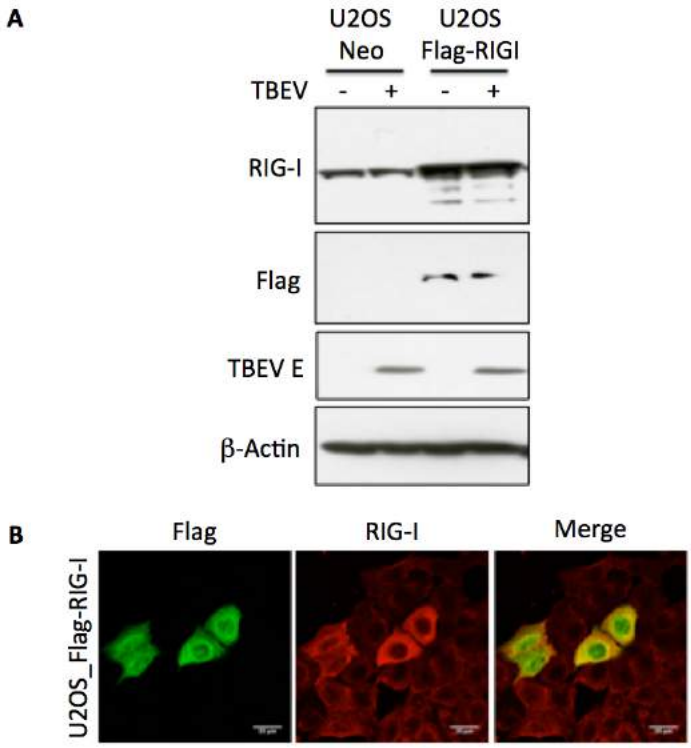

Figure 3.29 - Characterization of U2OS_Flag-RIG-I cells. A) U2OS_Flag-RIG-I and control cells U2OS_Neo were infected with TBEV at a MOI of 1. At different time during infection cell lysates were collected and immunoblotted with RIG-I and Flag antibodies. Immunoblot for infection and loading control are also shown (TBEV E and b-actin respectively). B) U2OS_Flag-RIG-I cells were fixed and immunostained with Flag and RIG-I antibodies to study efficiency of expression of the chimeric protein and its localization compare to the endogenous. Scale bars represent 35 μm.

RIG-I overexpression could be responsible of pre-activation of an antiviral-status that might inhibit the replication of TBEV. For this reason, and before continuing using these cells for our studies, we tested IFN-β mRNA levels, as well as TBEV replication, in U2OS_Flag-RIG-I mock or infected cells compare to the control cells U2OS_Neo.

Both cells population were infected, or mock infected, with TBEV at a MOI of 1 and RNA samples for this analysis were collected at 24 h p.i. As we can see from figure 3.30a, IFN-β levels in mock cells (grey bars) were comparable, as well as in infected cells (black bars). This data suggest that not only the antiviral response in U2OS_Flag-RIG-I cells was not pre-activated but also that upon TBEV infection the two population of cells were able to respond in the same way.

In figure 3.30b the result of the qRT-PCR analysis for TBEV replication in U2OS_Neo and Flag-RIG-I cells are shown. From this result we can demonstrate that TBEV replication is not affected by Flag-RIG-I overexpression.

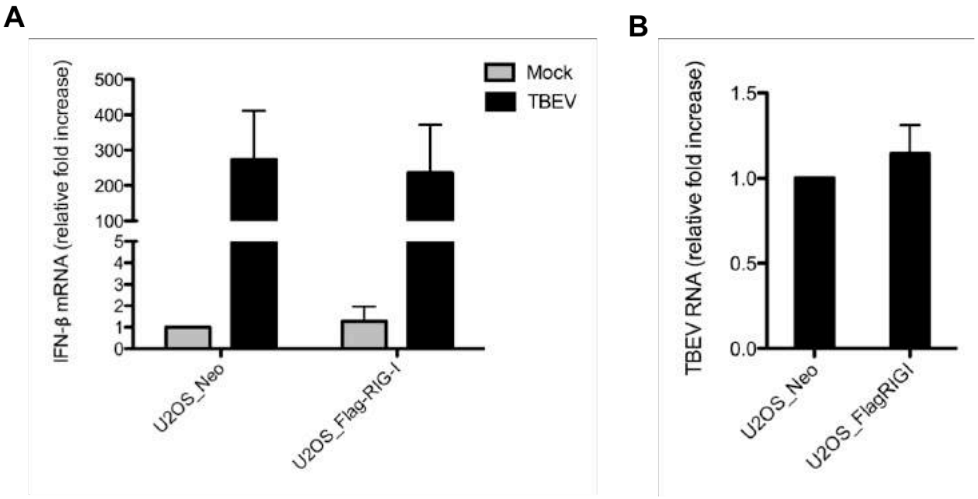

Figure 3.30 - IFN response and TBEV replication in U2OS_Flag-RIG-I cells. U2OS_Flag-RIG-I cells were infected (black bars), or mock infected (grey bars), with TBEV at a MOI of 1. At 24 hours post infection cell lysates were collected and total RNA was isolated and retro-transcribed. qRT-PCR analysis for IFN-b (A) and TBEV RNA (B) were performed. Levels are expressed as fold increase relative to U2OS_Neo. Data were averaged from two independent experiments and are represented as mean ± standard deviation.

This result might be due to the low number of cells (about 30%) in the population expressing the chimeric protein Flag-RIG-I.

Since, single cell analysis by IF do not require Flag-RIG-I expression in all cells, and moreover, a system in which IFN response is not affected by the overexpression of the chimeric protein is required, we continue our experiments with these cells.

3.6.3 Flag-RIG-I colocalize with TBEV in infected cells

In order to study the localization of Flag-RIG-I during infection U2OS_Flag-RIG-I and control cells U2OS_Neo were infected with TBEV at a MOI of 1 and fixed for immunofluorescence analyses at 24 h p.i. Anti-TBEV and anti-Flag antibodies were used.

Surprisingly no avSG containing Flag-RIG-I protein were found (Figure 3.31), suggesting that the chimeric protein could not be recruited to SG or that the amount of Flag-RIG-I in avSG is too low to be detectable by IF. On the other hand, co-localization of Flag-RIG-I with TBEV was visible in several cells confirming our previous data.

The last row of figure 3.31 shows IF images which were analysed for co-localisation using the Pearson's coefficient, also called Pearson's Correlation Coefficient (PCC). This coefficient is applied in microscopy to describe the degree of overlap between two signals (Manders, Verbeek, and Aten 1993). PCC calculation was performed with ImageJ software for selected region of interest. For values greater than 0.5 the two signals can be considered overlapped, co-localized.

These data confirm our previous observation (Figure 3.28) that RIG-I co-localizes together with TBEV at the sites of viral replication.

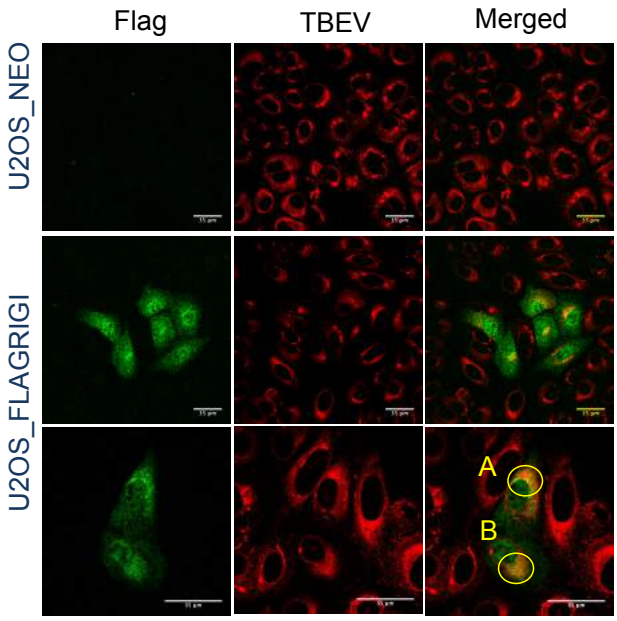

Figure 3.31 - Flag-RIG-I co-localize with TBEV during infection. U2OS_Flag-RIG-I and control U2OS_Neo cells were infected with TBEV at a MOI of 1. At 24 hours post infection cells were fixed and immunostained with Flag and TBEV antibodies. Circled in yellow are two point for which co-localization analyses was performed. Pearson's coefficient for the two points are 0,58 and 0,6 respectively for A and B.

3.7 Studying the activation status of RIG-I during TBEV infection

RIG-I binding to a target RNA triggers a conformational switch of the protein and its oligomerization. Usually RIG-I conforms to a closed structure, in which the CARD domain function is repressed due to interaction between the CTD and the helicase linker region. When viral infection produces short dsRNA or 5'ppp-RNA, these oligonucleotides bind the CTD in the presence of ATP and RIG-I changes its conformation and unmasks the CARD domain. CARD is able to interact with other CARD domains to form the RIG-I oligomers (Takahasi et al. 2008). This conformational switch is indicated by partial resistance to trypsin digestion and results in the generation of several fragments and in particular to a 30-kDa polypeptide (Saito et al. 2007).

In order to study the activation time of RIG-I during TBEV infection we took advantage of two different protocols reported in the work of Weber and colleagues (Weber et al. 2013).

3.7.1 Trypsin digestion indicates that RIG-I activation occurs at 8 hours of TBEV infection.

As explained above the conformational switch of RIG-I due to its activation makes the protein partially resistant to trypsin digestion.

We performed a time course experiment in which cells were either infected with TBEV at a MOI of 1 or mock infected and samples were collected at different time of infection: 0, 8, 10, 16 and 24 h p.i. In order to maintain the native conformation of the RIG-I protein, samples were collected with 0,5% Triton X-100 in PBS Native lysis buffer always working at 4°C. After sonication samples were centrifuged at 10000g for 10 minutes at 4°C and the supernatant was collected. Protein concentration was measured by the Bradford assay.

30 μg of protein from each sample were digested for 10 min at 37°C with 0.3 μg of trypsin. After the digestion samples were immediately mixed with Laemmli buffer, boiled and run in a 10% SDS PAGE.

As we can see from figure 3.32 at 0 h p.i. no differences between Mock and infected samples are visible. For both samples trypsin digestion was almost complete.

A first difference between mock and infected samples is visible at 8 h p.i. Here we can notice that at 8 h p.i. the infected sample result more resistant to trypsin, allowing

also the detection of the characteristic band at 30 kDa. Subsequently, at 10 and 16 h p.i. again no differences were evident. Finally, at 24 h p.i. a marked resistance to trypsin treatment was shown in the infected sample, where again we were able to detect the characteristic band at 30 kDa.

On the right part of the figure we report the WB analysis of RIG-I and TBEV levels in mock and TBEV infected samples collected at 24 h p.i. without trypsin digestion.

Due to the trypsin digestion the only loading control possible for this analysis is the Ponceau staining of the membrane, Figure 3.32b.

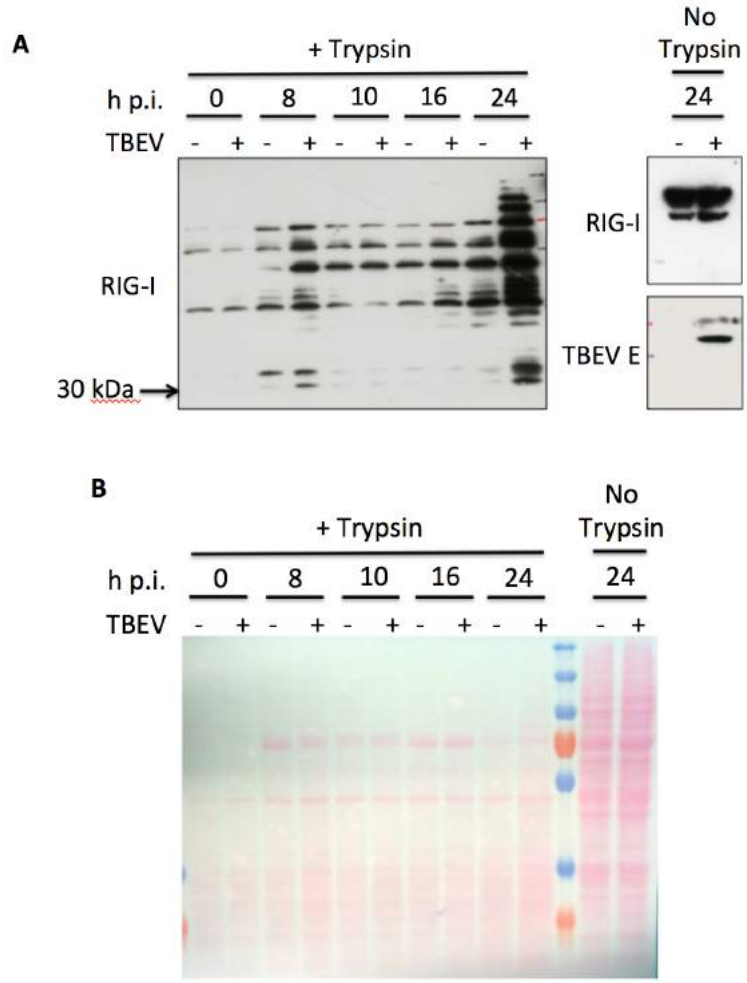

Figure 3.32 - RIG-I is activated early during infection with TBEV: the activated form is partially resistant to trypsin digestion. U2OS cells were infected, or mock infected, with TBEV at a MOI of 1. At different time of infection cell lysates were collected respecting the native condition and 30 mg of each sample digested with 0,3 mg Trypsin. A) Samples were immunoblotted with RIG-I antibody. Immunoblot with RIG-I and TBEV antibodies of samples collected at 24 hpi and not digested with trypsin are also shown. B) Ponceau staining of the membrane.

3.7.2 Native PAGE indicates RIG-I activation starting from 8 hours of TBEV infection.

Another way to test the activation status of RIG-I during infection is to perform a Native PAGE in order to assess its oligomerization, which occurs upon activation.

50 μg of cell lysates, the same collected for trypsin digestion assay, were loaded on a non-denaturing 8% polyacrylamide gel. As shown in figure 3.33 in TBEV infected samples RIG-I forms oligomers starting from 8 h p.i.

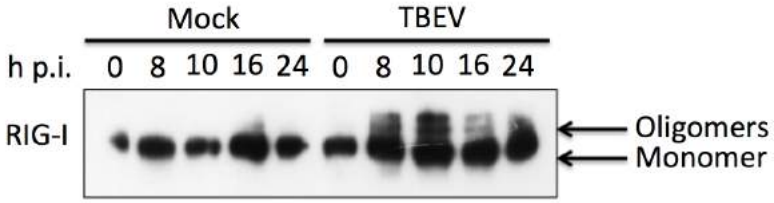

Figure 3.33 - RIG-I is activated early during infection with TBEV: the activated form is forming oligomers. U2OS cells were infected (TBEV, right part), or mock infected (Mock, left part), with TBEV at a MOI of 1. At different time of infection cell lysates were collected and loaded on a Native PAGE. Immunoblot with the RIG-I antibody was performed.

Taken together these results suggest that RIG-I is activated as early as 8 h p.i.

The experiment with trypsin suggests an oscillatory activation of RIG-I during the time of infection: the activation is visible at 8 h p.i. while at 10 and 16 h p.i. the WB suggest that RIG-I is not active, but at 24 h p.i. a pattern of bands suggesting the activation of the protein is again evident. On the other hand, the Native PAGE shows oligomerization of RIG-I starting at 8 h p.i. with no oscillatory pattern during the time of TBEV infection.

Even if both techniques demonstrate an early activation of RIG-I at 8 h p.i. the data obtained for 10 and 16 h p.i. points are discordant and for this reason further analysis has to be performed.

4 DISCUSSION

Flaviviruses are single-stranded RNA viruses with positive polarity. Viral RNA is directly translated into a single polyprotein, which is then cleaved into structural and non-structural proteins. Non-structural proteins induce rearrangements of cytoplasmic membranes leading to the formation of replication vesicles where viral RNA is replicated through a double-stranded RNA intermediate. It has been hypothesized that masking replication RNA intermediates within replication vesicles is a mechanism of viral escape from innate immunity mechanisms. Indeed, a delay between the appearance of such intermediates and the induction of interferon has been observed. However, the interferon response is nevertheless activated at later time points. In addition, cells respond to viral infection also by activating the stress-response, leading to a transient stop of translation and induction of stress granules. Studying the activation of these cellular responses and their possible crosstalk is becoming extremely important to better understand possible viral evasion or regulation mechanisms.

4.1 Main scope of this work

Previous studies performed in our lab (Miorin et al. 2012; Miorin et al. 2013) as well as by Overby and colleagues (Overby et al. 2010) have demonstrated that the IFN response to TBEV infection is delayed. Miorin and colleague demonstrated that the innate response to TBEV is RIG-I dependent and that its agonists are present in infected cells from early time of infection, as early as 8 h p.i., but are not able to trigger the response unless transfected as naked RNAs. Since viral proteins were unable to block the response (Overby et al. 2010), it has been proposed that the dsRNA of TBEV, an intermediate of viral replication, is sequestered into ER derived perinuclear vesicles, which would protect viral RNA from PRR recognition.

The cell responds to viral infection not only by activating the interferon response, but also by activating the stress response, which induce a transient arrest of translation. Recent studies suggest that the two pathways may be interconnected. For example, Onomoto and colleagues demonstrated that cells form SG upon infection with IAV and that these cytoplasmic aggregates contain viral RNA and antiviral proteins, which are involved in the activation of the IFN response during infection (Onomoto et al. 2012).

Despite initial observations that Flaviviruses did not induce SG, recent reports clearly showed that WNV (Courtney et al. 2012), HCV (Ruggieri et al. 2012) and TBEV (Albornoz et al. 2014) are indeed able to induce the formation of SG in infected cells.

Although a wealth of data described the induction of the stress and IFN responses in virally infected cells, very little is known about the timing of the events and their relationship. In particular, it is not clear how, where and when the PRR driven by the viral RNA intermediates are triggering their responses. During my doctoral studies I took the challenge of exploring these topics using TBEV as a model for flaviviral infection. I found that the major cellular pathway that is activated upon TBEV infection is the UPR. Activation of the UPR precedes both the IFN and stress response and, most importantly, appears to trigger them both. Furthermore, I could show that RIG-I is activated at early time points and localize to replication compartment before moving to SG during infection. These results provide a novel view of the cellular events that follow a viral infection, which may be extended to other viruses of the same family and beyond.

4.2 The IFN and stress responses are activated at the same time.

TBEV is able to induce SG upon phosphorylation of the initiation of translation factor eIF2α (Figure 3.1 and 3.4) (Albornoz et al. 2014). We also characterized this TBEV induced SG as *bona fide* SG, containing several typical SG's marker as G3BP1, eIF3 and eIF4B (FIG 3.1 and 3.2). The demonstration that a Flavivirus is able to induce SG is in agreement with similar recent studies on HCV (Ruggieri et al. 2012) and WNV (Courtney et al. 2012), but not with DENV (Emara and Brinton 2007). However it should be noticed that the suggestion that DENV was not capable of inducing SG was due to a TIA-1/TIAR staining, which we demonstrated to be recruited to replication sites during TBEV replication (Albornoz et al., 2014).

The percentage of infected cells showing SG was about 20%. Several could be the explanations for this phenotype. Courtney and colleagues suggested that it might depend on the pathogenicity of the virus used, since they demonstrated that natural lineages 1 and 2 of WNV do not induce SG during 24 hours of infection, but the infectious chimeric lineage 2/1 W956IC is able to induce SG in the first 12 hours of

infection. This chimeric virus is known to synthesize RNA faster during the early stages of replication and this characteristic correlates with the increase in SG formation and PKR activation. Ruggieri and colleagues demonstrated that formation of SG in HCV Huh-7 infected cells upon treatment with IFN-α is highly dynamic showing that SG are assembled and disassembled several times in a cell during a 24 hours infection experiment. Therefore, at a given time point the number of infected cells showing SG was always below 40%.

Also in our experiments the percentage of infected cells showing SG was always very low, about 20%, but we have to consider that the virus we are using in our experiments is TBEV strain Neudoerfl, a strain that has been demonstrated to be not as pathogenic as Hypr strain (Overby et al. 2010). For this reason we can speculate that with a different strain we could observe a higher percentage of cells presenting SG during TBEV infection.

Moreover, we did not have the possibility to perform a live cell imaging experiment to determine if, also during our experiment of infection, SG were showing an oscillatory behavior of assembly and disassembly. The major limitation is that the biosafety containment for TBEV is classified at the BL3 level, where we didn't have a live imaging station available. It is in our future plans to build a single-cycle recombinant virus to use in time-lapse microscopy experiments and determine the behavior of stress granules in TBEV infected living cells. This solution may be used to infect cells at BL2 level.

Finally, we should consider the fact that our analysis of SG formation stops at 24 h p.i., since we were mainly interested in early responses of the cell to the infection, but it might be that at later time points the percentage of cells presenting SG increases.

Notwithstanding the low number of infected cells showing SG, we could determine that these start to appear from 16 h p.i. (Figure 3.4). This data is extremely interesting since it demonstrates that the activation of the stress response during TBEV infection follows the same kinetic of the IFN response. Now we understand that both the stress and the IFN response are delayed during TBEV infection, suggesting that these two cellular responses are strictly interconnected and that other cellular events might play a key role in their activation

4.3 Whole genome transcriptome analysis reveals that the UPR is strongly activated upon TBEV infection.

Since we demonstrated that TBEV is abundantly replicating at 10 h p.i., when neither the IFN nor the stress response are activated, we decided to perform an RNA-Seq analysis of total cellular RNA of U2OS infected cells at these two critical time points of infection. After testing the integrity of the RNA (Figure 3.8) samples were sequenced. Thanks to the help of Dr.Danilo Licastro who performed for us the analyses of the raw data, we were able to understand the main differences in gene expression in infected cells at 24 h p.i. compared to 10 h p.i. As expected, and evidenced by the volcano plot of figure 3.9, we found that TBEV infection induces significant changes in the transcriptome of the cells.

We further analyzed these data with Ingenuity Pathway Analyses (IPA) and we found that the most significant pathway affected by TBEV infection is the Unfolded Protein Response. From the same analysis the Adipogenesis Pathway, the CDK5 Signalling Pathway as well as the Endoplasmatic Reticulum Stress resulted significantly affected. During our study we did not focus on these pathways, with the exception of the Endoplasmatic Reticulum Stress Pathway that share all the affected genes with the Unfolded Protein Response. It could be extremely interesting for future studies to analyse some of the genes involved in these other pathways. For example, we found that the gene SIRT2 in the adipogenesis pathway is up-regulated. SIRT2, NAD-dependent deacetylase Sirtuin-2, belongs to the Sirtuin proteins family that has been demonstrated to play a role as viral restriction factors (Koyuncu et al. 2014). In the same pathway we found XBP1s that has been studied in this work for its role in the UPR. However, several studies demonstrated that XBP1s is able to induces lipid biosynthesis in response to ER Stress (Sriburi et al. 2004), in order to increase the surface area and volume of the ER to better contain the stress. Since Flaviviruses are inducing lipid biosynthesis in order to increase ER membrane that is then required for the formation of replication sites (Heaton et al. 2010), it could be interesting to study if TBEV can positively regulate XBP1s in order to increase lipid biogenesis.

The CDK5 Signalling pathway is implicated in pathological degeneration of neurons and in particular the most up-regulated gene of this pathway is DRD1, a dopamine receptor in central nervous system that regulate neural growth and development. Among the down-regulated genes we found ITGA6, integrin-α6, and LAMB1, Laminin-β1,

both of them involved in regulating cell adhesion and neurite outgrowth. Knowing that TBEV infection induce a neuropathology characterized by encephalitis and that major hallmarks of the infection are neuroinflammation, neuronal death, and disruption of the blood-brain barrier (BBB), it would be extremely interesting to study the role of these genes in the pathogenesis of TBEV infection.

We next proceeded to the validation of the whole-genome transcriptome analysis by qRT-PCR of 9 up-regulated genes, 4 of them involved in the immune response to the infection and 5 involved in the UPR. The analysis was conducted with samples collected in an independent experiment.

The genes belonging to the UPR pathway that were chosen for the validation are: CHOP, XBP1s, DNAJC3, DNAJB9 and EDEM1. We found for their expression a very good agreement between RNA-Seq and qRT-PCR analyses, suggesting high accuracy of the transcriptome analyses.

Among the genes belonging to the immune response induced by the infection we decided to validate: IFIT2, IFIT3, IL8 and OASL. In this case we encountered several problems. In the RNA-Seq analyses IL8 and OASL were induced with a fold change of about 5 and 2 respectively, while during our qRT-PCR analyses we found an induction of approximately 80 and 20 fold changes. Concerning IFIT2 and IFIT3 expressions, we were never able to demonstrate their increased expression, while in the RNA-Seq they showed about 20 folds change induction. We also tried to perform the qRT-PCR on the same RNA samples that we used for the RNA-Seq analyses but also in this case we were not able to reproduce the data (data not show). We strongly doubt that the error is in the RNA-Seq since the data about these two genes are extremely significant, and also activation of this ISG during infection has been already demonstrated. More likely, the problem is due to the primer design. Several splicing variants have been identified for these genes and there might be discrepancy between the splicing variants found up-regulated by the RNA-Seq analysis and the ones for which our primers were designed. Since we decided to focus on the UPR we didn't investigate this aspect further.

4.3.1 The Unfolded Protein Response is activated before the Stress and IFN responses during TBEV infection.

TBEV, as other Flaviviruses, during its replication induce rearrangements of the host cell membranes originating from the ER. It has been demonstrated that ER membrane

reorganization is driven by flaviviral non-structural proteins, which induce not only changes in the protein composition of ER membranes but also in their lipid content (Heaton et al. 2010). The main non-structural proteins involved in membrane remodeling are NS4A (Miller et al. 2007) and NS4B (Kaufusi et al. 2014). As already mentioned before, in these complexes of rearranged membranes TBEV synthesizes new viral genomes that are then enclosed into virions that maturates in the Golgi complex along the secretory pathway. It is then evident that the interaction of TBEV, and more in general of Flaviviruses, with the ER during the viral life cycle is really strong and that ER plays a key role during infection.

For this reason it is not surprising that pathways such as the ER Stress and Unfolded Protein Response are activated during TBEV replication. Indeed, several are the reports that already demonstrate the activation of these pathways during Flaviviruses infection. However, what differentiates my work from that of others is the kinetics of activation.

4.3.2 All three pathways of the UPR are activated upon TBEV infection.

ATF6

The most accurate way to test activation of the ATF6 pathway is to investigate the cleavage of the protein and its nuclear localization. Since we didn't have an antibody for the detection of endogenous ATF6 we developed an alternative strategy. U2OS cells were transfected with a plasmid encoding EGFP-ATF6 (Chen, Shen, and Prywes 2002). Expression of EGFP-ATF6 was first evaluated by cytofluorimetric analyses (Figure 3.13), which revealed that about 52% of the cells were expressing the chimeric protein. The risk of this strategy is that overexpression of ATF6 might be able by itself to induce activation of the UPR, but we found that, in mock samples, only a low number of cells (8%) displayed nuclear translocation of ATF6 (Figure 3.14). From the time course experiment we found that infection with TBEV induce EGFP-ATF6 translocation from 8 h p.i. in about 15% of cells, and the number increase to 25% till 24 h p.i. (Figure 3.14). Moreover we found that XBP1 and BiP expression, which are strongly regulated by ATF6, are both induced at 16 h p.i. (Figure 3.15). We conclude that the ATF6 branch of the UPR is activated early during infection, between 8 and 16 h p.i.

Several published papers demonstrate that Flavivirus infection triggers the activation of ATF6 but, as it could be expected, the time of activation differs a lot between

different viruses. In particular, Pena (Peña and Harris 2011) and Yu (C.-Y. Yu et al. 2006) demonstrated that DENV-2 infection of 2fTGH and N18 cells induces the proteolitic cleavage of ATF6 at, respectively, 48 and 20 h p.i. On the other hand Ambrose (Ambrose and Mackenzie 2011) demonstrated that WNV_{KUN} infection induce activation of ATF6 branch of the UPR by qRT-PCR analyses of XBP1 and BiP expression and they proved that it occurs between 12-18 h p.i., similarly to what we have shown. Finally, Yu and colleagues (C. Yu, Achazi, and Niedrig 2013) demonstrated that TBEV infection of Vero cells induce ATF6 activation. First they checked nuclear translocation of EGFP-ATF6 upon infection but didn't succeed, then they tested the proteolitic cleavage of the protein by direct detection with a specific antibody. In this last experiment they showed activation of ATF6 at 24 h p.i. This data is not discordant with our since they did not performed a time course analysis of ATF6 activation during TBEV infection but they tested only one single time of infection.

For the first time we provided the evidence that also TBEV, as well as WNV (Ambrose and Mackenzie 2011), triggers the activation of ATF6 early during infection.

IRE-1

In this work we demonstrated, both by qRT-PCR analysis of XBP1 mRNA splicing (Figure 3.16) and by PstI digestion of XBP1 mRNA (Hirota et al. 2006) (Figure 3.17), that during TBEV infection the IRE1 pathway of the UPR is activated at 12 h p.i. Since splicing of XBP1 mRNA is a direct effect of IRE-1 activation we do not consider necessary to perform a WB for P-IRE-1 but obviously it can be a good experiment, together with XBP1s WB or nuclear translocation. The fact that TBEV is inducing splicing of XBP1 mRNA has already been demonstrated by Yu and colleagues (C. Yu, Achazi, and Niedrig 2013), but their analysis was performed only at 24 h p.i., not providing the information of the specific time of activation of this pathway. On the other hand, several reports on different Flaviviruses demonstrate that this branch of the UPR is activated early during infection: WNV_{KUN}, DENV2 and JEV induce XBP1 splicing at 12 h p.i (Ambrose and Mackenzie 2011; Peña and Harris 2011; C.-Y. Yu et al. 2006).

Afterwards, we demonstrate that the XBP1s target genes DNAJB9 and DNAJC3 are induced later during infection (Figure 3.18). In particular a small but not significant increase of DNAJC3 is detectable at 16 h p.i. and become more evident at 24 h p.i. while DNAJB9 show a little induction during the infection with a significant increase at

24 h p.i. Interestingly, also Yu and colleagues (C.-Y. Yu et al. 2006) demonstrated that these two chaperone proteins, during JEV and DENV2 infection, are induced only at 24 h p.i. while, TM treatment of N18 cells induce expression of these XBP1 target genes already after 6 hours of treatment. The reason of this delay during Flavivirus infection has not yet been studied, but it might be interesting to understand if it is due to a direct regulation of the virus.

PERK

Finally, we studied PERK activation during TBEV infection. PERK is one of the kinases, together with PKR, belonging to the Integrated Stress Response, an ancient stress response known to modulate the recover from different kind of stress. For this reason, while studying activation of PERK we also investigate the activation of PKR and the phosphorylation of the initiation of translation factor eIF2α.

We found that both PERK and eIF2α are phosphorylated starting from 8 h p.i. but that PERK phosphorylation is then negatively regulated by 16 h p.i. At this time P-PKR starts to be detectable by WB (Figure 3.19). These data indicate a time dependent regulation of eIF2α phosphorylation during TBEV infection by these two kinases.

It has been demonstrated that DNAJC3 has an inhibitory effect on the kinase activity of PERK (Yan et al. 2002). We have shown that DNAJC3 is slightly induced at 16 h p.i. (Figure 3.18) thus, we can speculate that its induction is regulating PERK activation during TBEV infection and, once PERK activity is inhibited, PKR takes over the phosphorylation of eIF2α.

As already discussed above, we demonstrated that SG formation occurs at 16 h p.i. Although two independent studies (Courtney et al. 2012; Ruggieri et al. 2012) have demonstrated that SG formation upon WNV and HCV infection is PKR dependent, we couldn't demonstrate in our system if SG formation depends on PERK, PKR or both. Furthermore, we demonstrated that CHOP and GADD34, both of which are direct target of ATF4, a transcription factor translated upon PERK activation, are activated during TBEV infection at 14 and 24 h p.i. respectively (Figure 3.20). The induction of these genes was described also upon infection with DENV2 (Umareddy et al. 2007) but in that case they studied their induction only at 24 h p.i. CHOP is known to mediate apoptosis and it has been demonstrated to play an important role in limiting WNV growth (Medigeshi et al. 2007). Interestingly, even if CHOP is induced early during

TBEV infection we never had evidences of an active programmed cell death, indeed, from our experience, cells can resist to TBEV infection for at least 72 hours (data not shown). We did not focus on this cellular response but it might be interesting to investigate this pathway in order to understand if TBEV is able to block or delay this cellular response. Interestingly, Clavarino and colleagues (Clavarino et al. 2012) have recently demonstrated that GADD34 expression is a direct consequence of PKR activation and dsRNA sensing. In their study they concluded that GADD34 and PKR are necessary to produce anti-viral cytokines during CHIKV infection. Since we saw a late induction of GADD34 it might be that this gene is regulated by PKR during TBEV infection instead of the PERK pathway. This hypothesis should be further investigated.

In the paper of Ambrose (Ambrose and Mackenzie 2011) it is shown that WNV_{KUN} infection of Vero cells does not induce strong phosphorylation of eIF2α. On the other hand Pena (Peña and Harris 2011) demonstrated that DENV2 infection leads to phosphorylation of eIF2α at 9 h p.i. but at later time the phosphorylation of this factor is negatively regulated. These data suggest that both WNV and DENV2 are regulating PERK pathway during infection. Interestingly, they both took advantage of MEF $PERK^{-/-}$ cells demonstrating that viral replication in absence of PERK is more efficient, suggesting an antiviral role of PERK during flavivirus replication.

Our hypothesis is that PERK is responsible of eIF2α phosphorylation during TBEV infection and consequently the responsible of SG induction. As we already discussed above, SG might have a critical role in the induction of the IFN response. For this reason we want to test TBEV replication in cells lacking PERK and, in particular, we want to study if SG induction and IFN response are affected in these cells.

During my doctorate studies, I tried to obtain stable U2OS cells expressing shPERK (data not shown). Unfortunately, even if several shRNAs against PERK were used I never succeed in obtaining an efficient knock down of PERK, and, consequently, I have never been able to see an effect on TBEV replication in these cells. We are now considering to use MEF $PERK^{-/-}$ or to produce U2OS PERK KO by using the CRISPR/Cas9 technology.

To conclude, we demonstrated that TBEV induce activation of the UPR at early time during infection, between 8 and 12 h p.i. Indeed, at 8 h p.i. we were able to detect a

weak signal for viral proteins both by IF and WB (Figure 3.25 and 3.26) suggesting that this is the time when viral proteins start accumulating in the ER, inducing activation of the unfolded protein response.

Furthermore, we also have to consider that the UPR during TBEV infection could induce ER membrane rearrangements typical of TBEV replication. Miorin and colleagues (Miorin et al. 2013) demonstrated by FRAP experiments that the viral RNA is secluded into compartments that are not accessible by the EYFP-MS2 protein starting from 12 hours post electroporation (h p.e.) of the TBEV replicon carrying the MS2 repeats, suggesting that in the period between 6 and 12 h p.e. the ER membrane start to be rearranged. We do not know if during infection the ER membranes are reorganized at this time since EM experiments on TBEV infected cells describing these structures were performed at 24 h p.i. (Miorin et al. 2013) or even later (Bílý et al. 2015). Nevertheless, we can speculate that during TBEV infection the rearrangements of the ER membranes follow a similar kinetic since in this range of time we observe the induction of the unfolded protein response.

4.4 Early activation of the UPR induce early IFN-β expression and SG formation

4.4.1 The Unfolded Protein Response triggers IFN-β expression during TBEV infection

After demonstrating that the UPR is activated in TBEV infected cells at earlier time of infection compared to the IFN response and SG formation, we investigate the possible role of the UPR in triggering these cellular responses. It is known that the UPR is involved in the development of immune cells and that it is implicated in several inflammatory conditions (J. A. Smith 2014). What remains unclear is its role in the induction of IFN.

By treating the cells with tunicamycin at the time of infection we obtained an early (4 h.p.i) activation of the UPR in TBEV infected cells (Figure 3.22). We demonstrated that TBEV replication is drastically affected by early activation of the UPR (Figure 3.23) and that in this condition IFN-β mRNA expression is induced at 8 h p.i. instead of 16 (Figure 3.24 b). Indeed, Smith and colleagues demonstrated that UPR induction by thapsigargin or tunicamycin in mouse macrophage cells is able to induce expression of IFN-β at low levels. When the same cells treated with these UPR inducers were

stimulated with LPS the IFN response was extremely enhanced compared to the situation in which the cells were only stimulated with LPS (Smith et al. 2008). In figure 3.24a we demonstrate that tunicamycin treatment of U2OS cells is sufficient to induce about 7 fold increase in IFN-β mRNA levels after 24 hours of treatment, while, in cells that were both treated with the drug and infected with TBEV the levels of IFN-β mRNA were 100 times higher than in cells that were only infected (Figure 3.24b).

With this experiment we were able to demonstrate for the first time that activation of the UPR in TBEV infected cells is able to trigger and amplify the IFN response, confirming the synergistic activity of these responses suggested by Smith (Smith et al. 2008).

Interestingly, a recent report (Cho et al. 2013) showed that exposure of human intestinal cell lines with cholera toxins induces inflammatory response and activation of IRE1. They demonstrated that IRE1 is required for the induction of inflammatory cytokine but XBP1s is dispensable for this process since the inflammatory response depends on the regulated IRE1α-dependent decay of mRNA (RIDD). The endonuclease domain of IRE1 has similar catalytic mechanisms of the protein RNaseL, which is able to produce RNA fragments that activate RIG-I. Cho and colleagues were able to demonstrate that the RIDD activity of IRE1 produced mRNA fragments that are recognized by RIG-I, but not MDA5, and induce the IFN response. We are considering the possibility that IRE1-RIDD activity might be responsible for the production of PRR agonists able to activate RIG-I during TBEV infection. For this reason, we are planning a time course infection experiment where RIDD will be specifically inhibited.

Moreover, we know that PRR agonists are present in the cells from early time of infection but they are not accessible to RIG-I recognition (Miorin et al. 2012). We already discussed the role of the UPR in lipid synthesis and speculate about the possibility that activation of UPR might coincide with ER membrane rearrangements in TBEV infected cells. We should consider also the possibility that the activation of the UPR might induce changes in the structure of these membranes vesicles where the virus is replicating and thus unmask the PRR agonists making them available for RIG-I recognition and activation, explaining why an earlier induction of this cellular response can activate early IFN response.

4.4.2 The Unfolded Protein Response triggers SG formation during TBEV infection

From the same experiment we demonstrated that not only IFN-β induction occurs at earlier time points of infection but that formation of SG in these conditions is triggered at 8 h p.i. as well (Figure 3.25) with phosphorylation of eIF2α starting at 4 h p.i. (Figure 3.26). This data is further confirming our hypothesis of a functional link between the UPR, the IFN response and the SG formation.

We know that both PERK and PKR are regulating the phosphorylation of eIF2α during TBEV infection in a time dependent manner. It could be hypothesized that early activation of PERK by TM treatment is inducing early formation of SG that will serve as platform for the IFN response as proposed by Fujita and collaborators (Onomoto et al. 2012).

It would be extremely interesting to repeat this experiment in MEF PERK$^{-/-}$ cells or in condition of PERK inhibition to evaluate if also TBEV replication is affected in these cells but also to measure at what time occurs SG formation in absence of PERK and, more important, if this affects the IFN response.

Tunicamycin is an inhibitor of N-glycosilation of newly synthesized peptides. It is known that for some Flavivirus the envelope protein is highly glycosylated (Brett D Lindenbach, Thiel, and Rice 2007). For this reason, it could be objected that the effect on TBEV replication upon tunicamycin treatment is due to misfolding of E protein, even if this would not explain the effect on IFN response and SG formation that we have demonstrated. To rule this out, we will repeat this experiment using a different drug, thapsigargin, a non-competitive inhibitor of the sarco/endoplasmic reticulum Ca^{2+} ATPase.

To conclude, with this experiment we have demonstrated the existence of a strong link between the unfolded protein response, the IFN response and the stress response, during TBEV replication. It would be extremely interesting to understand if this is a specific characteristic of TBEV replication or if it is a common issue of Flaviviruses. For this reason we already started to perform experiment with WNV (NY99) and DENV-2.

4.5 RIG-I activation occurs early during TBEV infection but is not sufficient to induce IFN response

4.5.1 RIG-I localize first to viral replication sites and later to SG during TBEV infection.

As previously discussed, the group of Fujita suggested an innovative role for SG in immune response during IAV infection (Onomoto et al. 2012) as platforms where the antiviral proteins recognize the viral RNA and activate the IFN response, renaming them antiviral SG (avSG). In the last part of this work we demonstrated that RIG-I localize in the SG starting from 16 h p.i. but that around 14 h p.i. some co-localization of RIG-I with dsRNA at viral replication sites was observed (Figure 3.28). In order to confirm this data and to exclude the possibility that what we were seeing was an artifact due to an unspecific activity of anti RIG-I antibody, we create U2OS cells expressing the chimeric protein Flag-RIG-I. After characterization of these cells by IF, WB and qRT-PCR analyses of IFN-β mRNA levels in mock condition and upon TBEV infection (Figure 3.29 and figure 3.30), the data regarding the co-localization of RIG-I with TBEV were confirmed (Figure 3.31). These data suggest that RIG-I is first recruited to viral replication sites where it might bind viral RNA, and then to SG where it activates the IFN response.

Despite the evidence of a correlation between RIG-I localization and IFN-β induction, we need to better characterize these TBEV induced SG in order to define them as avSG. In particular we should investigate if they contains other antiviral proteins like MDA5 and PKR and, above all, if they contains viral RNA. Indeed, during our IF experiments we were not able to detect any viral dsRNA in SG but we have to consider the limit of the IF analyses for which single dsRNA molecules could not be evidenced by the antibody. Moreover, other forms of viral RNA could be recruited to SG during infection. A possible solution could be to perform an RNA FISH on viral RNA (vRNA) to visualize if even single vRNA molecules are contained in SG.

Finally, as performed by Onomoto an colleagues, to prove that the TBEV induced SG are platforms from which the IFN response is triggered, we should be able to inhibit SG formation during TBEV infection and analyze IFN-β mRNA levels. One possibility that we are considering could be to infect the eIF2αA/A mutant cells (Scheuner et al. 2001) in which the protein eIF2α is phosphorylation deficient.

4.5.2 RIG-I activation occurs early during TBEV infection but is not sufficient to induce IFN-β expression

As already explained before, once that RIG-I binds a target RNA, that is commonly considered to be a short dsRNA or a 5'ppp-RNA, it changes its conformation unmasking the CARD domain that through interaction with other CARD domains induce oligomerization of the protein (Takahasi et al. 2008). This conformational switch is indicated by partial resistance to trypsin digestion, which results in the generation of several fragments and in particular of a 30-kDa polypeptide (Saito et al. 2007).

By performing trypsin digestion and Native PAGE (Figure 3.32 and 3.33) of samples collected during a time course infection experiment, we could demonstrate that an early activation of RIG-I occurs already at 8 h p.i. Unfortunately, the results of the two tests were partially discordant. In fact, the trypsin digestion indicates a possible oscillation of the activation status of RIG-I that was resistant to trypsin digestion only at 8 h p.i. and 24 h p.i. but not at intermediate times, while the Native PAGE showed oligomers from 8 h p.i. that are then conserved till 24 h p.i. Obviously, the experiments have to be repeated in order to confirm the data on the activation of RIG-I at 8 h p.i. and to understand if RIG-I is really following an oscillatory activation pathway during TBEV infection.

We know that PRR agonists are produced in infected cells at early time points but likely they remain hidden in the ER membrane rearrangements till later time of infection (Miorin et al. 2012). From our results it seems that RIG-I is activated early during infection but that this activation is not sufficient to trigger the induction of IFN-β that in fact occurs only at 16 h p.i. Moreover, even if we know that RIG-I is the only PRR responsible of IFN-β induction during TBEV infection of U2OS cells (Miorin et al. 2012), which kind of PAMP is produced and recognized by RIG-I during TBEV infection remains unknown. For this reason a RIP-seq analysis could be performed at different time of TBEV infection pulling down RIG-I and analyzing which RNA are bound to the antiviral proteins.

Finally, as suggested by the data of Cho and colleagues (Cho et al. 2013), RIG-I might be activated also by fragments of endogenous mRNA digested by RIDD activity of IRE-1, for this reason we should study activation status of RIG-I also in condition of UPR activation, and in condition of RIDD inhibition as well.

4.6 Conclusions and important remarks

In this doctorate study I have worked on several aspects of the cellular response to TBEV infection. We have quickly understood that more important than knowing which cellular responses are activated upon TBEV infection is to define the time of their activation in order to study their possible crosstalk. Figure 4.1 shows a schematic diagram of all the events described in this work that take place during the first 24 hours of TBEV replication.

We demonstrated that both IFN response and SG formation are delayed during viral replication, till 16 h p.i. but, thanks to the modern technique of RNA-seq, we were able to identified the unfolded protein response as early cellular response during TBEV infection. It has now become more important to understand if the induction of IFN-β is depending on the SG formation induced by UPR activation and which form of viral or host RNA is recognized by RIG-I to activate the IFN response.

For the first time in the field of Flavivirus, we determine that the UPR is responsible of triggering the expression of IFN-β and the formation of SG during TBEV infection. What remains to define is if this is a characteristic cellular response to TBEV or if it is a general issue for Flavivirus infected cells.

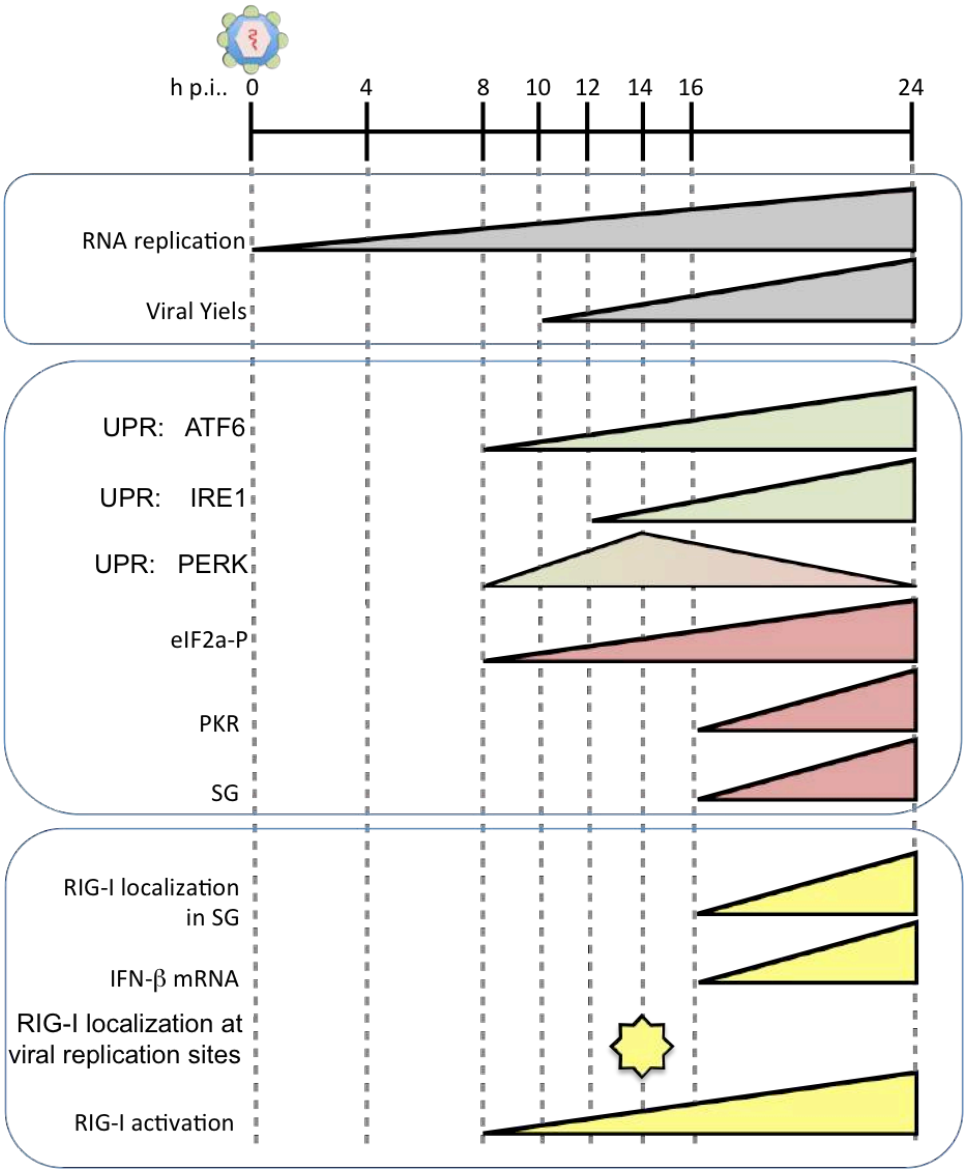

Figure 4.1 - Schematic diagram of all the events occurring during TBEV infection described in this work.

Albornoz Amelina, Tea Carletti, Gianmarco Corazza, and Alessandro Marcello. 2014. "The Stress Granule Component TIA-1 Binds Tick-Borne Encephalitis Virus RNA and Is Recruited to Perinuclear Sites of Viral Replication To Inhibit Viral Translation." *Journal of Virology* 88 (12) (June 15): 6611–6622. doi:10.1128/JVI.03736-13.

Alvarez Diego E., Maria F Lodeiro, Silvio J Luduen, Lia I Pietrasanta, and Andrea V Gamarnik. 2005. "Long-Range RNA-RNA Interactions Circularize the Dengue Virus Genome." *Journal of Virology* 79 (11): 6631–6643. doi:10.1128/JVI.79.11.6631.

Amberg Sean M, Ann Nestorowicz, David W McCourt, and Charles M Rice. 1994. "NS2B-3 Proteinase-Mediated Processing in the Yellow Fever Virus Structural Region: In Vitro and in Vivo Studies." *Journal of Virology* 68 (6) (June): 3794–802.

Ambrose Rebecca L, and Jason M Mackenzie. 2011. "West Nile Virus Differentially Modulates the Unfolded Protein Response to Facilitate Replication and Immune Evasion." *Journal of Virology* 85 (6) (March): 2723–32. doi:10.1128/JVI.02050-10.

Anderson Paul and Nancy Kedersha. 2002. "Stressful Initiations." *Journal of Cell Science* 115 (16) (August 15): 3227–34.

Anderson Paul and Nancy Kedersha. 2006. "RNA Granules." *The Journal of Cell Biology* 172 (6) (March 13): 803–8. doi:10.1083/jcb.200512082.

Ashour Joseph, Maudry Laurent-Rolle, Pei-Yong Shi, and Adolfo García-Sastre. 2009. "NS5 of Dengue Virus Mediates STAT2 Binding and Degradation." *Journal of Virology* 83 (11) (June): 5408–18. doi:10.1128/JVI.02188-08.

Avirutnan Panisadee, Anja Fuchs, Richard E Hauhart, Pawit Somnuke, Soonjeon Youn, Michael S Diamond, and John P Atkinson. 2010. "Antagonism of the Complement Component C4 by Flavivirus Nonstructural Protein NS1." *The Journal of Experimental Medicine* 207 (4) (April 12): 793–806. doi:10.1084/jem.20092545.

Baum Alina, Ravi Sachidanandam, and Adolfo Garcia-Sastre. 2010. "Preference of RIG-I for Short Viral RNA Molecules in Infected Cells Revealed by next-Generation Sequencing." *Proceedings of the National Academy of Sciences of the United States of America* 107 (37): 16303 – 16308. doi:10.1073/pnas.1100561108.

Beatty P Robert, Henry Puerta-Guardo, Sarah S. Killingbeck, Dustin R. Glasner, Kaycie Hopkins, and Eva Harris. 2015. "Dengue Virus NS1 Triggers Endothelial Permeability and Vascular Leak That Is Prevented by NS1 Vaccination." *Science Translational Medicine* 7 (304): 1–11.

Best Sonja M, Keely L Morris, Jeffrey G Shannon, Shelly J Robertson, Dana N Mitzel, Gregory S Park, Elena Boer, James B Wolfinbarger, and Marshall E Bloom. 2005. "Inhibition of Interferon-Stimulated JAK-STAT Signaling by a Tick-Borne Flavivirus and Identification of NS5 as an Interferon Antagonist." *Journal of Virology* 79 (20): 12828–12839. doi:10.1128/JVI.79.20.12828.2005.

Bílý Tomáš, Martin Palus, Luděk Eyer, Jana Elsterová, Marie Vancová, and Daniel Růžek. 2015. "Electron Tomography Analysis of Tick-Borne Encephalitis Virus Infection in Human Neurons." *Scientific Reports* 5: 10745. doi:10.1038/srep10745.

Bressanelli Stéphane, Karin Stiasny, Steven L Allison, Enrico a Stura, Stéphane Duquerroy, Julien Lescar, Franz X Heinz, and Félix a Rey. 2004. "Structure of a Flavivirus Envelope Glycoprotein in Its Low-pH-Induced Membrane Fusion Conformation." *The EMBO Journal* 23 (4) (February 25): 728–38. doi:10.1038/sj.emboj.7600064.

Caracciolo Ilaria, Matteo Bassetti, Giorgio Paladini, Roberto Luzzati, Daniela Santon, Maria Merelli, Giovanni De Sabbata, Tea Carletti, Alessandro Marcello, and Pierlanfranco D'Agaro. 2015. "Persistent Viremia and Urine Shedding of Tick-Borne Encephalitis Virus in an Infected Immunosuppressed Patient from a New Epidemic Cluster in North-Eastern Italy." *Journal of Clinical Virology* 69: 48–51. doi:10.1016/j.jcv.2015.05.019.

Chakrabarti Anirikh, Aaaron W Chen, and Jeffrey D. Varner. 2011. "A Review of the Mammalian Unfolded Protein Response." *Biotechnology and Bioengineering* 108 (12): 2777–2793. doi:10.1002/bit.23282.A.

Chambers, Thomas J, Chang S Hahn, Ricardo Galler, and Charles M Rice. 1990. "Flavivirus Genome Organization, Expression, and Replication." *Annual Review of Microbiology* 44: 649–88.

Chen, Xi, Jingshi Shen, and Ron Prywes. 2002. "The Luminal Domain of ATF6 Senses Endoplasmic Reticulum (ER) Stress and Causes Translocation of ATF6 from the ER to the Golgi." *Journal of Biological Chemistry* 277 (15): 13045–13052. doi:10.1074/jbc.M110636200.

Chmelík Václav, Ales Chrdle, and Daniel Ruzek. 2016. “Fatal Tick-Borne Encephalitis in an Immunosuppressed 12-Year-Old Patient.” *Journal of Clinical Virology* 74: 73–74. doi:10.1016/j.jcv.2009.05.033.

Cho Jin a, Ann-Hwee Lee, Barbara Platzer, Benedict C S Cross, Brooke M Gardner, Heidi De Luca, Phi Luong, et al. 2013. “The Unfolded Protein Response Element IRE1α Senses Bacterial Proteins Invading the ER to Activate RIG-I and Innate Immune Signaling.” *Cell Host & Microbe* 13 (5) (May 15): 558–69. doi:10.1016/j.chom.2013.03.011.

Chu P W, and E G Westaway. 1985. “Replication Strategy of Kunjin Virus: Evidence for Recycling Role of Replicative Form RNA as Template in Semiconservative and Asymmetric Replication.” *Virology* 140 (1) (January 15): 68–79.

Clavarino Giovanna, Nuno Cláudio, Thérèse Couderc, Alexandre Dalet, Delphine Judith, Voahirana Camosseto, Enrico K Schmidt, et al. 2012. “Induction of GADD34 Is Necessary for dsRNA-Dependent Interferon-β Production and Participates in the Control of Chikungunya Virus Infection.” *PLoS Pathogens* 8 (5) (January). doi:10.1371/journal.ppat.1002708.

Courtney S C, S V Scherbik, B M Stockman, and M Brinton. 2012. “West Nile Virus Infections Suppress Early Viral RNA Synthesis and Avoid Inducing the Cell Stress Granule Response.” *Journal of Virology* 86 (7) (April): 3647–57. doi:10.1128/JVI.06549-11.

Daffis Stephane, Kristy J Szretter, Jill Schriewer, Jianqing Li, Soonjeon Youn, John Errett, Tsai-Yu Lin, et al. 2010. “2’-O Methylation of the Viral mRNA Cap Evades Host Restriction by IFIT Family Members.” *Nature* 468 (7322) (November 18): 452–6. doi:10.1038/nature09489.

Deonarain R, A Alcamí, M Alexiou, M J Dallman, D R Gewert, and a C Porter. 2000. “Impaired Antiviral Response and Alpha/beta Interferon Induction in Mice Lacking Beta Interferon.” *Journal of Virology* 74 (7) (April): 3404–9.

Egloff Marie-pierre, Delphine Benarroch, Barbara Selisko, Jean-louis Romette, and Bruno Canard. 2002. “An RNA Cap (Nucleoside-2’-O-)Methyltransferase in the Flavivirus RNA Polymerase NS5: Crystal Structure and Functional Characterization.” *EMBO Journal* 21 (11): 2757–2768.

Emara Mohamed M, and Margo a Brinton. 2007. “Interaction of TIA-1/TIAR with West Nile and Dengue Virus Products in Infected Cells Interferes with Stress Granule Formation and Processing Body Assembly.” *Proceedings of the National Academy of Sciences of the United States of America* 104 (21) (May 22): 9041–6. doi:10.1073/pnas.0703348104.

Erbel Paul, Nikolaus Schiering, Allan D’Arcy, Martin Renatus, Markus Kroemer, Siew Pheng Lim, Zheng Yin, Thomas H Keller, Subhash G Vasudevan, and Ulrich Hommel. 2006. “Structural Basis for the Activation of Flaviviral NS3 Proteases from Dengue and West Nile Virus.” *Nature Structural & Molecular Biology* 13 (4) (April): 372–3. doi:10.1038/nsmb1073.

Falgout B, M Pethel, Y M Zhang, and C J Lai. 1991. “Both Nonstructural Proteins NS2B and NS3 Are Required for the Proteolytic Processing of Dengue Virus Nonstructural Proteins.” *Journal of Virology* 65 (5) (May): 2467–75.

Ferlenghi Ilaria, Mairi Clarke, Twan Ruttan, Steven L Allison, Juliane Schalich, Franz X Heinz, Stephen C Harrison, Felix A Rey, and Stephen D Fuller. 2001. “Molecular Organization of a Recombinant Subviral Particle from Tick-Borne Encephalitis Virus Henry Wellcome Building for Genomic Medicine.” *Molecular Cell* 7: 593–602.

Fernandez-Garcia Maria-Dolores, Michela Mazzon, Michael Jacobs, and Ali Amara. 2009. “Pathogenesis of Flavivirus Infections: Using and Abusing the Host Cell.” *Cell Host & Microbe* 5 (4) (April 23): 318–28. doi:10.1016/j.chom.2009.04.001.

Gething Mary-Jane. 1999. “Role and Regulation of the ER Chaperone BiP.” *Seminars in Cell & Developmental Biology* 10 (5): 465–472. doi:10.1006/scdb.1999.0318.

Gillespie Leah K, Antje Hoenen, Gary Morgan, and Jason M Mackenzie. 2010. “The Endoplasmic Reticulum Provides the Membrane Platform for Biogenesis of the Flavivirus Replication Complex.” *Journal of Virology* 84 (20) (October): 10438–47. doi:10.1128/JVI.00986-10.

Gould E A, and T Solomon. 2008. “Pathogenic Flaviviruses.” *Lancet* 371 (9611): 500–509. doi:10.1016/S0140-6736(08)60238-X.

Guirakhoo F, RA Bolin, and JT Roehrig. 1992. “The Murray Valley Encephalitis Virus prM Protein Confers Acid Resistance to Virus Particles and Alters the Expression of Epitopes within the R2 Domain of E Glycoprotein.” *Virology* 191 (2) (December): 921–31.

Guyatt Kimberley J, Edwin G Westaway, and Alexander A Khromykh. 2001. "Expression and Purification of Enzymatically Active Recombinant RNA-Dependent RNA Polymerase (NS5) of the Flavivirus Kunjin." *Journal of Virological Methods* 92 (1) (March): 37–44.

Harding Heather P, Yuhong Zhang, Anne Bertolotti, Huiqing Zeng, and David Ron. 2000. "Perk Is Essential for Translational Regulation and Cell Survival during the Unfolded Protein Response." *Molecular Cell* 5: 897–904.

Harding Heather P, Yuhong Zhang, David Ron. 1999. "Protein Translation and Folding Are Coupled by an Resident Kinase." *Nature* 397 (January).

Harding Heather P., Yuhong Zhang, Huiquing Zeng, Isabel Novoa, Phoebe D. Lu, Marcella Calfon, Navid Sadri, et al. 2003. "An Integrated Stress Response Regulates Amino Acid Metabolism and Resistance to Oxidative Stress." *Molecular Cell* 11 (3): 619–633. doi:10.1016/S1097-2765(03)00105-9.

Heaton Nicholas S, Rushika Perera, Kristi L Berger, Sudip Khadka, Douglas J Lacount, Richard J Kuhn, and Glenn Randall. 2010. "Dengue Virus Nonstructural Protein 3 Redistributes Fatty Acid Synthase to Sites of Viral Replication and Increases Cellular Fatty Acid Synthesis." *Proceedings of the National Academy of Sciences of the United States of America* 107 (40): 17345–17350. doi:10.1073/pnas.1010811107.

Hirota Morihiko, Masato Kitagaki, Hiroshi Itagaki, and Setsuya Aiba. 2006. "Quantitative Measurement of Spliced XBP1 mRNA as an Indicator of Endoplasmic Reticulum Stress." *The Journal of Toxicological Sciences* 31 (2) (May): 149–56.

Holden Katherin L., and Eva Harris. 2004. "Enhancement of Dengue Virus Translation: Role of the 3V Untranslated Region and the Terminal 3V Stem-Loop Domain." *Virology* 329: 119–133.

Hornung Veit, Hiroki Kato, Hendrik Poeck, Shizuo Akira, Karl-klaus Conzelmann, and Martin Schlee. 2006. "5'-Triphosphate RNA Is the Ligand for RIG-I." *Science Reports* 314: 994 – 997. doi:10.1126/science.1132505.

Kang Dong-chul, Rahul V Gopalkrishnan, Qingping Wu, Eckhard Jankowsky, Anna Marie Pyle, and Paul B Fisher. 2002. "Mda-5: An Interferon-Inducible Putative RNA Helicase with Double-Stranded RNA-Dependent ATPase Activity and Melanoma Growth-Suppressive Properties." *Proceedings of the National Academy of Sciences of the United States of America* 99 (2): 637–42. doi:10.1073/pnas.022637199.

Kato Hiroki, Shintaro Sato, Mitsutoshi Yoneyama, Masahiro Yamamoto, Satoshi Uematsu, Kosuke Matsui, Tohru Tsujimura, et al. 2005. "Cell Type-Specific Involvement of RIG-I in Antiviral Response." *Immunity* 23 (1) (July): 19–28. doi:10.1016/j.immuni.2005.04.010.

Katoh Hiroshi, Toru Okamoto, Takasuke Fukuhara, Hiroto Kambara, Eiji Morita, Yoshio Mori, Wataru Kamitani, and Yoshiharu Matsuura. 2013. "Japanese Encephalitis Virus Core Protein Inhibits Stress Granule Formation through an Interaction with Caprin-1 and Facilitates Viral Propagation." *Journal of Virology* 87 (1) (January): 489–502. doi:10.1128/JVI.02186-12.

Katze Michael G, Yupeng He, and Michael Gale. 2002. "Viruses and Interferon: A Fight for Supremacy." *Nature Reviews. Immunology* 2 (9) (September): 675–87. doi:10.1038/nri888. http://www.ncbi.nlm.nih.gov/pubmed/12209136.

Kaufman Randal J. 2002. "Orchestrating the Unfolded Protein Response in Health and Disease." *Journal of Clinical Investigation* 110 (10): 1389–1398. doi:10.1172/JCI200216886.The.

Kaufmann Bärbel, and Michael G Rossmann. 2011. "Molecular Mechanisms Involved in the Early Steps of Flavivirus Cell Entry." *Microbes and Infection / Institut Pasteur* 13 (1) (January): 1–9. doi:10.1016/j.micinf.2010.09.005.

Kaufusi Pakieli H., James F. Kelley, Richard Yanagihara, and Vivek R. Nerurkar. 2014. "Induction of Endoplasmic Reticulum-Derived Replication-Competent Membrane Structures by West Nile Virus Non-Structural Protein 4B." *PloS One* 9 (1): e84040. doi:10.1371/journal.pone.0084040.

Kawai Taro, and Shizuo Akira. 2006. "Innate Immune Recognition of Viral Infection." *Nature Immunology* 7 (2) (February): 131–7. doi:10.1038/ni1303.

Kedersha Nancy, Samantha Chen, Natalie Gilks, Wei Li, Ira J Miller, Joachim Stahl, and Paul Anderson. 2002. "Evidence That Ternary Complex (eIF2-GTP-tRNA iMet) Deficient Preinitiation Complexes Are Core Constituents of Mammalian Stress Granules." *Molecular Biology of the Cell* 13 (January): 195–210. doi:10.1091/mbc.01.

Kedersha Nancy L, Mita Gupta, Wei Li, Ira Miller, and Paul Anderson. 1999. "RNA-Binding Proteins TIA-1 and TIAR Link the Phosphorylation of eIF-2a to the Assembly of Mammalian Stress Granules." *Journal of Cell Biology* 147 (7): 1431–1441.

Khromykh Alexander A, Hedije Meka, Kimberley J Guyatt, and Edwin G Westaway. 2001. "Essential Role of Cyclization Sequences in Flavivirus RNA Replication." *Journal of Virology* 75 (14): 6719–6728. doi:10.1128/JVI.75.14.6719.

Kimball S R, M J Clemens, V J Tilleray, R C Wek, R L Horetsky, and L S Jefferson. 2001. "The Double-Stranded RNA-Activated Protein Kinase PKR Is Dispensable for Regulation of Translation Initiation in Response to Either Calcium Mobilization from the Endoplasmic Reticulum or Essential Amino Acid Starvation." *Biochemical and Biophysical Research Communications* 280 (1) (January 12): 293–300. doi:10.1006/bbrc.2000.4103.

King Nicholas J C, Daniel R Getts, Meghann T Getts, Sabita Rana, Bimmi Shrestha, and Alison M Kesson. 2007. "Immunopathology of Flavivirus Infections." *Immunology and Cell Biology* 85 (1) (January): 33–42. doi:10.1038/sj.icb.7100012. http://www.ncbi.nlm.nih.gov/pubmed/17146465.

Koyuncu Emre, B A, Hanna G. Budayeva, A, Yana V. Miteva, A, Dante P. Ricci, et al. 2014. "Sirtuins Are Evolutionarily Conserved Viral Restriction Factors." *The American Society for Microbiology* 5 (6): 1–10. doi:10.1128/mBio.02249-14.Editor.

Kümmerer Beate M, and Charles M Rice. 2002. "Mutations in the Yellow Fever Virus Nonstructural Protein NS2A Selectively Block Production of Infectious Particles." *Journal of Virology* 76 (10): 4773–4784. doi:10.1128/JVI.76.10.4773.

Lee Ann-hwee, Neal N Iwakoshi, and Laurie H Glimcher. 2003. "XBP-1 Regulates a Subset of Endoplasmic Reticulum Resident Chaperone Genes in the Unfolded Protein Response XBP-1 Regulates a Subset of Endoplasmic Reticulum Resident Chaperone Genes in the Unfolded Protein Response." *Molecular and Cellular Biology* 23 (21): 7448–7459. doi:10.1128/MCB.23.21.7448–7459.2003.

Li W, Y Li, N Kedersha, P Anderson, M Emara, K M Swiderek, G T Moreno, M A Brinton, and J V Irol. 2002. "Cell Proteins TIA-1 and TIAR Interact with the 3' Stem-Loop of the West Nile Virus Complementary Minus-Strand RNA and Facilitate Virus Replication." *Journal of Virology* 76 (23): 11989–12000. doi:10.1128/JVI.76.23.11989.

Lin Ren-Jye, Bi-Lan Chang, Han-Pang Yu, Ching-Len Liao, and Yi-Ling Lin. 2006. "Blocking of Interferon-Induced Jak-Stat Signaling by Japanese Encephalitis Virus NS5 through a Protein Tyrosine Phosphatase-Mediated Mechanism." *Journal of Virology* 80 (12) (June): 5908–18. doi:10.1128/JVI.02714-05.

Lindenbach B D, and C M Rice. 1999. "Genetic Interaction of Flavivirus Nonstructural Proteins NS1 and NS4A as a Determinant of Replicase Function." *Journal of Virology* 73 (6) (June): 4611–21.

Lindenbach Brett D, Heinz-Jurgen Thiel, and Charles M Rice. 2007. "Flaviviridae : The Viruses and Their Replication." In *Fields Virology, 5th Edition*, edited by M. Knipe and P.M. Howley, 5th Editio, 1101 – 1152. Philadelphia: Lippincott-Raven Publishers.

Lindquist Michael E, Aaron W Lifland, Thomas J Utley, Philip J Santangelo, James E Crowe Jr, and James E Crowe. 2010. "Respiratory Syncytial Virus Induces Host RNA Stress Granules To Facilitate Viral Replication." *Journal of Virology* 84 (23): 12274–12284. doi:10.1128/JVI.00260-10.

Lobigs M. 1993. "Flavivirus Premembrane Protein Cleavage and Spike Heterodimer Secretion Require the Function of the Viral Proteinase NS3." *Proceedings of the National Academy of Sciences of the United States of America* 90 (13) (July 1): 6218–22.

Loo Yueh-Ming, and Michael Gale. 2011. "Immune Signaling by RIG-I-like Receptors." *Immunity* 34 (5) (May 27): 680–92. doi:10.1016/j.immuni.2011.05.003.

Ma Lixin, Christopher T Jones, Teresa D Groesch, Richard J Kuhn, and Carol Beth Post. 2004. "Solution Structure of Dengue Virus Capsid Protein Reveals Another Fold." *Proceedings of the National Academy of Sciences of the United States of America* 101 (10) (March 9): 3414–9. doi:10.1073/pnas.0305892101.

Mackenzie J M, a a Khromykh, M K Jones, and E G Westaway. 1998. “Subcellular Localization and Some Biochemical Properties of the Flavivirus Kunjin Nonstructural Proteins NS2A and NS4A.” *Virology* 245 (2) (June 5): 203–15. doi:10.1006/viro.1998.9156.

Mackenzie Jason M, Mark T Kenney, and Edwin G Westaway. 2007. “West Nile Virus Strain Kunjin NS5 Polymerase Is a Phosphoprotein Localized at the Cytoplasmic Site of Viral RNA Synthesis.” *The Journal of General Virology* 88 (Pt 4) (April): 1163–8. doi:10.1099/vir.0.82552-0.

Mackenzie Jason M, and Edwin G Westaway. 2001. “Assembly and Maturation of the Flavivirus Kunjin Virus Appear To Occur in the Rough Endoplasmic Reticulum and along the Secretory Pathway , Respectively.” *Journal of Virology* 75 (22): 10787–10799. doi:10.1128/JVI.75.22.10787.

Mackenzie John S, Duane J Gubler, and Lyle R Petersen. 2004. “Emerging Flaviviruses: The Spread and Resurgence of Japanese Encephalitis, West Nile and Dengue Viruses.” *Nature Medicine* 10 (12 Suppl) (December): S98–109. doi:10.1038/nm1144.

Manders E. M. M., F. J. Verbeek, and J.A. Aten. 1993. “Measurement of Co-Localization of Objects in Dual-Colour Confocal Images.” *Journal of Microscopy* 169 (3): 375–382.

Manokaran, Gayathri, Esteban Finol, Chunling Wang, Jayantha Gunaratne, Justin Bahl, Eugenia Z Ong, Hwee Cheng Tan, et al. 2015. “Dengue Subgenomic RNA Binds TRIM25 to Inhibit Interferon Expression for Epidemiological Fitness.” *Science* 350 (6257): 217 – 221.

Markoff, Lewis. 2003. “5’- and 3'-noncoding Regions in Flavivirus RNA.” *Advances in Virus Research* 59 (January): 177–228.

Medigeshi Guruprasad R, Alissa M Lancaster, Alec J Hirsch, Thomas Briese, W Ian Lipkin, Victor Defilippis, Klaus Früh, Peter W Mason, Janko Nikolich-Zugich, and Jay a Nelson. 2007. “West Nile Virus Infection Activates the Unfolded Protein Response, Leading to CHOP Induction and Apoptosis.” *Journal of Virology* 81 (20) (October): 10849–60. doi:10.1128/JVI.01151-07.

Miller Sven, Stefan Kastner, Jacomine Krijnse-Locker, Sandra Bühler, and Ralf Bartenschlager. 2007. "The Non-Structural Protein 4A of Dengue Virus Is an Integral Membrane Protein Inducing Membrane Alterations in a 2K-Regulated Manner." *The Journal of Biological Chemistry* 282 (12) (March 23): 8873–82. doi:10.1074/jbc.M609919200.

Miller Sven, and Jacomine Krijnse-Locker. 2008. "Modification of Intracellular Membrane Structures for Virus Replication." *Nature Reviews. Microbiology* 6 (5) (May): 363–74. doi:10.1038/nrmicro1890.

Miller Sven, Sandra Sparacio, and Ralf Bartenschlager. 2006. "Subcellular Localization and Membrane Topology of the Dengue Virus Type 2 Non-Structural Protein 4B." *The Journal of Biological Chemistry* 281 (13): 8854–8863. doi:10.1074/jbc.M512697200.

Miorin Lisa, Amelina Albornoz, Marycelin M Baba, Pierlanfranco D'Agaro, and Alessandro Marcello. 2012. "Formation of Membrane-Defined Compartments by Tick-Borne Encephalitis Virus Contributes to the Early Delay in Interferon Signaling." *Virus Research* 163 (2) (February): 660–6. doi:10.1016/j.virusres.2011.11.020.

Miorin Lisa, Paolo Maiuri, V M Hoenninger, C W Mandl, and Alessandro Marcello. 2008. "Spatial and Temporal Organization of Tick-Borne Encephalitis Flavivirus Replicated RNA in Living Cells." *Virology* 379 (1) (September 15): 64–77. doi:10.1016/j.virol.2008.06.025.

Miorin Lisa, Inés Romero-Brey, Paolo Maiuri, Simone Hoppe, Jacomine Krijnse-Locker, Ralf Bartenschlager, and Alessandro Marcello. 2013. "Three-Dimensional Architecture of Tick-Borne Encephalitis Virus Replication Sites and Trafficking of the Replicated RNA." *Journal of Virology* 87 (11) (June): 6469–81. doi:10.1128/JVI.03456-12.

Mlakar Jernej, Misa Korva, Nataša Tul, Mara Popović, Mateja Poljšak-Prijatelj, Jerica Mraz, Marko Kolenc, et al. 2016. "Zika Virus Associated with Microcephaly." *New England Journal of Medicine*. doi:10.1056/NEJMoa1600651.

Mukhopadhyay Suchetana, Richard J Kuhn, and Michael G Rossmann. 2005. "A Structural Perspective of the Flavivirus Life Cycle." *Nature Reviews. Microbiology* 3 (1) (January): 13–22. doi:10.1038/nrmicro1067.

Munoz-Jordan Jorge L, Maudry Laurent-Rolle, Joseph Ashour, Luis Martinez-Sobrido, Mundrigi Ashok, W. Ian Lipkin, and Adolfo Garcıa-Sastre. 2005. "Inhibition of Alpha / Beta Interferon Signaling by the NS4B Protein of Flaviviruses." *Journal of virology*. 79 (13): 8004–8013. doi:10.1128/JVI.79.13.8004.

Muñoz-Jordan Jorge L, Gilma G Sánchez-Burgos, Maudry Laurent-Rolle, and Adolfo García-Sastre. 2003. "Inhibition of Interferon Signaling by Dengue Virus." *Proceedings of the National Academy of Sciences of the United States of America* 100 (24) (November 25): 14333–8. doi:10.1073/pnas.2335168100.

Muylaert Isabella R., Thomas J. Chambers, Ricardo Galler, and Charles M Rice. 1996. "Mutagenesis of the N-Linked Glycosylation Sites of the Yellow Fever Virus NS1 Protein: Effects on Virus Replication and Mouse Neurovirulence." *Virology* 222 (1) (August 1): 159–68. doi:10.1006/viro.1996.0406.

Nestorowicz Ann, Thomas J. Chambers, and Charles M. Rice. 1994. "Mutagenesis of the Yellow Fever Virus NS2A/2B Cleavage Site: Effects on Proteolytic Processing, Viral Replication, and Evidence for Alternative Processing of the NS2A Protein." *Virology* 199: 114–123.

Novoa Isabel, Huiqing Zeng, Heather P. Harding, and David Ron. 2001. "Feedback Inhibition of the Unfolded Protein Response by GADD34-Mediated Dephosphorylation of eIF2alpha." *The Journal of Cell Biology* 153 (5): 1011–1022. doi:10.1083/jcb.153.5.1011.

Onomoto Koji, Michihiko Jogi, Ji-Seung Yoo, Ryo Narita, Shiho Morimoto, Azumi Takemura, Suryaprakash Sambhara, et al. 2012. "Critical Role of an Antiviral Stress Granule Containing RIG-I and PKR in Viral Detection and Innate Immunity." *PloS One* 7 (8) (January): e43031. doi:10.1371/journal.pone.0043031.

Onomoto Koji, Mitsutoshi Yoneyama, Gabriel Fung, Hiroki Kato, and Takashi Fujita. 2014. "Antiviral Innate Immunity and Stress Granule Responses." *Trends in Immunology* 35 (9) (August 18): 420–428. doi:10.1016/j.it.2014.07.006.

Overby Anna K, Vsevolod L Popov, Matthias Niedrig, and Friedemann Weber. 2010. "Tick-Borne Encephalitis Virus Delays Interferon Induction and Hides Its Double-Stranded RNA in Intracellular Membrane Vesicles." *Journal of Virology* 84 (17) (September): 8470–83. doi:10.1128/JVI.00176-10.

Peña José, and Eva Harris. 2011. "Dengue Virus Modulates the Unfolded Protein Response in a Time-Dependent Manner." *The Journal of Biological Chemistry* 286 (16) (April 22): 14226–36. doi:10.1074/jbc.M111.222703.

Pijlman Gorben P, Anneke Funk, Natasha Kondratieva, Jason Leung, Shessy Torres, Lieke van der Aa, Wen Jun Liu, et al. 2008. "A Highly Structured, Nuclease-Resistant, Noncoding RNA Produced by Flaviviruses Is Required for Pathogenicity." *Cell Host & Microbe* 4 (6) (December 11): 579–91. doi:10.1016/j.chom.2008.10.007.

Ramanathan Mathura P, Jerome a Chambers, Panyupa Pankhong, Michael Chattergoon, Watcharee Attatippaholkun, Kesen Dang, Neelima Shah, and David B Weiner. 2006. "Host Cell Killing by the West Nile Virus NS2B-NS3 Proteolytic Complex: NS3 Alone Is Sufficient to Recruit Caspase-8-Based Apoptotic Pathway." *Virology* 345 (1) (February 5): 56–72. doi:10.1016/j.virol.2005.08.043.

Rey Félix A., Franx X. Heinz, Christian Mandl, Christian Kunz, and Stephen C. Harrison. 1995. "The Envelope Glycoprotein from Tick-Borne Encephalitis Virus at 2 A Resolution." *Nature* 375 (6529) (May 25): 291–8. doi:10.1038/375291a0.

Roby Justin A., Gorben P. Pijlman, Jeffrey Wilusz, and Alexander A. Khromykh. 2014. "Noncoding Subgenomic Flavivirus RNA: Multiple Functions in West Nile Virus Pathogenesis and Modulation of Host Responses." *Viruses* 6: 404–427. doi:10.3390/v6020404.

Romero-Brey, Ines, and Ralf Bartenschlager. 2014. *Membranous Replication Factories Induced by plus-Strand RNA Viruses*. *Viruses*. Vol. 6. doi:10.3390/v6072826.

Ruggieri, Alessia, Eva Dazert, Philippe Metz, Sarah Hofmann, Jan-Philip Bergeest, Johanna Mazur, Peter Bankhead, et al. 2012. "Dynamic Oscillation of Translation and Stress Granule Formation Mark the Cellular Response to Virus Infection." *Cell Host & Microbe* 12 (1) (July 19): 71–85. doi:10.1016/j.chom.2012.05.013.

Saito, Takeshi, Reiko Hirai, Yueh-Ming Loo, David Owen, Cynthia L Johnson, Sangita C Sinha, Shizuo Akira, Takashi Fujita, and Michael Gale. 2007. "Regulation of Innate Antiviral Defenses through a Shared Repressor Domain in RIG-I and LGP2." *Proceedings of the National Academy of Sciences of the United States of America* 104 (2): 582–587. doi:10.1073/pnas.0606699104.

Samuel, Charles E. 2001. "Antiviral Actions of Interferons." *Clinical Microbiology Reviews* 14 (4): 778–809. doi:10.1128/CMR.14.4.778.

Satoh, Takashi, Hiroki Kato, Yutaro Kumagai, Mitsutoshi Yoneyama, Shintaro Sato, Kazufumi Matsushita, Tohru Tsujimura, Takashi Fujita, Shizuo Akira, and Osamu Takeuchi. 2010. "LGP2 Is a Positive Regulator of RIG-I- and MDA5-Mediated Antiviral Responses." *Proceedings of the National Academy of Sciences of the United States of America* 107 (4): 1512–1517. doi:10.1073/pnas.0912986107.

Scheuner, D, B Song, E McEwen, C Liu, R Laybutt, P Gillespie, T Saunders, S Bonner-Weir, and R J Kaufman. 2001. "Translational Control Is Required for the Unfolded Protein Response and in Vivo Glucose Homeostasis." *Molecular Cell* 7 (6): 1165–76. doi:S1097-2765(01)00265-9.

Schröder, Martin, and Randal J Kaufman. 2005. "The Mammalian Unfolded Protein Response." *Annual Review of Biochemistry* 74 (January): 739–89. doi:10.1146/annurev.biochem.73.011303.074134.

Shinohara, Yoshiyasu, Kento Imajo, Masato Yoneda, Wataru Tomeno, Yuji Ogawa, Hiroyuki Kirikoshi, Kengo Funakoshi, et al. 2013. "Unfolded Protein Response Pathways Regulate Hepatitis C Virus Replication via Modulation of Autophagy." *Biochemical and Biophysical Research Communications* 432 (2): 326–332. doi:10.1016/j.bbrc.2013.01.103.

Smith Judith a, Matthew J Turner, Monica L DeLay, Erin I Klenk, Dawn P. Sowders, and Robert A. Colbert. 2008. "Endoplasmic Reticulum Stress and the Unfolded Protein Response Are Linked to Synergistic IFN-β Induction via XBP-1." *European Journal of Immunology* 38 (5): 1194–1203. doi:10.1002/eji.200737882.Endoplasmic.

Smith Judith A. 2014. "A New Paradigm: Innate Immune Sensing of Viruses via the Unfolded Protein Response." *Frontiers in Microbiology* 5 (May): 1–10. doi:10.3389/fmicb.2014.00222.

Sriburi Rungtawan, Suzanne Jackowski, Kazutoshi Mori, and Joseph W. Brewer. 2004. "XBP1: A Link between the Unfolded Protein Response, Lipid Biosynthesis, and Biogenesis of the Endoplasmic Reticulum." *Journal of Cell Biology* 167 (1): 35–41. doi:10.1083/jcb.200406136.

Stapleton Jack T., Steven Foung, A. Scott Muerhoff, Jens Bukh, and Peter Simmonds. 2011. "The GB Viruses: A Review and Proposed Classification of GBV-A, GBV-C (HGV), and GBV-D in Genus Pegivirus within the Family Flaviviridae." *Journal of General Virology* 92 (2): 233–246. doi:10.1099/vir.0.027490-0.

Stetson Daniel B, and Ruslan Medzhitov. 2006. “Type I Interferons in Host Defense.” *Immunity* 25 (3) (October): 373–81. doi:10.1016/j.immuni.2006.08.007.

Stiasny Karin, and Franz X Heinz. 2006. “Flavivirus Membrane Fusion.” *The Journal of General Virology* 87 (Pt 10) (October): 2755–66. doi:10.1099/vir.0.82210-0.

Takahasi Kiyohiro, Mitsutoshi Yoneyama, Tatsuya Nishihori, Reiko Hirai, Hiroyuki Kumeta, Ryo Narita, Michael Gale, Fuyuhiko Inagaki, and Takashi Fujita. 2008. “Nonself RNA-Sensing Mechanism of RIG-I Helicase and Activation of Antiviral Immune Responses.” *Molecular Cell* 29 (4): 428–440. doi:10.1016/j.molcel.2007.11.028.

Todd Derrich J, Ann-Hwee Lee, and Laurie H Glimcher. 2008. “The Endoplasmic Reticulum Stress Response in Immunity and Autoimmunity.” *Nature Reviews. Immunology* 8 (9) (September): 663–74. doi:10.1038/nri2359.

Tourrière Helene, Karim Chebli, Latifa Zekri, Brice Courselaud, Jean Marie Blanchard, Edouard Bertrand, and Jamal Tazi. 2003. “The RasGAP-Associated Endoribonuclease G3BP Assembles Stress Granules.” *The Journal of Cell Biology* 160 (6) (March 17): 823–31. doi:10.1083/jcb.200212128.

Umareddy Indira, Olivier Pluquet, Qing Yin Wang, Subhash G Vasudevan, Eric Chevet, and Feng Gu. 2007. “Dengue Virus Serotype Infection Specifies the Activation of the Unfolded Protein Response.” *Virology Journal* 4 (January): 91. doi:10.1186/1743-422X-4-91.

Walter Peter, and David Ron. 2011. “The Unfolded Protein Response: From Stress Pathway to Homeostatic Regulation.” *Science* 334: 1081 – 1086. doi:10.1126/science.1209038.

Warrener Paul, James K Tamura, Marc S Collett, West Watkins, and Mill Road. 1993. “RNA-Stimulated NTPase Activity Associated with Yellow Fever Virus NS3 Protein Expressed in bacteriaVirus NS3 Protein Expressed in Bacteria.” *Journal of Virology* 67 (2): 989–996.

Weber Michaela, Ali Gawanbacht, Matthias Habjan, Andreas Rang, Christoph Borner, Anna Mareike Schmidt, Sophie Veitinger, et al. 2013. “Incoming RNA Virus Nucleocapsids Containing a 5’-triphosphorylated Genome Activate RIG-I and Antiviral Signaling.” *Cell Host & Microbe* 13 (3) (March 13): 336–46. doi:10.1016/j.chom.2013.01.012.

Welsch Sonja, Sven Miller, Ines Romero-Brey, Andreas Merz, Christopher K E Bleck, Paul Walther, Stephen D Fuller, Claude Antony, Jacomine Krijnse-Locker, and Ralf Bartenschlager. 2009. "Composition and Three-Dimensional Architecture of the Dengue Virus Replication and Assembly Sites." *Cell Host & Microbe* 5 (4) (April 23): 365–75. doi:10.1016/j.chom.2009.03.007.

Wengler Gerd, and Gisela Wengler. 1993. "The NS3 Nonstrutural Protein of Flaviviruses Contains an RNA Triphosphatase Activity." *Virology* 197: 265–273.

Wengler Gerd, Gisela Wengler, and Hans J. Gross. 1978. "Studies on Virus-Specific Nucleic Acids Synthesized in Vertebrate and Mosquito Cells Infected with Flaviviruses." *Virology* 89 (2): 423–437.

Wilson Jason R, Paola Florez de Sessions, Megan a Leon, and Frank Scholle. 2008. "West Nile Virus Nonstructural Protein 1 Inhibits TLR3 Signal Transduction." *Journal of Virology* 82 (17) (September): 8262–71. doi:10.1128/JVI.00226-08.

Yan Wei, Christopher L Frank, Marcus J Korth, Bryce L Sopher, Isabel Novoa, David Ron, and Michael G Katze. 2002. "Control of PERK eIF2alpha Kinase Activity by the Endoplasmic Reticulum Stress-Induced Molecular Chaperone P58IPK." *Proceedings of the National Academy of Sciences of the United States of America* 99 (25): 15920–15925. doi:10.1073/pnas.252341799.

Ye Jing, Bibo Zhu, Zhen F Fu, Huanchun Chen, and Shengbo Cao. 2013. "Immune Evasion Strategies of Flaviviruses." *Vaccine* 31 (3) (January 7): 461–71. doi:10.1016/j.vaccine.2012.11.015.

Yoneyama Mitsutoshi, and Takashi Fujita. 2009. "RNA Recognition and Signal Transduction by RIG-I-like Receptors." *Immunological Reviews* 227 (1) (January): 54–65. doi:10.1111/j.1600-065X.2008.00727.x.

Yoneyama Mitsutoshi, Mika Kikuchi, Kanae Matsumoto, Tadaatsu Imaizumi, Makoto Miyagishi, Kazunari Taira, Eileen Foy, et al. 2005. "Shared and Unique Functions of the DExD/H-Box Helicases RIG-I, MDA5, and LGP2 in Antiviral Innate Immunity." *Journal of Immunology* 175 (5): 2851–2858. doi:175/5/2851 [pii].

Yoneyama Mitsutoshi, Mika Kikuchi, Takashi Natsukawa, Noriaki Shinobu, Tadaatsu Imaizumi, Makoto Miyagishi, Kazunari Taira, Shizuo Akira, and Takashi Fujita. 2004. "The RNA Helicase RIG-I Has an Essential Function in Double-Stranded RNA-Induced Innate Antiviral Responses." *Nature Immunology* 5 (7) (July): 730–7. doi:10.1038/ni1087.

Yoshida Hiderou, Toshie Matsui, Akira Yamamoto, Tetsuya Okada, and Kazutoshi Mori. 2001. "XBP1 mRNA Is Induced by ATF6 and Spliced by IRE1 in Response to ER Stress to Produce a Highly Active Transcription Factor." *Cell* 107 (7): 881–891. doi:10.1016/S0092-8674(01)00611-0.

Yu Chao, Katharina Achazi, and Matthias Niedrig. 2013. "Tick-Borne Encephalitis Virus Triggers Inositol-Requiring Enzyme 1 (IRE1) and Transcription Factor 6 (ATF6) Pathways of Unfolded Protein Response." *Virus Research* 178 (2) (December 26): 471–7. doi:10.1016/j.virusres.2013.10.012.

Yu Chia-Yi, Yun-Wei Hsu, Ching-Len Liao, and Yi-Ling Lin. 2006. "Flavivirus Infection Activates the XBP1 Pathway of the Unfolded Protein Response to Cope with Endoplasmic Reticulum Stress." *Journal of Virology* 80 (23) (December): 11868–80. doi:10.1128/JVI.00879-06.